Design of cancer-selective and nuclei-targeting cell-penetrating peptides and their characterization

Inaugural-Dissertation

zur

Erlangung des Doktorgrades

der Mathematisch-Naturwissenschaftlichen Fakultät

der Universität zu Köln

vorgelegt von

Anja Gronewold

aus Bonn

Köln 2017

Berichterstatter:	Prof. Dr. Ines Neundorf
	Prof. Dr. Ulrich Baumann
Tag der mündlichen Prüfung:	18. Dezember 2017

Die im Rahmen der vorliegenden Arbeit durchgeführten Experimente und Untersuchungen wurden im Zeitraum von April 2014 bis August 2017 am Institut für Biochemie der Universität zu Köln unter der Anleitung von Frau Prof. Dr. Ines Neundorf durchgeführt.

Abstract

Nowadays, cancer still remains one of the leading causes of death in the world. Therefore, cancer research is a present and central topic. Current drawbacks in cancer therapeutics are the lack of tumor specificity and the inefficient drug accumulation in cancer cells, resulting in non-specific agents that also affect healthy cells and thus their application provokes many side effects. Many possibilities for cancer cell-selective targeting of drugs are currently in focus. One includes the use of cell-penetrating peptides (CPPs), which are able to overcome the plasma membrane barrier and to transport various cargoes inside cells. Recently, it was shown for some CPPs, that they can specifically target cancer cells and therefore be used to promote the effective transport of anticancer drugs into various neoplastic cells. Furthermore, a certain intracellular targeting feature to various organelles was presented in the last years, which is important for the successful delivery of certain drugs to their point of action. This makes these amino acid sequences a promising research field in cancer treatment.

In this study, the focus was set to the development and characterization of specific cancer-selective peptides that accumulate in the cell nuclei and can moreover be used to deliver various cargoes to cancer cells.

The design of the CPPs was based on the *C*-terminal domain of the cationic antimicrobial peptide CAP18 (sC18), which was modified in various ways. For instance, it could be demonstrated that dimerization of the sequence and the *N*-terminally introduction of nuclear targeting sequences led to higher uptake rates of the CPP. Furthermore, the branched variant $(sC18)_2$ exhibited a certain cancer cell-selectivity and was able to disrupt the neoplastic plasma membranes resulting in higher cytotoxicity. Next to this, the combination of sC18 with N50 and NrTP - two sequences that specifically target the cell nuclei - are approving the intracellular trafficking into the cell nucleus in cancer cells. Furthermore, an application as drug delivery system in breast cancer cells was elucidated.

Zusammenfassung

Krebs ist eine der häufigsten Todesursachen weltweit, weshalb die Forschung nach neuen Therapieansätzen zur Krebsbekämpfung eine zentrale Rolle annimmt. Die maßgeblichen Nachteile heutiger Therapien sind sowohl die ungezielte Ansteuerung von Krebszellen als auch eine ineffiziente Anhäufung der Medikamente in Tumoren. Das macht viele Therapeutika zu nicht zufriedenstellenden Lösungen, da diese ebenfalls gesunde Zellen angreifen und daher sehr viele Nebeneffekte mit sich bringen. Zurzeit sind viele andere Herangehensweisen, um Krebszellen spezifisch anzusteuern, im Fokus der Wissenschaft. Eine davon ist der Einsatz von zellpenetrierenden Peptiden (cell-penetrating peptides, CPPs), die in der Lage sind, sich selber in Zellen einzuschleusen und zusätzlich Wirkstoffe in diese zu transportieren. Kürzlich konnte für einige dieser CPPs gezeigt werden, dass sie Krebszellen spezifisch ansteuern und gleichzeitig als Transporter für Zytostatika dienen können. Außerdem haben einige Peptide die Eigenschaft, in speziellen Zellorganellen wie dem Zellkern zu akkumulieren, was nötig ist, um spezielle Medikamente an ihren Wirkungsort zu transportieren.

In dieser Arbeit sollten Peptide entwickelt werden, die selektiv gegenüber Krebszellen sind. Weiterhin wurde untersucht, ob sich diese Peptide selektiv im Zellkern anlagern und als Transportsystem genutzt werden können.

Das Design der neuen CPPs basierte auf dem Peptid sC18, eine von der *C*-terminalen Domäne des antimikrobiellen kationischen Peptides CAP18 abgeleiteten Sequenz. Dieses zellpenetrierende Peptid wurden auf unterschiedlichen Wegen modifiziert. Es konnte gezeigt werden, dass eine Dimerisierung über die Seitenkette eines Lysins zu höheren Aufnahmeraten und einer Lokalisation der Peptide im Zellkern führt. Für das verzweigte $(sC18)_2$ konnte eine erhöhte Krebsselektivität gezeigt werden. Das Peptid sorgt für eine Permeabilisierung der Zellmembran von Krebszellen und induziert dadurch eine gewisse Zytotoxizität.

Außerdem wurde sC18 durch das *N*-terminale Kuppeln von speziellen Zellkern-ansteuernden Sequenzen modifiziert. Die Kombination des Peptids mit N50 und NrTP – zwei Peptidsequenzen, die in der Lage sind, den Zellkern selektiv anzusteuern – führte zu einer erhöhten Anreicherung der Peptide im Nukleus von Krebszellen. Zudem konnte ein erfolgreicher Transport eines Therapeutikums in Brustkrebszellen gezeigt werden.

Table of contents

1. INTRODUCTION

1.1 Overcoming cell membrane barriers

About four billion years ago, the first cells and with them, the primary cell membranes emerged. Cellular plasma membranes have a lot of duties and functions towards the cell. It is a semi-permeable lipid bilayer, which defines the cell shape and separates the intracellular space from the surrounding environment, protecting the cell from invading pathogens and toxic substances. [1, 2] Due to their particular biological structure, the membrane is only permeable for small hydrophobic compounds with less than 1,000 Daltons [3]. Uptake of large or hydrophilic molecules can only occur through transmembrane protein channels and transporter molecules. Furthermore, cellular membranes are involved in various physiological processes such as signal transduction, energy synthesis and cell-cell communication. [4, 5]

Since the plasma membrane has extraordinary properties in protecting the cell from the surrounding environment, the problem occurs that delivery processes of drugs, proteins and nucleotides into cells and compartments are limited. Several studies about strategies to overcome membrane barriers have received major attention in the last years. Penetration of the cellular plasma membrane can either be achieved by the use of certain biological or chemical compounds, like prodrugs, carriers and permeation enhancers, or by physical units generating an energy-dependent disruption of the membrane. [2] Within this, cell membranes have already been permeabilized by sonoporation, resulting in a successful gene delivery to HeLa and PC-3 cells [6, 7]. However, for most of the physical methods, a power source is necessary. Therefore, they can be potentially expensive, which reduces the attraction of these methods. A variety of biological approaches like prodrugs, liposomes and nanoparticles were recently developed and investigated. In this context, liposomes were shown to transport anti-cancer, anti-fungal and antibiotic drugs as well as anti-inflammatory agents and gene medicines into a variety of cells [8]. Moreover, PEGylated nanoparticles have been used to deliver proteins and peptide-drugs *in vivo* [9].

Another group of transport vehicles has been discovered in the last decades; these are short peptides, able to cross membranes in a receptor-independent manner. These so-called cell-penetrating peptides (CPPs) have the ability to interact electrostatically with biological membranes and internalize into a number of different cell types, like microorganisms, fungi, mammalian and plant cells. [10, 11] In general, they are known to be usually positively charged, water soluble and partly hydrophobic. Advantages of these peptides are their small size, good biocompatibility and their easy and cost-effective synthesis. Furthermore, CPPs can be easily

modified concerning, for example their affinity, hydrophobicity, charge, solubility, and stability. Additionally, they do usually not evoke an immune response. [12, 13] The most important feature of these recently discovered peptides is certainly their capability to efficiently transport different cargos into cells [14]. Anyway, also disadvantages of CPPs are known, like their low cell, tissue and organ specifity and their limited stability *in vivo*. Moreover, another problem to overcome is their often occurred internalization by endocytosis and the need of a subsequent endosomal release, essential for the transport of peptides and cargos to their targets. [15]

Nevertheless, cell-penetrating peptides represent a promising and precious tool for the transport and internalization of otherwise impermeable molecules.

1.2 Commonly used cell-penetrating peptides

Cell-penetrating peptides can be divided into different subgroups based on their specific properties. One classification is based on the origin of the peptide sequence divided in protein-derived, chimeric or synthetic peptides. [10] An overview about some CPPs and their sequences is presented in table 1.

Table 1: Examples for commonly used cell-penetrating peptides and their origin.

Peptide	Sequence	Origin	Reference
TAT(48-60)	GRKKRRQRRRPPQ	Protein-derived	[16]
Penetratin	RQIKIWFQNRRMKWKK	Protein-derived	[17]
hCT(9-32)	LGTYTQDFNKFHTFPQTAIGVGAP	Peptide-derived	[18]
sC18	GLRKRLRKFRNKIKEK	Protein-derived	[19]
$(sC18)_2$	GLRKRLRKFRNKIKEK | GLRKRLRKFRNKIKEK	Chimeric	[20]
Transportan	GWTLNSAGYLLGKINLKALAALAKKIL	Chimeric	[21]
Oligoarginines	R8, R9, R10, R12	Designed	[22]
Pep-1	KETWWETWWTEWSQPKKKRKV	Designed	[23]

The peptides TAT and penetratin are examples for CPPs that are derived from natural proteins. TAT(48-60) is a cationic and hydrophilic peptide derived from the transcription activating factor

of human immunodeficiency virus (HIV-1), that is able to translocate through the plasma membrane and accumulate in the cell nucleus. [16] Also penetratin is derived from a transcription factor, precisely from the Drosophila *Antennapedia* homeodomain, and is an extensively studied cell-penetrating peptide. Penetratin is declared to be a secondary amphipathic peptide, meaning that its amphipathic structure is only formed when the CPP is interacting with phospholipid membranes. [17] Furthermore, also a hydrophobic peptide, derived from the human peptide hormone calcitonin (hCT) has been reported to translocate membranes. The shorter fragment hCT(9-32) is able to transport small organic molecules as well as proteins into cells. The efficient delivery of DNA and RNA has been reported for hCT(18-32), which was further combined with a lysine- and arginine-rich sequence (k7), representing an example for a chimeric peptide built from a peptide-derived and designed sequence. [18, 19, 24] Another well-studied CPP is derived from a cationic antimicrobial protein from rabbit leucocytes, which is assumed to inactivate pathogens by permeabilizing their membranes. This cathelicidin-derived, short peptide sequence from the *C*-terminal domain is called sC18 and exhibits an α-helical structure. It was already demonstrated that its uptake rates are comparable to those of TAT(48-60) and hCT(18-32)-k7. [19, 25] Furthermore, also a branched, dimeric version of sC18 was examined by Hoyer *et al.* with even higher internalization capacity and an increased cytotoxicity. $(sC18)_2$ is also able to efficiently transport cytostatic compounds into tumor cells. [20]

Transportan is classified as a chimeric CPP, which is composed of two sequences, mastoparan and galanin. Mastoparan is known as a wasp toxin that can penetrate and lyse cell membranes, while galanin is a neuropeptide, which inhibits the release of neurotransmitter from vesicles. Their chimeric combination connected via a lysine results in a cell-penetrating peptide with high internalization rates. [21] Examples for synthetically designed peptides are Pep-1 and oligoarginines. The amphipathic peptide Pep-1 was shown to deliver unbound active proteins or peptides into cells and different oligoarginines were reported to translocate through membranes due to their high hydrophilicity. [22, 23]

1.3 Cellular uptake mechanisms of cell-penetrating peptides

The cellular uptake of cell-penetrating peptides is a complex process, which is intensively studied. Unfortunately, the general uptake mechanism is still not fully understood, since the internalization of peptides can occur in several ways simultaneously. Moreover, the uptake is dependent on the peptide sequence, the concentration, temperatures as well as the cell type investigated. In addition, specific cargoes attached to the CPP can also influence the uptake mechanism. Generally, two different ways of CPP entry are discussed – the direct translocation over the membrane and the uptake via endocytosis. [26, 27]

Direct penetration is an energy-independent process that can even occur at low temperatures when all endocytotic uptake routes are repressed. Hereby, it is thought that the mainly positively charged peptides interact electrostatically with negatively charged components of biological membranes, inducing finally the insertion of the peptide in the membrane and resulting in cell entry. In this context, the internalization by inverted micelles, direct translocation, pore formation, carpet-like model and membrane thinning can be differentiated as shown in figure 1.

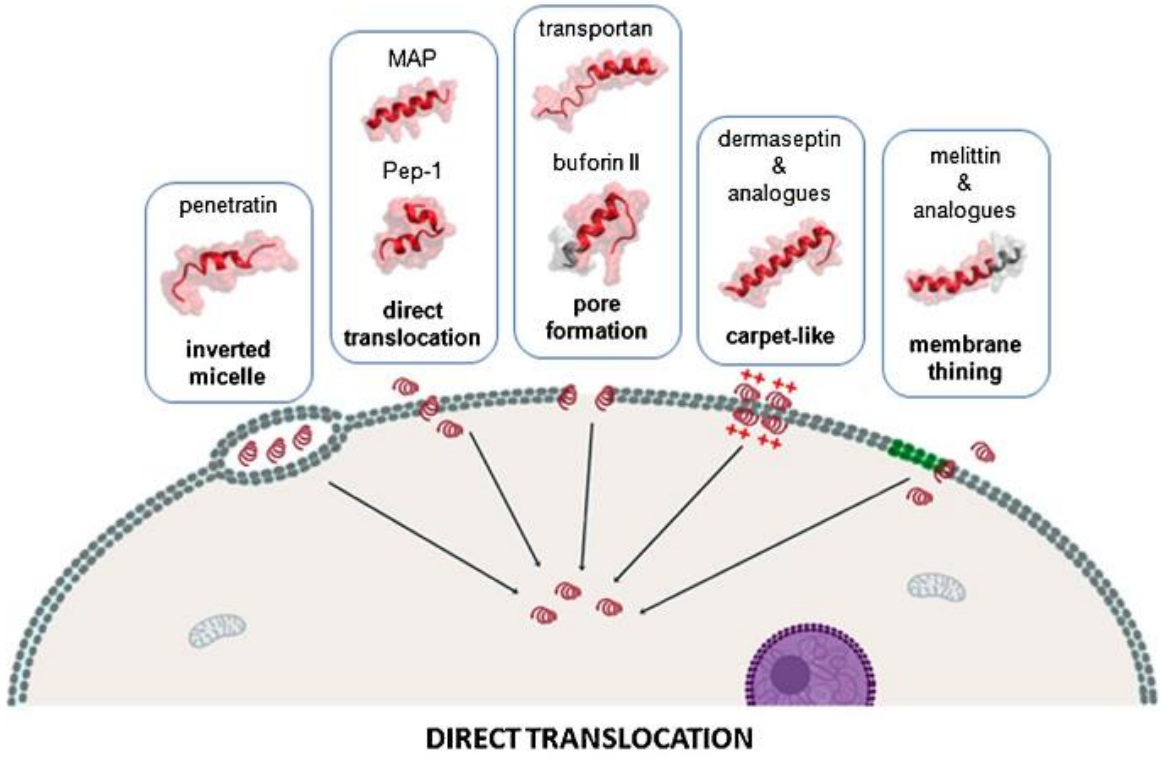

Figure 1: Overview of the main mechanisms of cellular internalization used by cell-penetrating peptides among non-endocytotic direct penetration ways, with representative corresponding examples. [28]

For penetratin for example, the translocation via inverted micelles has been shown, whereby the membrane is destabilized and a curvature is induced. The formed micelle is then enclosing the peptides in its interior and the disruption of the inner membrane is resulting in the release of the CPPs into the cytoplasm. [29] Pore-formation, which is presumed for transportan can arise via the barrel stave or the toroidal model. The CPPs organize in barrel-like structures, where the hydrophilic residues of the sequences form the pore, or as in the toroidal model, the peptides and headgroups of membrane lipids built the pore together. [10]

Also the endocytic uptake pathway, which is an energy-dependent process, can be classified in various mechanisms like macropinocytosis, clathrin- or caveolin-dependent or -independent

endocytosis as depicted in figure 2. After endosomal uptake, the CPPs and CPP-cargo conjugates are enclosed in vesicles. The following endosomal release is a challenging mechanism, and also indispensable for the effect of many drugs taken up by endocytosis. [30] Moreover, the uptake and release depends, among others, on the size and physicochemical nature of the cargo molecule [31].

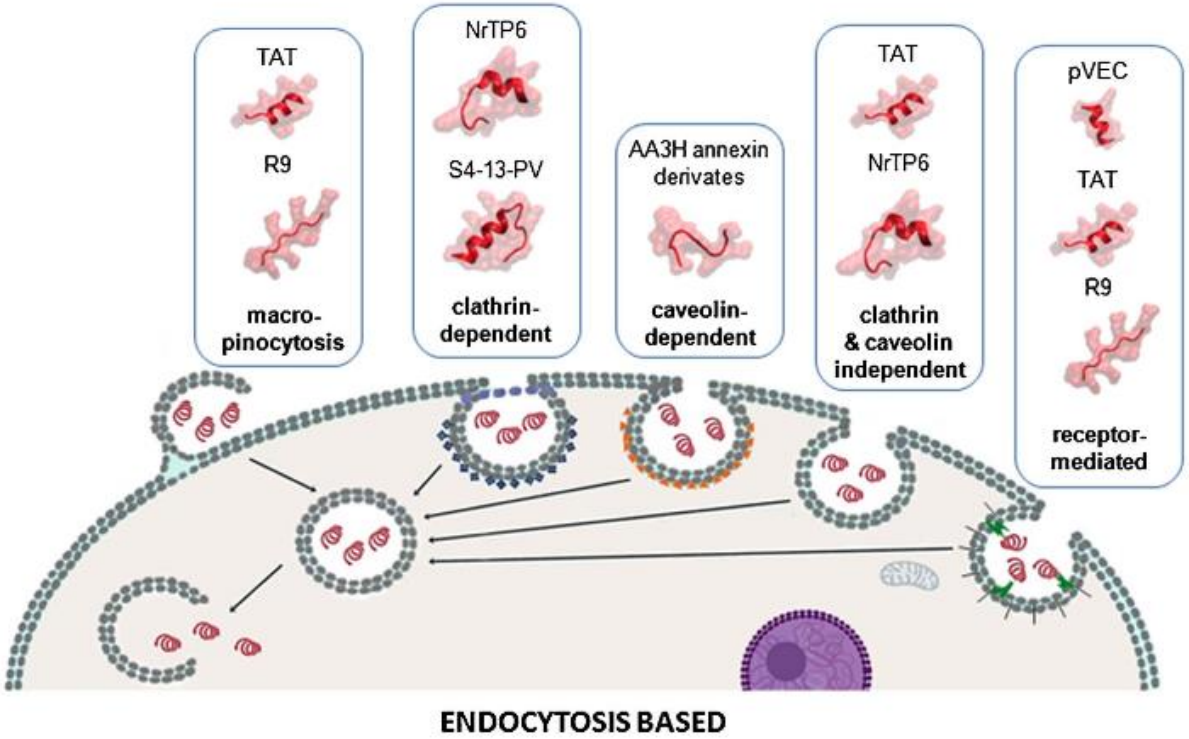

Figure 2: Overview of the main mechanisms of cellular internalization used by cell-penetrating peptides among endocytotic-based mechanisms, with representative corresponding examples. [28]

For the well-studied TAT(48-60) peptide, various uptake routes have been demonstrated including a direct penetration, but also macropinocytosis, as well as clathrin- or caveolin-independent internalization could be presented [28]. During macropinocytosis an inward folding of the plasma membrane to the outer surface takes place and results in a vesicle inside the cell [32]. The different uptake ways are dependent on concentration, time of incubation and composition of membrane phospholipids. [33, 34] NrTP analogues, which are also used in this thesis, crosses the cell membrane by clathrin-dependent endocytosis. [35]

For the cathelicidin-derived CPP sC18, an endocytotic uptake pathway is supposed, but a more precise declaration is still in study [19]. Also for the dimeric variant $(sC18)_2$, internalization by endocytosis was postulated, which was further investigated in this study [20].

1.4 Cell-penetrating peptides for selective targeting of cancer cells

Cancer remains one of the main causes of death globally, and it is one of the most common in the United States responsible for nearly 25% of deaths. A majority of treatments includes the surgical removal of the tumor tissue. Furthermore, chemo- and radiotherapy are used to inhibit tumor growth – nevertheless, a major issue is that also healthy tissue is affected by these therapeutical approaches. [36, 37] The major drawbacks of cancer therapeutics are not only the lack of tumor specificity, but also drug resistance, inefficient drug accumulation and cancer cell heterogeneity. The traditional chemotherapeutic systems poorly distinguish between cancer and non-cancer cells, leading to non-negligible side effects. [12] Hence, a broad field of scientific studies try to find solutions to specifically target cancer cells and prevent the affection of healthy cells.

From this point of view, CPPs have been intensively studied and discussed, since for some of them showed a tumor targeting ability. Interaction, binding and translocation depends on the components of the extracellular matrix of the cell membrane as well as on their sugar and lipid composition. In fact, plasma membranes of cancer and non-cancer cells differ from each other, as neoplastic cell membranes have an increased amount of anionic molecules such as the phospholipid phosphatidylserine, sialylated gangliosides, O-glycosylated mucins and heparin sulfate. This results in a more negative net charge in contrast to healthy mammalian cell membranes, which occur mostly zwitterionic. [38, 39] Especially positively charged CPPs are able to interact with the more negatively charged cancer cell membranes, which is primarily responsible for their tumor cell selectivity. The positively charged, amphipathic peptide NK-2, which is derived from the cationic core region of an antibacterial effector protein from porcine immune cells, specifically attacks cancer cells that have a high content of phosphatidylserine. Healthy human lymphocytes are not harmed by this membranolytic peptide. [40] Lim *et al.* presented in 2013 a derivative of the anticancer peptide buforin IIb with extraordinary cancer-specificity. This peptide BR2 targets cancer cells by interaction with gangliosides, which are found in high amounts within tumor cells, and translocates the membrane via lipid-mediated macropinocytosis. [41]

Another strategy to specifically target cancer cells is the combination of cell-penetrating peptides with homing peptides, which are able to recognize particular cell types. Homing peptides are often membrane impermeable, which could be advanced by the conjugation to CPP sequences. Tumor homing peptides usually interact with receptors that are overexpressed on the cancer cell surface like integrins, somatostatin, transferrin or epidermal growth factor receptors (EGFR). [12] The conjugation of a CPP with S3, an EGFR-binding domain from vaccinia virus growth factor, increases the tumor selectivity extremely. The uptake

rates of the conjugate were 80-times higher than of the peptide alone, whereas the internalization in non-cancer cells remained at a low level. [42] The tripeptide Arg-Gly-Asp (RGD) is often used for the specific targeting of integrins because this sequence is specifically recognized by the transmembrane receptors. Recently, a study was published, whereby an RGD reverse sequence was conjugated to octaarginine. This conjugation peptide could specifically bind to integrin αvβ3, which is highly upregulated in some tumors, and translocate into various cancer cells with increased uptake rates compared to the controls. [43, 44]

1.5 Application of CPPs as delivery vectors in cancer cells

Very recently, in last August 2017, the company Novartis introduced the first chimeric antigen receptor T cell therapy on the market, which is based on gene transfer for the treatment of B-cell precursor acute lymphoblastic leukemia [https://novartis.gcs-web.com/novartis-receives-fda-approval-for-KymriahTM (29.09.2017)]. For this immunocellular therapy, named Kymriah, the patient's T-cells were taken and transduced with a lentiviral vector encoding a specific antigen receptor for the overproduced B-cells in this type of cancer. Transferring the cells back to the patient, they are able to express the antigen and the immune system starts to fight the cancerous B-cells. [45] In clinical phase II, 83% of the patients treated with the new therapy achieved complete remission, even if the treatment is associated to many side effects [Novartis media release, Basel, August 30, 2017].

A challenging process in this new treatment is the transfection of the T-cells with the lentiviral vector. In general, it is not just important to target specific cells with an application system, but also the transport capability of these systems should be reliable. Anyway, based on this example, there are some promising methods to treat cancer besides the use of conservative therapies like resection or chemotherapy.

Also cell-penetrating peptides received attention as potential candidates for anticancer drug delivery systems. [12] These peptides were shown to transport biologically active cargoes such as drugs, proteins, peptides, nanoparticles and nucleic acids into cells. CPPs were also used as anticancer peptidic vaccines in various approaches. [46, 47] Li *et al.* presented the amphipathic peptide CADY-1, which is able to form a stable complex with the cytotoxic anti-cancer drug doxorubicin (DOX) and triggers its transport over the cell membrane increasing its toxicity. This CADY-1/doxorubicin complex even exhibits anti-tumor activity in animals. [48] Also TAT-DOX conjugates were investigated, showing a high decrease in viable cells compared to the incubation with TAT or DOX alone. They were even able to overcome the multidrug resistance of cervical cancer cells by circumventing drug efflux. [49] A human ovarian cancer cell line that is resistant to the chemotherapeutic agent taxol was treated efficiently with a conjugate of taxol and octaarginine. The approach to overcome this taxol resistance was

next to cell culture also observed in mouse models with ovarian cancer. [50] The CPP BP16 with delivery features for the anticancer drug chlorambucil was presented by Soler *et al*. The efficacy of chlorambucil increased between 6 and 9-times when linked to BP16 in various cancer cells. [51] Also other compounds used in tumor therapy were transported to target cells, for example organometallic compounds, like cisplatin, were efficiently carried by the well-studied CPP Transportan 10 to two different cell lines, whereas no internalization of the drug in non-cancer cells could be observed [52].

For the above described recently introduced immunocellular gene therapy, a delivery of nucleic acids, in this case a DNA vector, is necessary. In this topic, a high number of studies with successful delivery by CPPs could be published. Mussbach *et al.* demonstrated in 2011 that various cell-penetrating peptides in non-covalent complexes with nucleoside phosphates were able to transport them in high amounts into a cervix cancer cell line. Their binding to functional proteins in signal transduction or translation process can induce many intracellular reactions. [53] The delivery of RNA or DNA is exceedingly challenging, because these nucleic acids need to be non-covalently bound to the CPPs and transported to the nuclei as well. This so-called transfection was first described in 1997 by Morris *et al.* using a 27 residue-long peptide sequence built from a hydrophobic domain of HIV gp41 and a hydrophilic domain from the nuclear localization sequence of SV40 T-antigen. They showed a rapid and efficient delivery into the nucleus of fibroblasts by the formation of peptide vector/oligonucleotide complexes. [54] But also in cancer cells, transfection could be successfully conducted by CPPs. The basic amphiphilic peptide ppTG1 is efficiently triggering the transport of vector DNA into HeLa cells. The luciferase reporter assay presented gene expression rates comparable to standard transfection reagents as polyethylenimine (PEI) and Lipofectin. [55] A short cell-penetrating peptides (RRWQW) from bovine lactoferrin was presented to deliver a plasmid, encoding the enhanced green fluorescent protein (EGFP) into human lung carcinoma cells, which was subsequently expressed. Also the efficiency of this peptide was comparable to the commonly used transfection reagent Lipofectamine. [56]

1.6 Specific targeting of organelles using CPPs

Many cargoes or drugs need in fact to be transported to specific targets within the cell. Some of them are depicted in figure 3. Especially organelles like mitochondria, the Golgi apparatus or the nucleus can be reached combining cell-penetrating peptides with a specific localization sequence. This intracellular targeting is a very promising feature of these peptides.

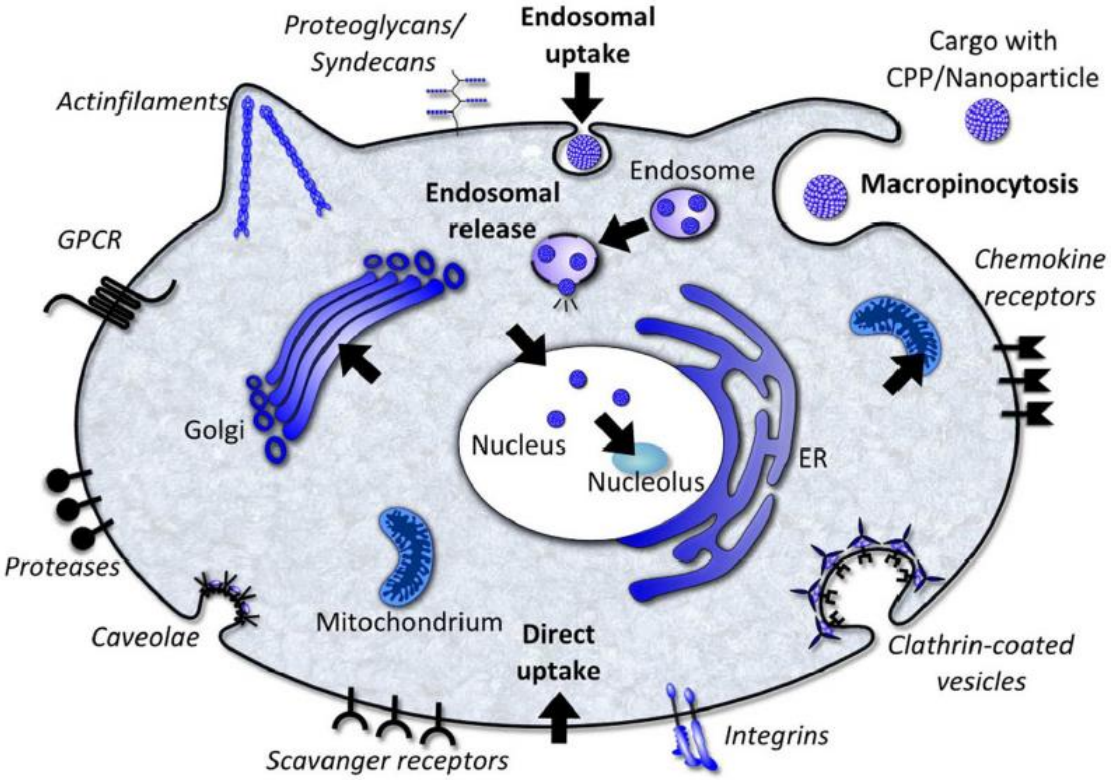

Figure 3: Uptake mechanisms and intracellular targeting of organelles. [15]

The so called mitochondria-penetrating peptides composed of a CPP and a mitochondria-targeting sequence are of great interest, since a lot of intracellular processes as intermediary metabolism, calcium signaling and apoptosis are controlled by these energy-generating organelles. Furthermore, a high number of human diseases such as Parkinson's disease are caused by mitochondrial dysfunctions [57, 58]. The uptake and mitochondrial localization of a mitochondria-penetrating peptide in two cancer cell lines (HeLa and MCF-7) could already be demonstrated by Horton *et al*. [59].

Moreover, of a great interest is the targeting of the cell's control center, the nucleus. This organelle contains the genetic information and controls cell growth, development and reproduction as well as many other intracellular processes. The nuclei are enveloped by a nuclear membrane that separates the nucleoplasm from the cytoplasm and protects the DNA from the surrounding cytoplasm [60, 61]. For some CPPs, an accumulation in the nuclei could be demonstrated. For example, the well-studied trans-activator of transcription TAT(48-60) is able to translocate through the plasma and nuclear membrane [16]. But also some nuclear localization sequences (NLS) were presented in the last years, natural as well as synthetic ones. NLS sequences can be found in cellular or viral proteins that need to be transported to the nucleus after translation or viral infection of a host cell. They often contain high amounts of lysines and arginines. After covalent attachment of a nuclear localization signal motif of the

Simian-Virus 40 (SV40)-T-antigen (PKKKRK) to a peptide, derived from dermaseptin, which failed to enter the nuclei, the conjugate was accumulating in this compartment of HeLa cells [62]. Lewis *et al.* showed that the synthesis of a novel CPP consisting of a glutamate-rich peptide (EEEAA) coupled to the nuclear localization signal of the Oct6 transcription factor results in nuclear localization as well as uptake in prostate and pancreatic cancer cell lines [63].

Nuclear factor-κB (NFκB) is a family of structurally related transcription factors bearing an essential role in inflammation, innate immunity and cancer development. The protein complex that controls DNA transcription is imported into the nucleus through the nuclear pores by importin. The NFκB1/p50 subunit contains a hydrophilic N50 motif patterned on its NLS region. This N50 motif is known to bind the importin α and is therefore responsible for the efficient transport of the transcription factor into the cell nucleus. [64, 65] This N50 peptide sequence (VQRKRQKLMP) was used in this thesis for nuclear targeting of CPPs.

Another desirable target for intracellular delivery of drugs, transcription factors and siRNAs is the nucleolus. A cell contains between one and five of these dense granular structures in the nucleus, which are mostly composed of RNA and proteins. The ribosomal RNA transcription and synthesis of ribosome subunits takes plays in this compartment, and is involved in viral infection, regulation of oncogenesis and tumor suppression. [66, 67] For D-octa-arginine an accumulation in the nucleoli could be reported by Fretz *et al*. [68]. Lately, NrTP was designed by structural minimization of the rattlesnake toxin crotamine. The peptide sequence showed strong membrane-translocating properties and it was capable to penetrate various carcinoma cells and accumulate in their nucleoli. This sequence contains a lysine-rich palindrome hexad in the middle of the peptide (YKQCHKKGGKKGSG). Also the capability of NrTP for intracellular delivery of large molecules like β-galactosidase has been previously demonstrated. [35, 69] The NrTP peptide sequence was used in this thesis to target cell nucleoli.

1.7 Preliminary work

This work is based on the studies that were performed during my master thesis. In this context, the dimeric cell-penetrating peptide $(sC18)_2$ was investigated regarding its internalization, toxicity and membrane interaction in comparison to the monomeric sC18.

In this recent work, it could be shown that sC18 does not exhibit toxicity to three studied cancer cell lines (MCF-7, HeLa and HCT-15) and the non-cancer cell line HEK-293. In contrast, it could be executed that the toxicity of $(sC18)_2$ is extremely increased when incubated with the cancer cell lines HeLa and MCF-7 compared to HCT-15 and HEK-293 cells. Moreover, $(sC18)_2$ presumably acts via disrupting the plasma membranes of HeLa and MCF-7 cells.

Also the internalization of the dimeric versus the monomeric peptide differed from each other, which was verified by microscopic studies. It was observed in all cell lines that the internalization rates of $(sC18)_2$ were much higher compared to the uptake of the monomeric sC18. Furthermore, a detailed observation of a non-cancer and a cancer cell line presented, that sC18 and $(sC18)_2$ seemed to internalize in HEK-293 cells via an endocytic uptake way. Afterwards, the peptides were entrapped in the vesicles and did not appear in the nucleus. On the contrary, in MCF-7 cells, the peptides were distributed in the cytoplasm as well as in the nucleus, which could be explained by an endocytotic uptake with followed release from the endosomes or a direct translocation over the plasma membrane. It is also likely that both uptake ways occur simultaneously. The high internalization rates and the accumulation in the nuclei is probably correlated with the cytotoxic effect on MCF-7 cells. The difference in cancer and non-cancer cells was further investigated using an artificial membrane-like system, precisely different composed giant unilamellar vesicles (GUVs). In this context, it was demonstrated that the interaction of the peptides with negatively charged membranes is much higher than with GUVs composed of zwitterionic phospholipids, which is in accordance with the fact that the peptides showed increased penetration rates and lytic effects on the negatively charged cancer cell membranes.

2. AIMS OF THE THESIS

The main goal of this thesis was the development and characterization of cancer-selective and nuclei-targeting cell-penetrating peptides. Therefore, the well-studied CPP sC18 was chosen as candidate and modified in several ways.

In part I (**"Linear and branched dimeric versions of sC18"**) new variants of sC18 should therefore be developed and characterized. The focus was set on the dimerization of sC18 and its truncated form sC18* (lacking the four *C*-terminal amino acids). The aim was to investigate the impact of the dimerization strategy that yielded either linear or branched derivatives. Therefore, all new peptides should be analyzed concerning their cell-penetrating and membrane damaging properties. In this regard, internalization studies via flow cytometer and microscopy, but also cytotoxicity experiments and furthermore, studies with artificial membrane systems should be performed.

The first part revealed that $(sC18)_2$ showed the highest anticancer potential. Therefore, the focus was set on this peptide in part II of the thesis (**"Characterization of a CPP with potential anticancer activity"**). Within this part, the detailed uptake mechanism and cell selectivity were of great interest. Therefore, uptake studies in different cancer and non-cancer cell lines, studies about the uptake pathway and cargo delivery should be performed. The investigation should initiate with different uptake studies with various peptide concentrations and temperatures. Also flow cytometric analysis should be performed, as well as endosomal release experiments. Next to membrane interaction and disruption studies, also a screening on 16 different cell lines should be performed to further prove the cancer selectivity of the peptide. As a last approach, the drug transport capability should be investigated.

For the delivery of various cargoes, it is important that the transport is not just triggered over the plasma membrane. It is also necessary that the transport vehicle is able to deliver the cargo to its point of action, which could be for example the nucleus. In the third part (**"Specific targeting of nuclei and nucleoli using modified CPPs"**) the CPP sC18* should be combined with the two nuclear localization sequences N50 and NrTP. These fusion peptides should be investigated concerning their translocation efficiency, nuclear localization and toxicity in MCF-7 and HeLa cells. Furthermore, their capability to form complexes with plasmid DNA and the followed transfection ability should be elucidated, as well as the non-covalently conjugation of an anticancer drug and its delivery into cancer cells.

3. MATERIALS AND METHODS

3.1 Materials

3.1.1 Chemicals

All chemicals, reagents and consumables used in this work were purchased from Alfa Aesar (Karlsruhe, Germany), Applichem (Darmstadt, Germany), Fluka (Taufkirchen, Germany), Merck (Darmstadt, Germany), Roth (Karlsruhe, Germany) Sarstedt (Nürmbrecht, Germany), Sigma-Aldrich (Taufkirchen, Germany) and VWR (Darmstadt, Germany), if not specified otherwise. N^{α}-Fmoc protected amino acids were obtained from IRIS Biotech (Marktredwitz, Germany).

3.1.2 Instrumentations

Balances	Analytical balance FA-210-4, Faust
	Laboratory balance SBA52, Scaltec
CD spectrometer	Jasco Corp. J715
Cell culture clean bench	Heraeus Herasafe HS12
Centrifuges	Multifuge X1R, Thermo Scientific
	Pico 17, Thermo Scientific
CO_2-Incubator	BINDER
ESI mass spectrometer	Bruker Esquire HCT
Flow cytometer	Guava easyCyte, Merck
Hemocytometer	Neubauer improved, Superiour Marienfeld, Germany, Depth 0.100 mm, 0.0025 m2
Heating block	Thermomixer compact, Eppendorf
HPLC (analytic)	Hewlett Packard Series 1100, Agilent 1100 Series
	column: Phenomenex Kinetex, 2,6 u, C18, 100A,
	100 x 4,60 mm or Machery Nagel, C18ec Elite Lachrom
	Hitachi Pump L-2130, Elite

HPLC (preparative)	Elite Lachrom Hitachi Pump L-2130, Elite Lachrom Hitachi Autosampler L-2200, Elite Lachrom Hitachi Diode Array Detector L-2455, Teledyne ISCO Fraction Collector Foxy R1, column: Phenomenex Jupiter, 4 u Proteo 90 A, 250 x 15 mm, 4 micron or Machery Nagel, C18ec
LC - mass spectrometer	LC: Hewlett Packard Series 1100 MS: Finnigan MAT – LCQ or MS: Thermo Scientific LTQ-XL
Lyophilizer	Lyovac GT2 with CertomaT SII and a Thermo Savant Refridgerated Vapor Trap RVT5105 or Christ; Alpha 2-4 LDplus
Microscope	Inverted microscope (Motic AE31, Wetzlar) 20x objective (N.A. 0.25)) Confocal laser scanning system (Nikon D-Eclipse C1), inverted microscope (Nikon Eclipse Ti), 60x oil immersion objective (N.A. 1.4, Plan PO VC; Nikon)
Multipette® plus	Eppendorf Research
NanoDrop	NanoDrop™ 1000 Spectrophotometer, Thermo Scientific
PCR Thermal Cycler	FlexCycler analytikjena
Pipetting aid	NeoLab
Pipettes	Eppendorf Research
Plate reader	Tecan infinite M200
Rotary Shaker	KL-2 (Edmund Bühler GmbH)
Spectrophotometer	Thermo Scientific Genesys 10S UV-Vis
Speed-Vac	Thermo Scientific Speedvac Concentrator Savant SC210A, RVT5105 Refrigerated Vapor Trap VLP80 Vacuum Pump
Synthesis robot	MultiSynTech Syro I

Thermomixer compact	Eppendorf
Vacuum pump	VWR
Vortex	Scientific Industries – Vortex Genie 2
Water bath	Julabo SW22
XcelVap™	Horizon Technology

3.1 Methods

3.1.1 Peptide synthesis

All syntheses were performed in open polypropylene reactor vessels (2 ml syringes) stocked with a fritted filter disc. Manual coupling steps were performed under the hood and solvents were removed from the resin using a vacuum pump.

For each synthesis 15 µmol of resin were used and calculated according to the specific resin loading. The mentioned equivalents correlated with the amount 15 µmol per equivalent.

Following to all coupling steps a Kaiser test was performed to examine the presence of free amino groups and the completeness of a coupling. If the test was positive, the coupling step was repeated.

Since carboxyfluorescein is light sensitive, all experiments including CF-coupling, as well as all following steps were executed avoiding light, and all peptides were protected from light by covering with aluminum foil.

The theoretical molecular masses were calculated using the software Peptide Companion, Version 1.25, CoshiSoft/PeptiSearch or the peptide property calculator by Innovagen, 2015.

2.3.1.1 Automated peptide synthesis

For automated peptide synthesis, a multiple Syro I peptide synthesizer from MultiSynTech was used. The software SyroXP is able to calculate the amounts of amino acids that are needed to synthesize the peptides. All amino acids were dissolved in DMF except from phenylalanine that needed to be dissolved in NMP. After filling the reaction vessels with 15 µmol (30 mg) of Fmoc-Rink amide resin beads and starting the software, the robot performs all synthesis steps automatically using the Fmoc/t-Bu strategy. In the first step, the beads were swollen in DMF and the Fmoc protection group was cleaved from the resin using first a 40% piperidine solution in DMF and afterwards a 20% piperidine solution in DMF. After washing the beads four times

with DMF, coupling of the first N^{α}-Fmoc protected amino acid was performed using Oxyma and DIC. The amino acid was introduced in 8-fold excess and every coupling step was performed twice, each for 40 min respectively including four washing steps with DMF in between. Before repeating deprotection and coupling of the next amino acid, the sample was washed another time with DMF. In the last step, the vessels were again incubated with piperidine to cleave off all Fmoc protection groups and washed four times with DMF. After the complete synthesis, the samples were washed with CH_2Cl_2, MeOH and Et_2O manually and the resin beads were dried in the Speedvac.

2.3.1.2 Coupling procedure with Oxyma/DIC

For the manual coupling of amino acids, the resin was swollen for 15 min in 1 ml DMF at RT shaking with 200 rounds/min. After removing the solvent with a vacuum pump, a solution containing the amino acid (7 eq. for general amino acids, 2 eq. for Dde-L-Lys-(Fmoc)-OH) and Oxyma (7 or 2 eq.) in 300 µl DMF and 7 or 2 eq. of DIC was added to the resin, respectively. The solution was incubated for 2 h or o/N at RT and under shaking conditions. After washing the resin five times with DMF, the coupling procedure was repeated. In the end, the solvent was removed, the resin was washed five times with DMF, CH_2Cl_2, MeOH and Et_2O, respectively, and afterwards it was dried for 10 min at low speed in the Speedvac.

2.3.1.3 Kaiser test (after Kaiser *et al*. 1970)

To monitor whether the coupling was successful and all free amino groups were successfully coupled with an amino acid, a protection group or carboxyfluorescein, a Kaiser test was performed on a few resin beads [70]. After transferring some beads into a 1.5 ml reaction vessel, one drop of the solutions I to III (table 2) was added in quick succession.

Table 2: Chemicals used for the Kaiser test.

Solution I	1.0 g ninhydrin in 20 ml EtOH
Solution II	80 g phenol in 20 ml EtOH
Solution III	0.4 ml aq. KCN-solution (1 mM) in 20 ml pyridine

The mixture was incubated at 95 °C for 5 min in a Thermomixer. The test was defined positive, if the solution showed a blue color, indicating free amino groups. If the mixture was yellow, no free amino groups could be detected and the coupling was complete.

2.3.1.4 Cleavage of a Dde protecting group

To cleave the special Dde protecting group, the resin was swollen for 15 min in 1 ml DMF at RT. After removing the solvent, 1 ml of a 3% hydrazine solution in DMF was added to the resin and incubated for 10 min. The solvent was collected in a Falcon tube, the resin was washed twice with DMF and the flow through was harvested in the same Falcon tube. This procedure was performed ten times, collecting just the last phase. The amount of Dde in the first and the last sample was determined by measuring the absorption at 301 nm in a spectrophotometer. A mixture of 2 ml DMF and 1 ml 3% hydrazine served as reference. If the absorption of the last washing step was lower than 0.1, the entire cleavage of the Dde group was successful. If it was higher than 0.1, a few cleavage steps with 3% hydrazine were repeated. Afterwards the resin was washed five times with DMF, CH_2Cl_2, MeOH and Et_2O, respectively, and dried for 10 min at low speed in the Speedvac.

2.3.1.5 Cleavage of an Fmoc protecting group

Before coupling the following amino acid in the coupling procedure, the Fmoc protecting group had to be cleaved off. Therefore, the resin was swollen for 15 min in 1 ml DMF, the solvent was removed and 500 µl of a 30% piperidine solution in DMF was added. The resin was incubated shaking for 20 min at RT and afterwards washed five times with DMF. The procedure was done twice.

2.3.1.6 Coupling of carboxyfluorescein

For the modification of the peptide with the reporter group carboxyfluorescein, the resin was swollen as described previously and after removing the solvent, a solution was added that contained 10 eq. 5(6)-carboxyfluorescein and 10 eq. HATU in 300 µl DMF. Afterwards, 10 eq. DIPEA were pipetted directly to the resin. The syringe was shaken at RT for 2 h. After washing the resin five times with DMF the coupling was repeated o/N using Oxyma and DIC as described above. Thereafter, the resin was washed five times with DMF, CH_2Cl_2, MeOH and Et_2O respectively and dried for 10 min at low speed in the Speedvac. The successful coupling was verified by a Kaiser test.

If the test was negative, a polymer cleavage was performed to avoid CF polymers. Therefore, the resin was swollen in DMF, 1 ml of a 20% piperidine solution in DMF was added and the syringe was incubated shaking for 45 min at RT. In the end, the resin was washed five times with DMF, CH_2Cl_2, MeOH and Et_2O, respectively, and dried for 10 min at low speed in the Speedvac.

2.3.1.7 Coupling of DOTA and NODAGA

The *N*-terminal coupling of the chelators DOTA (1,4,7,10-tetraazacyclododecane-1,4,7,10-tetraacetic acid – Sigma Aldrich) and NODA-Ga(tBu)$_3$ (4-(4,7-bis(2-tert-butoxy-2-oxoethyl)-1,4,7-triazonan-1-yl)-5-tert-butoxy-5-oxopentaoic acid – CheMatech / Dijon, France) was carried out in the same way as described for CF except from using 3 eq. of the substance to be coupled and activating with 3 eq. HATU/DIPEA in DMF under vigorous shaking for 2 h. A double coupling process was not desired.

After full cleavage and preparative HPLC (chapter 2.3.1.9 and 2.3.1.11), a salt exchange was done to eliminate the TFA salts in the peptide solution. Therefore, the lyophilized CPPs were dissolved in 5 ml of 80 mM HCl solution and incubated at RT shaking for 1 h. After freezing the sample for 30 min at - 80 °C, it was dried o/N by lyophilisation. The procedure was repeated two to four times, until no TFA adducts could be detected via analytical ESI-MS spectrometry anymore.

2.3.1.8 Sample cleavage

A sample cleavage was done to ensure that the manual coupling of amino acids, CF or chelator and the synthesis of the robot was successful. Some dry beads of the resin were transferred to a 1.5 ml tube and 2.5 µl of the scavenger triisopropylsilane mixed with 2.5 µl H_2O_{dd} was added. After the addition of 95 µl TFA using a multipette, the syringe was incubated at RT shaking for 3 h. Peptide sequences that contain cysteine, methionine or tryptophan were cleaved from the resin with 7 µl thioanisole, 3 µl 1,2-ethandithiole and 90 µl TFA. The peptide was precipitated in 1 ml of ice-cold diethyl ether and the mixture was incubated for at least 20 min at - 20 °C. The samples were centrifuged at 10,000 x g for 5 min at 4 °C. After removing the supernatant, the pellet was again resuspended in 1 ml ice-cold ether and centrifuged for 5 min at 10,000 x g at 4 °C. This procedure was repeated at least five times until no scavenger smell could be noted anymore. The pellet was then dried for 10 min at low speed in the Speedvac. After resuspending the peptide in 100 µl H_2O or H_2O/^{t}BuOH (3:1 (v/v)) according to the solubility, the sample was centrifuged for 1 min at 10,000 x g to separate the beads from the peptide and the supernatant was analyzed via HPLC/ESI-MS (chapter 2.3.1.10).

2.3.1.9 Full cleavage

To cleave the peptides from the resin, a full cleavage was performed. A mixture of 25 µl of the scavenger triisopropylsilane and 25 µl H_2O_{dd} was added to the resin. After the addition of 950 µl TFA using a multipette, the syringe was incubated at RT shaking for 3 h. Peptide sequences that contain cysteine, methionine or tryptophan were cleaved from the resin with 70 µl

thioanisole, 30 µl 1,2-ethandithiole and 900 µl TFA. To precipitate the peptide, the solvent was pressed through the fritted disc in a 15 ml Falcon tube containing 10 ml of ice-cold diethyl ether. Furthermore, 200 µl of TFA were added to the resin and also harvested in the tube. After incubation for at least 20 min at - 20 °C to allow precipitation of the peptide, the sample was centrifuged at 5,000 x g for 5 min at 4 °C. The supernatant was removed, the pellet was resuspended in 10 ml ice-cold diethyl ether and the solution was again centrifuged. This procedure was repeated five times until no scavenger smell could be noted anymore. The pellet was then dried for 15 min at low speed in the Speedvac and afterwards resuspended in 2 ml H_2O or H_2O/^{t}BuOH (3:1 (v/v)), respectively. The peptide solution was transferred into a balanced glass vessel and covered with paper. After freezing the sample for 30 min at - 80 °C, it was freeze-dried o/N by lyophilisation. The amount of the peptide could then be detected by weight and after subtraction of the TFA residues that bind to all free NH_2-ends and the side chains of the positively charged amino acids arginine and lysine.

2.3.1.10 Analytical high performance liquid chromatography-electrospray ionization mass spectrometry (HPLC/ESI-MS)

For the identification of the synthesized sequences, a high performance liquid chromatography/electrospray ionization mass spectrometry (HPLC/ESI-MS) method was performed. After sample or full cleavage from the resin, peptides were usually diluted 1:10 with 10% ACN/90% H_2O containing 0.1% trifluoroacetic acid or formic acid, depending on the chosen method. Generally, the peptides were separated on the column with a flow rate of 6 ml/min via an increasing linear gradient from 10 – 60% ACN in H_2O (inclusive 0.1% TFA or FA). After the HPLC, the sample passed the electrospray ionization source, whereby ions were generated and their m/z ratios were determined.

2.3.1.11 Preparative reverse phase high performance liquid chromatography (RP-HPLC)

After lyophilisation, the dry peptide, but not more than 30 mg, was dissolved in 960 µl of ACN/H_2O (incl. 0.1% TFA) according to the initial ratio of gradient and centrifuged in a 1.5 ml tube for some seconds to separate the sample from possible debris. The supernatant was transferred to a bellied HPLC glass vessel.

The purification of the peptide was done with a preparative HPLC and the software EZChromElite. First, the column was equilibrated with ACN/H_2O (incl. 0.1% TFA) according to the start gradient. Afterwards, the concentration of ACN was increased gradually and the peptide containing fractions were collected. The solvent was removed via evaporation in the XcelVap at 65 °C using a gradient of 880 – 1640 mbar twice for 30 min, respectively.

Afterwards, 15 µl were taken for the analytical HPLC and the rest was transferred to balanced glass vessels and covered with paper. After freezing the samples for 30 min at - 80 °C, they were freeze-dried by lyophilisation o/N.

According to the weight and the purity, the dried peptides were dissolved in H_2O_{dd} to a concentration of 1 mM regarding the accumulation of TFA on every arginine, lysine and free NH_2-group at the terminal end.

2.3.2 CD spectroscopy

For the structural characterization of the synthesized peptides, circular dichroism spectra were recorded. The cell-penetrating peptides were analyzed in 10 mM potassium phosphate buffer (pH 7.0) with and without TFE (1:1 dilution), respectively. Therefore, 20 µM peptide solutions in the two different buffers were measured in 3 accumulations in the CD spectrometer according to the apparatus instructions. The peptides were measured in a 0.1 cm quartz cuvette with a sensitivity of 100 mdeg in the range from 260 to 180 nm in 0.5 nm intervals. The scanning mode was continuous and a scanning speed of 50 nm/min was chosen. The results of pure buffer were subtracted from the spectra of the peptides. The ratio between the molar ellipticity at 222 nm and 207 nm is a good indicator to confirm an α-helical structure of peptides. For α-helices, these R-values should be around a value of one. [71]

2.3.3 Cell culture methods

All cell culture work was done in sterile conditions under the sterile hood wearing disinfected gloves. All working materials that were transferred under the hood were disinfected with 70% EtOH before using. Autoclaved pipette tips and sterile serological pipettes were used for the cell culture work. A vacuum pump was utilized to remove media during washing or splitting steps.

All cell lines were grown in sterile culture dishes (diameter 10 cm) in a CO_2-Incubator (5% CO_2) at 37 °C. The cell line HEK-293 was grown in MEM containing 15% Fetal Bovine Serum (FBS) and 4 mM L-Gln. The cell lines HeLa, HCT-15 and MCF-7 were grown in RPMI-1640 medium containing 10% FBS and 4 mM L-Gln. For PC-3 cells, DMEM F-12 Ham's medium was completed with 4 mM L-Gln and 5% FBS. HaCaT cells were grown in high glucose DMEM supplemented with 2 mM L-Gln and 10% FBS. Each medium was also prepared without FBS.

2.3.3.1 Mycoplasma testing

All used cell lines were tested at least once a year but anywhere after taking new cell lines in culture using the PCR Mycoplasma Test Kit II and the *Superhot Taq* DNA Polymerase provided

by Applichem following the manufacture´s protocol. After the polymerase chain reaction using the supernatant of centrifuged consumed medium of cells, 6x loading dye was added to the samples which were then loaded on a 1.5% agarose gel stained with GelRed™ (Biotium, USA) in Tris Acetate-EDTA (TAE) buffer and electrophoresed for 40 min at 100 V.

2.3.3.2 Splitting and seeding cells

For trypsinization of the cells, the cell layer was washed twice with 4 ml of phosphate buffered saline (PBS). To detach the cells from the surface and from each other, 1 ml of Trypsin-EDTA solution was added and incubated for 3 – 15 min at 37 °C, depending on the cell line. Detachment of cells was checked microscopically in bright-field mode with a 20x objective (N.A. 0.25)). Cells were then resuspended and mixed with 9 ml of medium containing serum to inhibit trypsin activity.

To split the cells, they were transferred to new culture dishes and mixed with new medium depending on the splitting ratio. Cells were grown in approximately 10 ml fresh medium. The number of passages was mentioned on each plate, HEK-293 cells were not used above the 30^{th} passage and HeLa, HCT-15, MCF-7 and PC-3 cells not above the 40^{th} passage. HaCaT cells could be used until passage number 100.

For seeding a defined number of cells, a hemocytometer was used for cell counting. Therefore, 10 µl of the cell suspension was pipetted between the hemocytometer and the cover slip. The cells in 4 squares (volume of each 1×10^{-4} ml) were counted under the microscope, divided by 4 to get the average number of one square, and multiplied with 10^4 to get the number of cells per ml. The determined concentration was used to calculate the needed volumes to seed the requested amount of cells.

2.3.3.3 Freezing and thawing cells

To freeze cells, they were trypsinized and after adding medium to inhibit trypsin activity, they were centrifuged for 5 min at 300 x g. After removing the supernatant, the cell pellet was resuspended in 1.5 ml freezing medium (requested medium containing FBS and Gln and 10% sterile filtered DMSO), transferred to a freezing tube and cooled down at 4 °C for 15 min. Afterwards, the tubes were stored at - 20 °C for 2 – 4 h and then incubated o/N at - 80 °C. The next day, the tubes were transferred into liquid nitrogen.

To thaw cells, the freezing tubes were taken from liquid nitrogen and put on ice. The solution was thawed at 37 °C in the water bath and directly transferred to a culture dish containing the required medium. After incubation in the CO_2-Incubator (5% CO_2) at 37 °C for 24 h, dead cells and rests of DMSO were removed by washing the cell layer twice with PBS before adding new

medium. HaCaT cells were centrifuged and the cell pellet was resuspended in fresh medium before transferring them into TC Flask T75, Cell+ from Sarstedt. After satisfying growth, cells were transferred in usual culture dishes.

2.3.4 Cell viability assay based on resazurin

To detect the relative cell viability after treatment with the CPPs in various concentrations, a cytotoxicity assay was performed. The first day, a total volume of 200 µl of cells (HEK-293 $7*10^4$, HeLa, PC-3 and HaCaT $4*10^4$, MCF-7 and HCT-15 $5*10^4$ cells per well) were seeded in 96-well plates.

After approximately 24 h of incubation at 37 °C, when the cells reached a confluency about 80%, the medium was removed and the peptide or substance solutions diluted in serum-free medium were added in a total volume of 100 µl to the cells. In the wells that served as positive and negative controls, the medium was replaced by fresh medium missing FBS. The plates were incubated for 24 h or 48 h at 37 °C.

Afterwards, the positive control was treated with 100 µl of 70% EtOH for 10 min. In the meantime, the other wells were washed with PBS as well as the positive control in the end. To start the reaction, cells were covered with 100 µl of a 10% resazurin solution in medium without FBS and incubated for 1 – 2 h at 37 °C. Afterwards, the fluorescent product of the reaction, namely resorufin was quantified by measuring the fluorescence with the Tecan infinite M200 plate reader (Excitation: 550 nm, Emission: 595 nm).

To achieve comparably results, the positive control was in most of the cases subtracted from all data and the negative control was set to 100%, so that the results of the peptide treated cells represent relative cell viability values in %.

2.3.5 Cell lysis assay based on LDH release

The CytoTox-ONE™ Homogenous Membrane Integrity Assay from Promega was performed to detect disrupted cell membranes. Thereby, the released lactate dehydrogenase from permeabilised cells can be monitored. The first day, a total volume of 200 µl of cells (HEK-293 $7*10^4$, HeLa and PC-3 $4*10^4$, MCF-7 and HCT-15 $5*10^4$ cells per well) were seeded in 96-well plates. The next day, the wells, except for the ones of the positive and negative control, were treated with the peptide or substance solutions in medium without FBS for 1 h at 37 °C. After the plate was brought to room temperature, 2 µl of lysis solution from the Kit were added to the positive control. The CytoTox-ONE™ reagent was prepared as described in the protocol and 100 µl were added to each well. The cells were incubated at RT for 10 min before stopping the reaction with 50 µl of stop solution also provided with the kit. The release of LDH was

monitored via measuring the fluorescence using the plate reader Tecan infinite M200 (Excitation: 560 nm, Emission: 590 nm).

The results are shown in relative cell lysis compared to the average value of the positive control, which was set to 100%, after subtraction of the fluorescent intensity of the negative control, which represents the background LDH release.

2.3.6 Microscopy

For microscopic analyses, a confocal laser scanning system (Nikon D-Eclipse C1) with an inverted microscope (Nikon Eclipse Ti) was used. The pictures were taken with the 60x oil immersion objective (N.A. 1.4, Plan APO VC; Nikon) and the software EZ-C1 3.91 from Nikon.

The cells were seeded in 350 µl medium in an 8-well ibidi plate (HEK-293 $1.2*10^5$, HeLa $4.5*10^4$, MCF-7 $7*10^4$, HCT-15 $2*10^5$, PC-3 $8*10^4$, HaCaT $1.2*10^5$ cells per well) and were grown to 70 – 80% confluency. The next day, the medium was removed and the cells were treated with the peptides and substances in various concentrations for the requested time periods. The cells were incubated at 4 °C or 37 °C and 10 min prior to the end of incubation 0.6 µl of Hoechst stain (bisbenzimide H33342, 1 mg/ml in H_2O, sterile filtered) was added to each well to stain the cell nuclei. After removing the solutions, the cells were quenched with 200 µl of 150 µM trypan blue solution (in acetate buffer) for 30 s. The stain was removed and the cells were washed twice with medium. After adding 300 µl of fresh medium, pictures were taken under the microscope with pinhole S, Offset green: 100, blue: 38, red: 0 and various gain values. The gains for the blue and red channel were individually chosen due to the fact, that the staining was different depending on the mixing after addition of Hoechst, Lysotracker or ER-tracker and the cell density. The images were edited in Image J 1.43m.

2.3.7 Flow cytometry

For flow cytometric analyses, cells were seeded the day before (HEK-293 $5*10^5$, HeLa $1.7*10^5$ and MCF-7 $2*10^5$ cells per well) in 24-well plates and grown to 70 – 80% confluency o/N. Then, the cells were treated with 400 µl of peptide or substance solutions dissolved in serum-free medium for the appropriate time at 4 °C or 37 °C. Afterwards, the cells were washed twice with PBS and detached using 200 µl of Trypsin-EDTA 1X in PBS without phenol red for 3 – 5 min followed by adding 800 µl of indicator-free medium. The cells were resuspended and 200 µl of the suspension were transferred to a 96-well plate for measuring the fluorescence in the guava easy cyte flow cytometer. In each sample, 10’000 cells were measured and each experiment was done in triplicate. Cells treated with medium only served as negative control and their fluorescent signal was subtracted from all other samples in each set of experiment.

2.3.8 Radiolabeling of the NODAGA-coupled peptides and uptake experiments

The following experiments were done in cooperation with Sergio Muños Vázquez and Beate Zimmermanns in the working group of Prof. Dr. Klaus Schomäcker in the Department of Nuclear Medicine, University of Cologne.

The radioisotope [^{68}Ga]Ga^{3+} was eluted in 0.05 M ultrapure HCl from a ^{68}Ga/^{68}Ga generator (Isotope Technologies Garching GmbH). For the labeling of [^{68}Ga]Ga-NODAGA-sC18, a stock solution was prepared with 1 mg of peptide dissolved in 1235 ml of ultrapure water; 30 ml of a stock solution (10 nmol) was mixed with 15 ml of 2 M sodium acetate buffer; 200 ml of the eluted ^{68}Ga (50 – 70 MBq) was added to the reaction vial resulting in a solution at pH 4.5. For the labeling of [^{68}Ga]Ga-NODAGA-(sC18)$_2$, a stock solution was prepared with 2 mg of peptide dissolved in 1339 ml of ultrapure water; 30 ml of a stock solution (10 nmol) was mixed with 15 ml of 2 M sodium acetate buffer; 200 ml of the eluted [^{68}Ga]Ga^{3+} (50 – 70 MBq) was added to the reaction vial resulting in a solution at pH 4.5. The labeling mixture was incubated for 30 min at RT, respectively. The radiochemical yield was determined by HPLC, which was performed with Azura ASM 2.1L equipped with two P4.1S pumps with pressure transducer and 10 ml titanium pump head, a degasser DG 2.1S 2-channels, a Smartmix 350 mixer and a manual 6-port/3-channel injection valve with a sample loop of 20 ml. The compounds were analyzed by a Nucleodur C18 Gravity, 250 mm x 4 mm, 5 mm column and a linear A – B gradient (80% A to 70% A in 15 min) at a flow rate of 1 ml/min. Solvent A consisted of H_2O containing 0.1% TFA, and solvent B was ACN with 0.1% TFA. The compounds were analyzed by a UV detector UVD2.1L (λ = 254 nm) and the radioactive ones were determined by a radioactivity counter STEFFI Raytest. The peak analyses were done by OpenLAB CDS EZChrom edition version A.04.05.

For uptake studies, HEK-293 and MCF-7 cells were seeded in 24-well plates. The next day, when they were grown up to 80% confluency, the peptides were added to the cells in serum-free medium and incubated for 30 min. Afterwards, the cells were washed twice with PBS and detached with trypsin-EDTA. The cells were centrifuged and the radioactivity in the cell pellet was determined in a gamma spectrometer (LB2045 Berthold technologies).

2.3.9 Plasmid transformation in *E.coli* and plasmid isolation

For plasmid transformation, competent *Escherichia coli* DH5α cells, produced with the $CaCl_2$ method [72], were kindly provided by Annika Klimpel. An aliquot of competent cells was thawed on ice and gently mixed with 0.5 µl of vector DNA (pEGFP-N1 or pGL4.13). After an incubation of 30 min on ice, the cells were heat shocked at 42 °C for 45 s and incubated for another 2 min

on ice. Thereafter, 500 µl of LB-medium (25 g Luria/Miller in 1 l H_2O_{dd}) without antibiotics were added and shaken for 45 min at 37 °C. 50 µl of the solution were plated on an LB agar plate with the appropriate antibiotic (100 µg/ml ampicillin) and incubated o/N until colonies are grown. The next day, colonies were picked using sterile pipette tips and transferred to 3 ml of LB-medium containing ampicillin. The cultures were incubated under vigorous shaking o/N and thereafter, the PureYield™ Plasmid Miniprep System from Promega was used following the manufacture´s protocol to isolate the plasmid. The vector concentration was determined with a NanoDrop and the plasmids were stored at - 20 °C.

2.3.10 Electrophoretic mobility shift assay

An electrophoretic mobility shift assay (EMSA) was performed to examine if the positively charged CPPs are able to form complexes with negatively charged plasmid DNA, namely the vectors pEGFP-N1 and pGL4.13. The peptides were incubated with the plasmid DNA in various charge ratios (1:1, 5:1, 10:1 and 30:1) for 30 min in 37 °C warm nuclease free water at RT in a total volume of 40 µl. Afterwards, the solution was supplemented with 8 µl 6x loading dye and around 30 µl were loaded on a 1% agarose gel in TAE-buffer (Tris-acetate-EDTA) stained with GelRed™ (Biotium, USA). The DNA was electrophoresed for around 30 min at 100 V and the gel was then observed in a gel documentation system. Naked plasmid DNA was used as negative control.

2.3.11 Examination of transfection with pEGFP-N1 plasmid

For transfection with the enhanced green fluorescent protein encoding plasmid pEGFP-N1, cells were seeded in an 8-well ibidi plate (HeLa $4.5*10^4$, MCF-7 $7*10^4$ cells per well) and grown to 70 – 80% confluency. Then, the CPPs N50-sC18* or NrTP-sC18* were complexed with the pEGFP-N1 vector in 50 µl nuclease free water as described before (2.3.10), the solution was filled up with 250 µl medium without FBS and added to the cells. Additionally, in one set of experiments, 100 µM chloroquine was added to the complexation solution. The plasmid itself served as negative control, cells treated with plasmid and Lipofectamine®2000 transfection reagent (ThermoFisher scientific), that were complexed for 5 min, were used as positive control. After 6 h incubation, the solution was replaced by fresh serum-free medium. 48 h later, the nuclei were stained with Hoechst and the cells were observed under the microscope.

2.3.12 Examination of transfection with pGL4.13 plasmid

For transfection with the luciferase encoding plasmid pGL4.13 [luc2/SV40], cells were seeded in 96-well plates (HeLa $4*10^4$, MCF-7 $5*10^4$ cells per well). The next day, the CPPs N50-sC18* or NrTP-sC18* were complexed with the pGL4.13 [luc2/SV40] vector in 100 µl medium without

FBS as described before (2.3.10) and added to the cells. Additionally, in one set of experiments, 100 µM chloroquine was added to the complexation solution. Plasmid alone served as negative control, cells treated with plasmid and Lipofectamine®2000 transfection reagent (ThermoFisher scientific), that were complexed for 5 min, were used as positive control. After 6 h incubation, the solution was replaced by fresh serum-free medium and the cells were incubated for 48 h at 37 °C. Afterwards, the luciferase activity was determined using the ONE-Glo™ Luciferase Assay System by Promega. The solution was brought to RT and 100 µl were added to each well without removing the medium, respectively. After 3 min of incubation at RT, the solutions were transferred to white 96-well polystyrol plates with clear bottoms and the luminescence was measured in the Tecan infinite M200.

2.3.13 Cargo delivery of actinomycin D or doxorubicin

For cargo delivery studies using the drugs actinomycin D or doxorubicin, cells were seeded in 96-well plates (HeLa $4*10^4$, MCF-7 $5*10^4$ cells per well). The day after, the drug alone or co-incubated with the respective peptides in various concentrations were added in 100 µl to the cells and incubated for 24 or 48 h. Afterwards, a resazurin based cell viability assay was performed as described previously (2.3.4).

4 RESULTS AND DISCUSSION

4.1 Linear and branched dimeric versions of sC18

Previous studies have shown that the dimerization and branching of the cell-penetrating peptide sC18 led to higher uptake rates and membrane disrupting properties. In addition, the dimeric sequence $(sC18)_2$ seemed to have a certain selectivity for cancer cells, as demonstrated by the different internalization patterns between cancerous versus non-cancerous cells. [Gronewold, master thesis 2014] [20]

The branched variant $(sC18)_2$ represents just one of many examples of structures derived from the CPP sC18. In other experiments, it was observed that a shorter variant of sC18 lacking the four *C*-terminal amino acids Ile-Lys-Glu-Lys could improve the formation of the α-helical, amphipathic structure. In this truncated version sC18*, the positively charged face of the helix is not interrupted by glutamic acid as in sC18, as presented in figure 4. The cell-penetrating ability of sC18* could be observed in HEK-293 and MCF-7 cells [73].

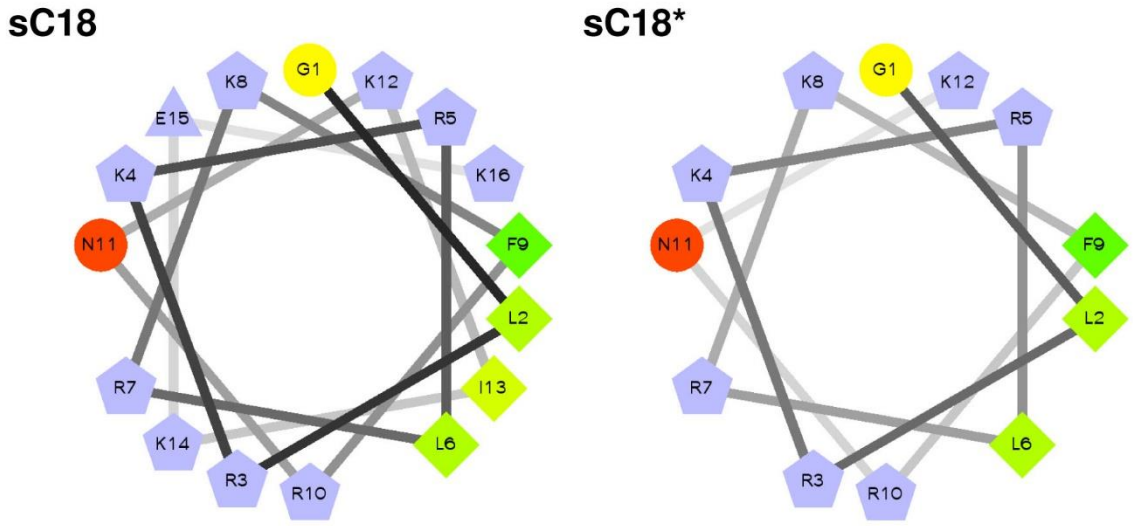

Figure 4: Helical wheel projection of sC18 and sC18*. The projection is showing the hydrophilic (circles), hydrophobic (diamonds), potentially negatively (triangles), and positively charged (pentagons) residues. The most hydrophobic residues are represented in green and the amount of brightness is decreasing proportionally to the hydrophobicity, with zero hydrophobicity coded as yellow. Hydrophilic residues are coded red with pure red being the most hydrophilic (uncharged) residue. The charged residues are light blue. Projection was made with the software created by Don Armstrong and Raphael Zidovetzki. Version: Id: wheel.pl,v 1.4 2009-10-20 21:23:36 don Exp (http://rzlab.ucr.edu/scripts/wheel/wheel.cgi).

Until now, it was not elucidated, if the positive effects of $(sC18)_2$ are a consequence of to the simple dimerization of the sC18 sequence or the branching. To figure this out, a linear version $lin(sC18)_2$ containing two sC18 sequences in line was examined. Furthermore, the truncated sC18* was investigated as well as its dimeric versions $(sC18^*)_2$ and $lin(sC18^*)_2$. All peptides were synthesized via solid-phase peptide synthesis, cleaved from the resin, purified and used for further studies. For localization and uptake studies, CF-labeled sequences were also generated. The successful synthesis of the linear and branched variants was confirmed by HPLC/ESI-MS and in table 3 the calculated and experimentally obtained molecular masses, purities, yields and net charges are shown. All peptide sequences could be synthesized in satisfying purities and yields. Subsequently, the synthesis of a branched variant is exemplarily shown.

Table 3: Calculated and experimentally determined molecular weights, purities and yields of the synthesized sC18 derivatives, unlabeled and labeled with carboxyfluorescein (CF). The peptides $(sC18^*)_2$ and CF-$(sC18^*)_2$ were provided by Dr. Stephanie Natividad-Tietz.

Peptide	Sequence	MW_{calc} [Da]	MW_{exp} [Da]	Net charge	Purity [%]	Yield [%]
sC18	GLRKRLRKFRNKIKEK-NH_2	2069.60	2070.47	+ 9	> 99	~ 36
CF-sC18	CF-GLRKRLRKFRNKIKEK-NH_2	2427.92	2428.89	+ 8	> 98	~ 36
$(sC18)_2$	GLRKRLRKFRNKIKEK-NH_2 | GLRKRLRKFRNKIKEK	4122.16	4122.44	+ 17	> 99	~ 22
CF-$(sC18)_2$	CF-GLRKRLRKFRNKIKEK-NH_2 | GLRKRLRKFRNKIKEK	4480.50	4481.81	+ 16	> 98	~ 30
sC18*	GLRKRLRKFRNK-NH_2	1570.96	1571.36	+ 8	> 99	~ 29
CF-sC18*	CF- GLRKRLRKFRNK-NH_2	1929.28	1929.76	+ 7	> 97	~ 32
$(sC18^*)_2$	GLRKRLRKFRNK-NH_2 | GLRKRLRKFRNK	3124.91	3125.04	+ 15	> 98	~ 43
CF-$(sC18^*)_2$	CF-GLRKRLRKFRNK-NH_2 | GLRKRLRKFRNK	3483.23	3483.30	+ 14	> 97	~ 49
lin$(sC18)_2$	GLRKRLRKFRNKIKEKGLRKRLRKFRNKIKEK-NH_2	4122.16	4122.05	+ 17	> 99	~ 38
CF-lin$(sC18)_2$	CF-GLRKRLRKFRNKIKEKGLRKRLRKFRNKIKEK-NH_2	4480.50	4480.36	+ 16	> 99	~ 39
lin$(sC18^*)_2$	GLRKRLRKFRNKGLRKRLRKFRNK-NH_2	3124.91	3126.10	+ 15	> 99	~ 44
CF-lin$(sC18^*)_2$	CF-GLRKRLRKFRNKGLRKRLRKFRNK-NH_2	3483.23	3482.99	+ 14	> 99	~ 51

The synthesis of $(sC18^*)_2$ was performed by SPPS from the C- to the N-terminus using the Fmoc/tBu-strategy. The synthesis strategy with the single steps is shown in figure 5.

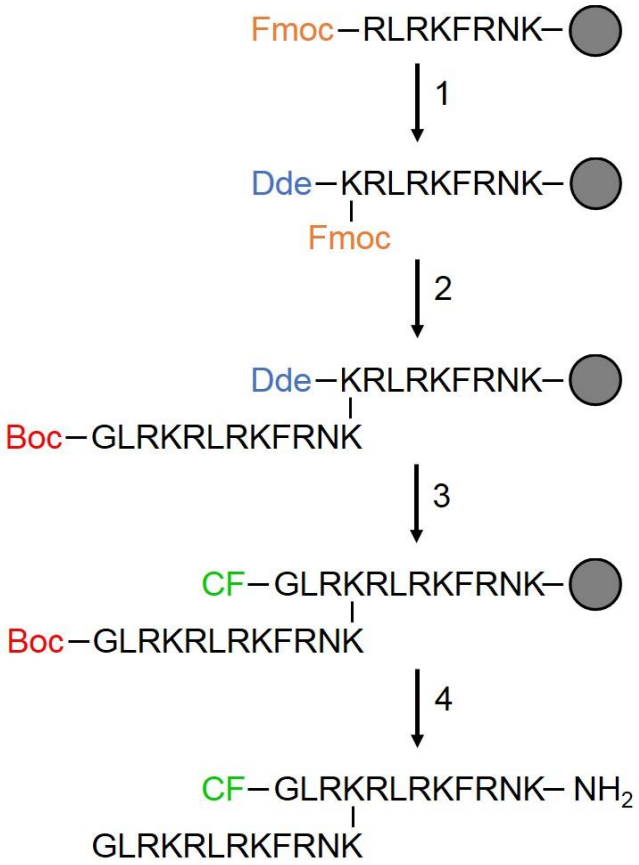

Figure 5: Reaction scheme of the stepwise peptide synthesis of the branched $(sC18^*)_2$. The grey circle represents a rink amide resin bead and the single steps 1 - 4 are explained in the running text.

The sequence RLRKFRNK, anchored to the resin, was automatically synthesized by the robot. After the cleavage of the Fmoc protection group from the arginine at the N-terminus, the amino acid Dde-L-Lys-(Fmoc)-OH was manually coupled. Importantly, the lysine carries a special Dde protection group at the amino group and an Fmoc protection group at the ε-amino group of the side chain (figure 5-1). The peptide was then extended by automatized synthesis with the sequence GLRKRLRKFRNK at the side chain. The glycine at the N-terminus of this second chain was Boc-Gly-OH (figure 5-2). A sample cleavage was performed and analytic HPLC-ESI/MS proved successful synthesis of this fragment (data not shown). In the next step, the three missing amino acids GLR needed to be coupled to the peptide chain. Due to the presence of the Boc-protected glycine, an elongation of this sequence of the peptide was avoided. Instead, the Dde group of the manually bound lysine was cleaved off from the peptide chain using hydrazine and the amino acids GLR were

coupled manually using the activating reagents Oxyma and DIC. After labeling with 5(6)-carboxyfluorescein (figure 5-3), the peptide was cleaved from the resin with TFA. In the end, the product was identified via HPLC/ESI-MS and purified by preparative HPLC. The UV chromatogram and ESI-MS spectra of the purified CF-(sC18*)$_2$ are depicted in figure 6.

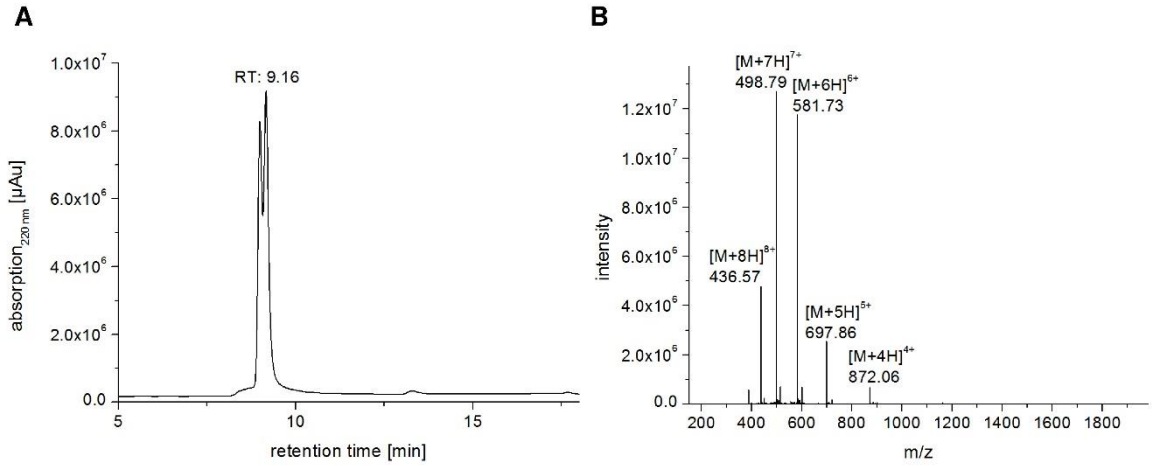

Figure 6: Analysis of CF-(sC18*)$_2$ by HPLC-ESI/MS. UV chromatogram (**A**) and ESI-MS (**B**) from analytic HPLC of (sC18*)$_2$ labeled with carboxyfluorescein after preparative HPLC using a gradient of 10 to 60% acetonitrile in water containing 0.1% TFA. The four-fold to eight-fold charged pseudomolecular ions are marked and comply with the calculated ones ([M+4H]$^{4+}$ = 871.81; [M+5H]$^{5+}$ = 697.65; [M+6H]$^{6+}$ = 581.54; [M+7H]$^{7+}$ = 498.60; [M+8H]$^{8+}$ = 436.40).

The two main peaks in the UV chromatogram in figure 6 correspond to the two isomers of the 5(6)-carboxyfluorescein-labeled peptide. Successful synthesis of the CF-labeled cell-penetrating peptide CF-(sC18*)$_2$ could be confirmed by ESI-MS.

4.1.1 CD spectroscopy of linear and truncated versions

Peptides or proteins that are able to interact with biological membranes of cells or organelles, often contain secondary structures as α-helices or β-sheets [10]. To gain a first insight about the cell-penetrating capability of the sequences, the secondary structure formation was investigated by circular dichroism spectroscopy.

In previous work, it was already shown, that the peptides sC18 and (sC18)$_2$ display a random coil structure when measured in phosphate buffer environment. On the contrary, when the secondary structure inducing solvent trifluoroethanol is present, they exhibit an α-helical structure. [19, 20] Furthermore, it was shown that the fluorophore carboxyfluorescein has no significant influence on the formation of the secondary structure and hence on uptake, activity and properties of CPPs [74]. It is probable, that, like in the

presence of TFE, the peptides also exhibit α-helical structures when interacting with cell membranes. [75, 76]

However, the newly synthesized peptides were measured in the CD spectrometer with a concentration of 20 µM in phosphate buffer (pH 7) with and without TFE, respectively. The spectra are shown in figure 7.

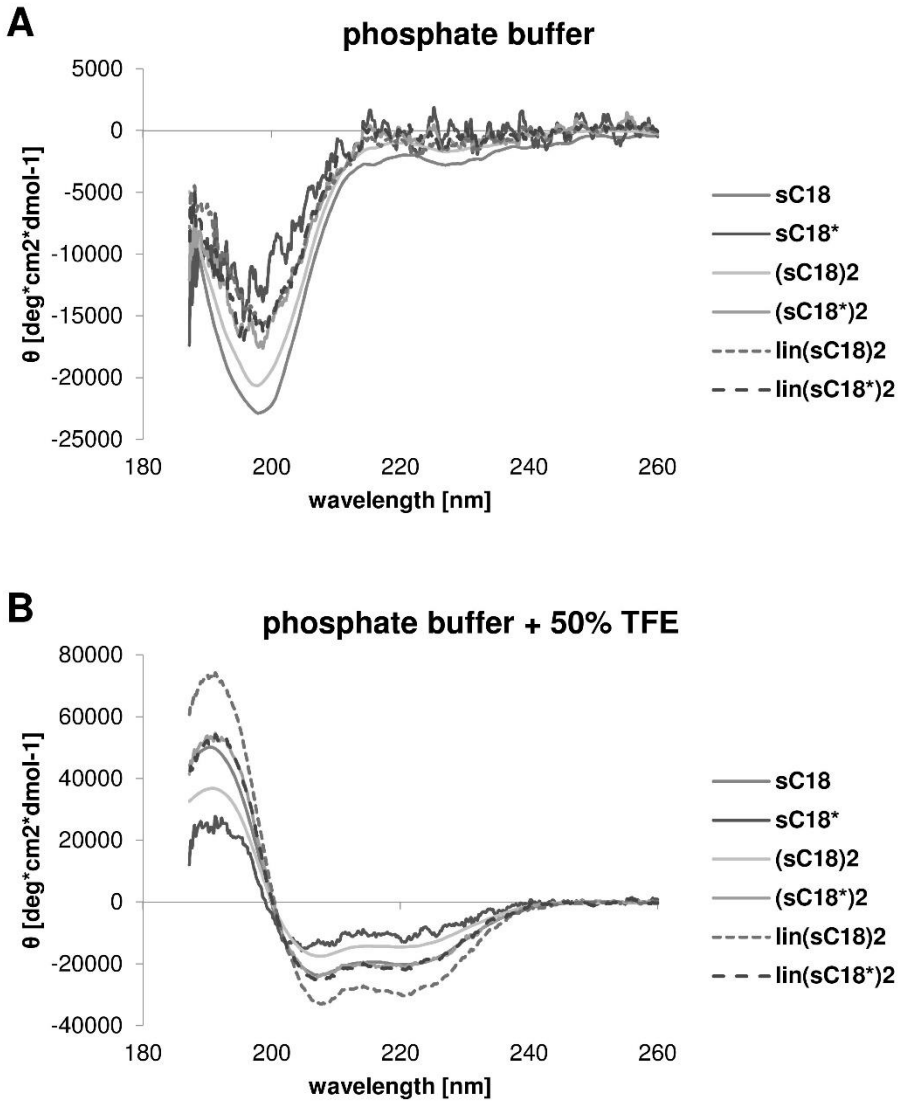

Figure 7: Secondary structure analysis of CPP variants. Circular dichroism spectra of the investigated peptides sC18, sC18*, $(sC18)_2$, $(sC18^*)_2$, $lin(sC18)_2$ and $lin(sC18^*)_2$. Peptides were measured in a concentration of 20 µM in 10 mM phosphate buffer (pH 7) with **(B)** and without **(A)** 50%-trifluoroethanol (TFE) (*n = 1*).

All investigated peptides exhibited a random coil structure in phosphate buffer (figure 7 A), whereby in the presence of trifluoroethanol they all built an α-helical structure, even if the intensities of the amplitudes appeared to be different depending on the structures. The spectrum of sC18* in phosphate buffer with TFE showed a notable lower intensity in the

peak amplitudes, which is maybe due to its shorter sequence. The graphs of the peptides $(sC18^*)_2$ and $lin(sC18^*)_2$ have very similar shapes, probably because of the same amino acid composition. The higher intensities of the amplitudes visible in the spectrum of the $lin(sC18)_2$ can be explained because its sequence is longer than the others. To confirm the formation of α-helices, the R-value, which is calculated by the quotient between the molar ellipticity at 222 nm and 207 nm, can be adduced. Thereby, a perfect formed helix results in the R-value of one. In table 4, the values corresponding to all peptide variants, which were measured in buffer containing TFE, are shown.

Table 4: Calculated R-values [Θ_{222}/ Θ_{207}] of the synthesized peptides in phosphate buffer with 50% TFE.

Peptide	R-value [θ_{222} / θ_{207}]
sC18	0.85
sC18*	0.84
$(sC18)_2$	0.82
$(sC18^*)_2$	0.82
$lin(sC18)_2$	0.89
$lin(sC18^*)_2$	0.84

It can be seen that all values were close to one, supporting the visual determination of α-helices. The values of the linear versions were slightly higher compared to the corresponding branched dimeric versions, which indicated a more regular helix formation. The sequences of the branched variants are interrupted by the peptide bond over the lysine side chain, which is probably resulting in a disruption of the helix. In contrast to that, the linear versions can probably form a continuous helix.

Anyway, it can be concluded, that neither the dimerization, nor the branching of sC18 and sC18* disturbs the formation of helices and therefore, all peptides should be theoretically able to interact with biological membranes.

4.1.2 Uptake studies using different sC18 variants

Next, the internalization of the branched and linear dimeric versions of sC18 and sC18* were examined. Recently, studies using sC18 and $(sC18)_2$ were published, indicating a difference in the uptake and localization in the non-cancer cell line HEK-293 and the breast cancer cell line MCF-7 [77]. Hence, these two cell lines were chosen to get an overview about the uptake and localization of the new variants. After incubating the cells for 30 min

with 10 µM of the peptides, the external fluorescence was quenched and the cells were observed under the fluorescence microscope, as shown in figure 8.

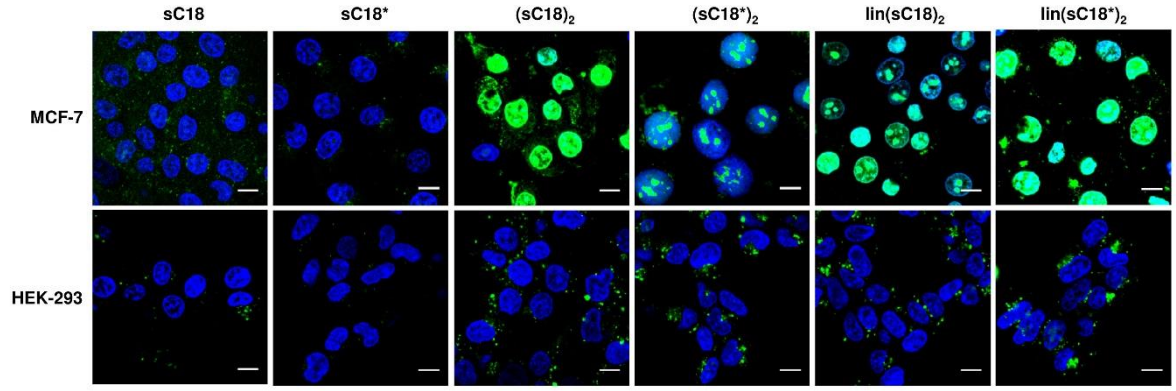

Figure 8: Uptake of CPP variants in MCF-7 and HEK-293 cells. Fluorescence microscopy images after 30 min incubation with 10 µM CF-sC18, CF-sC18*, CF-$(sC18)_2$, CF-$(sC18^*)_2$, CF-lin$(sC18)_2$ and CF-lin$(sC18^*)_2$. Blue: Hoechst nuclear stain, Green: carboxyfluorescein-labeled peptides, external fluorescence was quenched with trypan blue for 30 s, Scale bars are 10 µm.

Notably, all peptides seemed to have cell-penetrating properties and they seemed to behave differently in their uptake mechanisms and intracellular distribution depending on the tested cell line. All CPPs showed apparently higher internalization into the cancer cell line MCF-7 than into the non-cancer cells. To be more precise, in HEK-293 cells, the peptides presumably internalized by endocytosis, accumulating in vesicles, which could be detected by the punctual distribution within the cytoplasm. Furthermore, they were not present in the nucleus, which is a consequence of the fact that the peptides were probably hold in the endosomes and could thereby not enter the nuclei. Comparing the patterns of the different CPPs, it seemed that the internalization of sC18* is not that efficient as the uptake of the longer, parent peptide sC18. Florian Reichart showed in his dissertation by microscopy and flow cytometry experiments with 10 µM peptides, that the uptake of the truncated version is similar to the uptake of sC18 in HEK-293 cells, while in MCF-7 cells the internalization is reduced for sC18* compared to the longer sC18 [Reichart, Dissertation 2015]. The uptake rates and intracellular distribution of the four dimeric variants were higher compared to the sC18 but within these CPPs, no obvious difference could be registered.

In contrast, for MCF-7 cells, it can be seen that the uptake for all peptides probably occurred via direct penetration and endocytosis with a subsequent endosomal release, as the CPPs accumulated within the cytoplasm as well as within the nucleus. This can just occur, when the peptides are free in the cytoplasm and not trapped in endosomes. In detail, looking at the differences between the peptides, one can see that the internalization rates of sC18*

are reduced compared to the longer sC18 peptide. As already pointed out for HEK-293 cells, the internalization rates of the dimeric, branched and linear versions, respectively, are much higher in comparison to the monomeric CPPs. For all variants, a strong accumulation within the nuclei could be noticed as shown in figure 8 and no significant differences between the internalization patterns could be seen. For instance, the cells treated with $(sC18^*)_2$ did not look very healthy and may have suffered from the incubation with the peptides. Therefore, it was investigated if the incubation of the peptides has an influence on the cell viability of the cells.

4.1.3 Cytotoxicity profile of linear and truncated versions

To get more insights about the influence of the peptides on cell viability and selectivity, two different cytotoxicity tests were performed with MCF-7 and HEK-293 cells.

With the cell viability assay based on resazurin the viable cell number was monitored after incubation with the CPPs in different concentrations and compared to untreated cells. Therefore, cells were exposed to the non-labeled peptides in various concentrations for 24 h and were afterwards treated with the cell permeable redox indicator resazurin. The viable cells with active metabolism were able to reduce resazurin into the fluorescent substance resorufin, which was detected using a Tecan reader at a defined wavelength. [78] Treatment with 70% EtOH served as positive control and untreated cells were measured as negative control. The results are shown in figure 9.

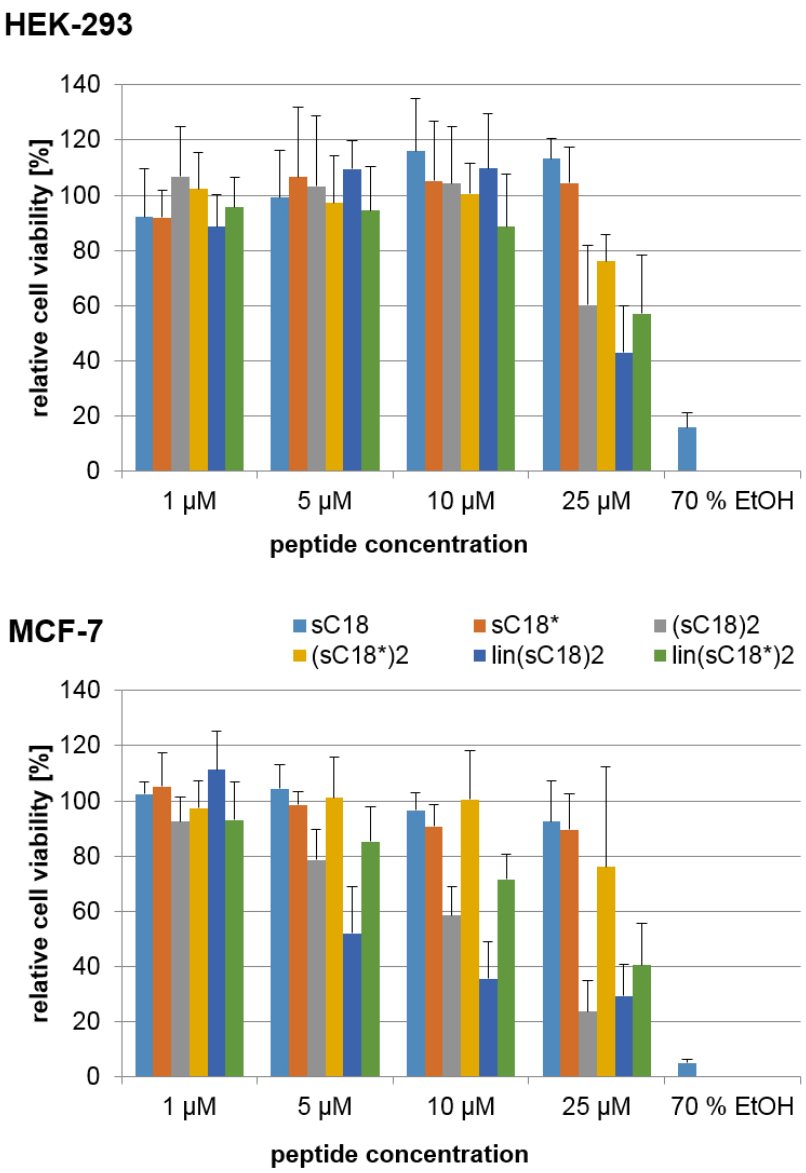

Figure 9: Cytotoxic profile of CPP variants on HEK-293 and MCF-7 cells. Cell viability of truncated, linear and branched variants, namely sC18, sC18*, $(sC18)_2$, $(sC18^*)_2$, lin$(sC18)_2$ and lin$(sC18^*)_2$ after incubation for 24 h with the CPPs in different concentrations, untreated cells served as negative control and were set to 100%. 70% EtOH was used as positive control. Experiments were conducted in triplicate with *n = 2* (HEK-293) or *n = 3* (MCF-7). Error bars represent the standard deviations.

In general, it could be observed that all peptides were slightly more toxic to the cancer cell line MCF-7 than to the embryonic kidney cells. The peptides demonstrated no toxic effects on HEK-293 cells up to a concentration of 10 µM, whereas in MCF-7 cells, a certain toxicity at 5 µM could be detected in some cases. In detail, the short sequences sC18 and sC18* were not toxic to both cell lines and showed a very similar profile. Regarding the two branched variants $(sC18)_2$ and $(sC18^*)_2$ in HEK-293 cells, also no difference could be noticed. In contrast, looking at the results in the cancer cells, the truncated version $(sC18^*)_2$

was less toxic compared to the longer version $(sC18)_2$. This could be explained by the missing amino acids (IKEK in both chains, respectively) in the truncated version. Maybe, $(sC18)_2$ can better interact with the plasma membrane of MCF-7 and therefore induce a higher cytotoxicity. Coming to answer the main question, which was, if the linear forms behave the same as the branched variants, the observation of the results in figure 9 showed that the linear derivatives are minimally more toxic to MCF-7 cells, whereby for the HEK-293 cells, no difference could be detected. This could be proven by comparing the $lin(sC18)_2$ with the $(sC18)_2$ as well as the $lin(sC18^*)_2$ with the $(sC18^*)_2$, forming the idea that the interruption of the two sC18 or sC18* sequences by branching leads to a reduction of cytotoxicity. The cytotoxic profiles of sC18 and $(sC18)_2$ are in agreement with published results [77].

To get a better insight into the behavior of the CPPs on the cell membrane, another cytotoxicity assay was performed. The LDH assay is a test to estimate if substances permeabilize cell membranes. Lactate dehydrogenase leaks from the cytoplasm through the damaged cell membrane into the environmental medium. LDH converts lactate to pyruvate in the surrounding whereby the present resazurin is reduced to resorufin. This fluorescent substance can again be detected using the Tecan reader. [79] First, cells were treated with the different peptides in various concentrations for 1 h and afterwards incubated for 10 min with a mixture containing all needed substances for the reaction explained above. A lysis solution provided with the Kit served as positive control and was set to 100% cell lysis; the results of untreated cells served as negative control. The test was performed in triplicates and the average values are shown in figure 10 for HEK-293 and MCF-7 cells.

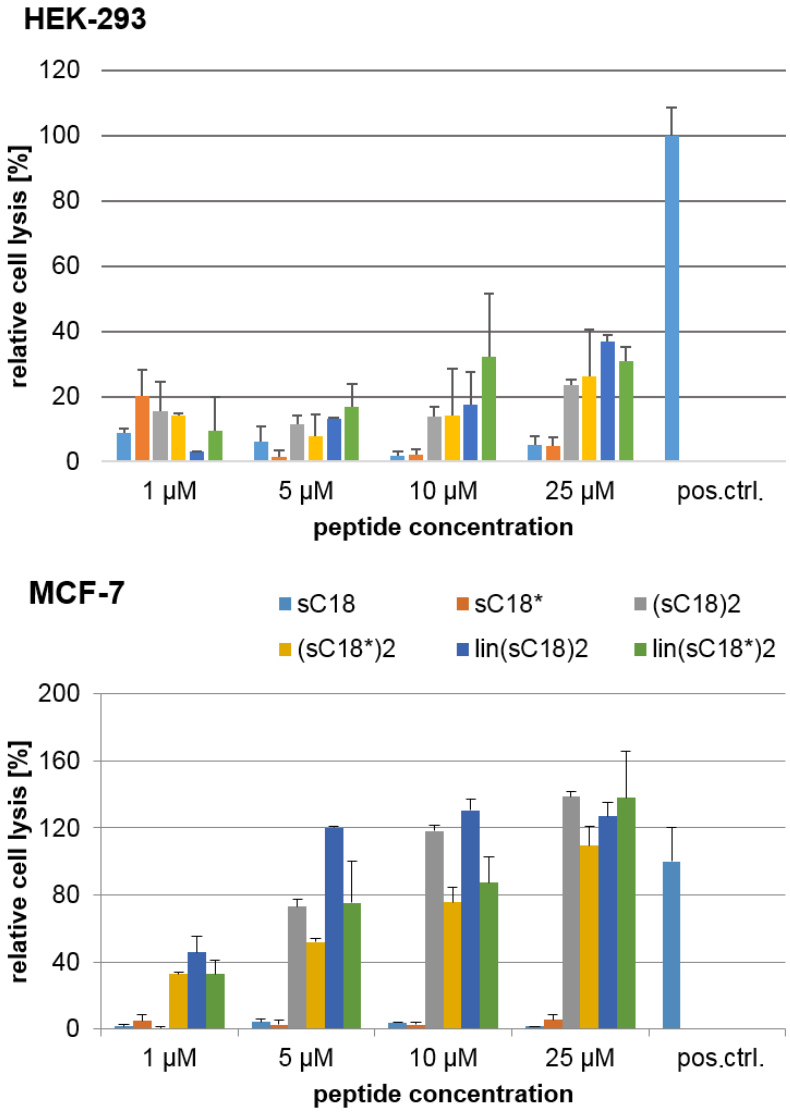

Figure 10: Membrane disruption of CPP variants on HEK-293 and MCF-7 cells. Cell lysis assay based on lactate dehydrogenase release after 1 h incubation with the CPPs sC18, sC18*, $(sC18)_2$, $(sC18^*)_2$, lin$(sC18)_2$ and lin$(sC18^*)_2$ in different concentrations. Cells treated with lysis solution served as positive control and were set to 100%, untreated cells were used as negative control and were subtracted from each result. Experiments were conducted in triplicate with $n = 1$. Error bars represent the standard deviations.

As shown in figure 10, already at low concentrations the peptides induced cell lysis in MCF-7, which is quite opposite to the treatment of HEK-293 cells, whereby just some CPPs induce a slight cell lysis at higher concentrations. In detail, it can be concluded that the monomeric peptides sC18 and sC18* do not permeabilize the cell membranes of both cell lines. This is in consistence with previously published results [77]. For the embryonic kidney cells, a significant cell lysis was visible for the branched and linear peptides at a concentration of 25 µM, whereas about 20 to 30% of the cells were lysed. On the contrary, the cell lysis pattern seemed to be completely different looking at the cancer cell line MCF-7.

Here, the $(sC18)_2$ started to lyse the cells at a concentration of 5 µM, whereas already 80% of the cells were permeabilized. At higher concentrations, the cell lysis rate even exceeded the ones of the positive control. As already shown in the resazurin based toxicity assay (figure 9), the shorter variant $(sC18^*)_2$ was a bit less toxic to the cells and their number of lysed cells was always a bit smaller compared to the ones of the longer parent peptide. Especially for 5 and 10 µM, it can be noticed that the cell lysis by the linear versions was triggered in higher extent, but this result was not significant except for 5 µM. It could be shown that the peptides $(sC18)_2$, $(sC18^*)_2$, $lin(sC18)_2$ and $lin(sC18^*)_2$ have a certain cell selectivity, because they all harmed the plasma membranes of the breast cancer cells, which could not be shown for HEK-293. Apart from that, the monomeric short variants sC18 and sC18* do not have an effect on cell lysis. The membrane lysing activity of sC18 and $(sC18)_2$ is in correlation with published results [77].

4.1.4 Membrane interaction studies

The internalization and toxicity studies of the peptide variants showed differences between cancer and non-cancer cells. Considering the fact that the first interaction of the peptides with the cells is directly correlated to the composition, charge and fluidity of the cell membrane, which are different in cancer and non-cancer cells, studies on artificial membrane systems were performed. Definitely, the interaction with membrane lipids is a crucial step for peptide internalization. As for the longer versions $(sC18)_2$ and $lin(sC18)_2$, the highest activities on cell membrane destabilization was observed (figure 9 and 10), these two peptides were investigated in the following experiments. The interaction, destabilization and pore forming capability with different membrane systems were thereby tested by Mareike Horn as described in previously published studies [77].

Two different artificial membrane systems were generated. First, large unilamellar vesicles (LUVs) with a diameter of about 100 nm composed of a different lipid arrangement were prepared and carboxyfluorescein was enclosed in these vesicles. The CF-release could then be detected if the treatment with the unlabeled CPPs leads to a pore-forming or membrane disrupting event. The unlabeled peptides were incubated with the artificial membranes and the CF-release from the vesicles was determined using a plate reader. At the end of each experiment, Triton X-100 was applied to measure the maximum of dequenching, which was set to 100% and then used to normalize data. Each experiment was carried out three times in duplicate. Furthermore, the interaction of CF-labeled $(sC18)_2$ and $lin(sC18)_2$ with giant unilamellar vesicles (GUVs), also composed of different formula of phospholipids, doped with 0.2 mol% Atto550-DOPE to visualize their membranes was investigated. The advantage of GUVs is their bigger size of 5 – 10 µm diameter, which

makes a microscopic observation possible. Moreover, due to their magnitude, the membrane curvature is comparable to that of cell membranes. [80] The interior of the GUVs was filled with a blue stain, namely Oyster405, to detect pore formation within the membranes [81, 82]. After incubating the GUVs with the CPPs, the behavior was observed by confocal laser scanning microscope.

Both, the LUVs and GUVs were prepared in the following compositions: zwitterionic, non-charged, phospholipid vesicles (made from DOPC/DOPE, 50:50) resembling the asymmetric distribution within electrostatically neutral mammalian membranes, which is simplified comparable to the cell membrane of HEK-293 cells [83, 84]. Neoplastic cells often comprise a more negatively charged membrane than healthy cells [85] and therefore, vesicles with negatively charged membranes made from DOPC, DOPG, DOPE (40:30:30) were investigated, too. [86, 87] To not only compare the effect of peptides on zwitterionic and anionic lipid membranes, the effect of different membrane fluidities was also studied by adding sphingomyelin and cholesterol to the latter mixture, resulting in vesicles with the composition DOPC/DOPG/SM/Chol (25:5:20:20). [88, 89] The results for the interaction of the two candidates $(sC18)_2$ and $lin(sC18)_2$ are depicted in figure 11.

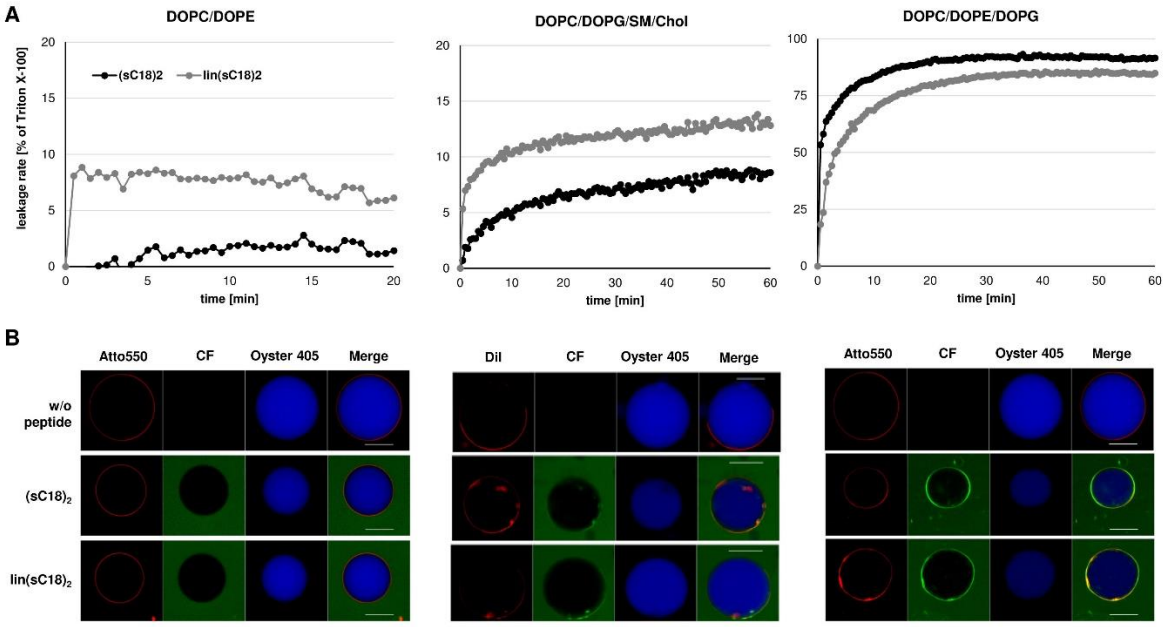

Figure 11: Lipid-peptide interaction studies using artificial membrane systems. (A) Peptide-induced CF leakage experiments from LUVs composed of DOPC/DOPE (50:50), DOPC/DOPG/SM/Chol (25:5:20:20), DOPC/DOPE/DOPG (40:30:30) as a function of time. The results shown are representative of three independent preparations of LUVs. LUVs are treated with 1 µM $(sC18)_2$ and $lin(sC18)_2$ for 60 min. **(B)** CLSM analysis of GUVs composed of DOPC/DOPE (50:50), DOPC/DOPG/SM/Chol (25:5:20:20), DOPC/DOPE/DOPG (40:30:30) treated with 10 µM $(sC18)_2$ and $lin(sC18)_2$ for 90 min. Red: Membrane Stain Atto550 or DiI, Green: CF-labeled peptides, Blue: Oyster 405. Scale bar is 30 µm. Experiments were performed by Mareike Horn.

Having a look on the membrane interaction studies depicted in figure 11, it is obvious that the behavior of the peptides with the artificial systems differed from each other depending on the lipid composition that was used. The zwitterionic membranes composed of the lipids DOPC and DOPE mimicking a neutral, non-charged phospholipid membrane were not interacting with the peptides. In figure 11 A, left graph, it is visible that for $(sC18)_2$ no leakage of the enclosed CF in the large unilamellar vesicles could be detected, whereas for the linear version, a tight leakage between 5 to 10% compared to the maximum of dequenching could be seen. Also, no accumulation on the membrane of neutral GUVs was detectable (figure 11 B). The peptides seemed to stay in the surrounding environment and did not bind to the vesicles. Due to this, no release of the blue Oyster dye could occur. This observation indicates only low peptide-lipid interactions and no lytic activities of both peptide variants $(sC18)_2$ and $lin(sC18)_2$.

On the contrary, the studies with both vesicles that are more mimicking a cancer cell membrane due to the negatively charged phospholipid DOPG, resulted in a completely different pattern. From the CF-leakage experiments with LUVs in figure 11 A, right graph, one can argue that the interaction with the membranes was strong and led to a fairly fast release of the carboxyfluorescein from the vesicles. The percentage number of leakage rate reached 80% within 20 min. This can occur either by forming pores within the membranes so that the dye can escape from the LUVs or by a complete disruption of the structures. Hereby, the effect is minimally more intense for the branched $(sC18)_2$ than for the $lin(sC18)_2$. These results could be confirmed observing the CLSM analysis of the GUVs consisting of the same lipid composition (figure 11 B right picture). For both peptides, a strong accumulation on the membrane and an evident release of the blue stain out of the vesicles could be detected. Moreover, the GUVs that were treated with $(sC18)_2$ seemed to be smaller and their appearance differed from the normal round feature of a vesicle. This proved that the CPPs were able to interact with the negatively charged DOPG within the membranes and the tight interaction led to its disruption and pore formation.

It is known, that cholesterol and sphingomyelin have an effect on membrane fluidity and can thereby also have an influence on the peptide-membrane interaction [89]. Thus, another lipid composition for the vesicle studies was chosen, namely LUVs and GUVs that are composed of DOPC, DOPG, sphingomyelin and cholesterol. As shown in figure 11 A, middle graph, the leakage rate compared to the maximum leakage using Triton-X also increased up to a percentage of 5 to 10% for the branched $(sC18)_2$, whereas for the linear version, a leakage of 10 to 15% could be measured. One can say that the pore-forming events were not that present as they were for the negatively charged LUVs, but anyway a

certain release of the dye could be noticed. Looking at the microscopic analysis, a binding to the vesicles could be detected. Furthermore, one can say that a minimal amount of the blue Oyster stain left the vesicles, which were incubated with the branched CPP $(sC18)_2$. This effect was not visible for the linear version. Notably, the dimeric peptides accumulated especially within the DiI-labeled disordered phases of the vesicle membranes, which are containing less sphingomyelin and cholesterol (Figure 11 B). Therefore, the positively charged CPPs presumably interacted with the anionic DOPG but the ordered phase of the lipid rafts in the cell membrane hinders cell membrane disruption or stronger pore-forming processes. Interestingly, by adding cholesterol and sphingomyelin, the strong membrane attack can be somehow lowered. On the one hand, this may be a consequence of the presence of cholesterol that has profound effects on the membrane fluidity and regulates also endocytosis. On the other hand, sphingomyelin together with cholesterol are reported to be enriched in distinct membrane domains, often referred as rafts [90].

Apart from that, these experiments prove that the dimeric peptides play a prominent role in cell penetration and membrane destabilization, which is also in correlation with the performed toxicity assays. The higher release of the CF out of the LUVs and the blue stain out of the GUVs after incubation with $(sC18)_2$ and $lin(sC18)_2$ corresponds to the LDH release out of the cells tested in this study (figure 10).

Consequently, the results showed that the CPPs were not able to overcome neutral charged membranes corroborating the importance of negatively charged constituents at the outer leaflet of the membrane. This could explain why the CPPs show a preference for the cancer cell line MCF-7 in internalization and cell killing. Apart from that, the addition of cholesterol and sphingomyelin led to a decrease of this interaction.

In conclusion, it can be said that for $(sC18)_2$, the highest difference between cancer and non-cancer cells could be shown. This was mostly visible in the cytotoxicity studies and led to the presumption that this variant owned the best anticancer properties. Furthermore, the branched peptide showed less pore-formation in the membrane vesicle studies, which revealed a lower cytotoxicity compared to $lin(sC18)_2$. Therefore, this CPP was studied in more detail in the following part of the thesis.

4.2 Characterization of a CPP with potential anticancer activity

In chapter 4.1, it was already shown that the branched dimeric variant $(sC18)_2$ exhibited the best selectivity for cancer cells compared to the other dimeric, branched and linear versions. Regarding these results, this cell-penetrating peptide should be examined in more detail. Within all experiments, the monomeric parent peptide sC18 served as control.

4.2.1 Microscopic analysis of uptake at 4 °C

It is already known from previous studies that the uptake of sC18 occurs mainly via endocytosis. After internalization in HEK-293 cells, sC18 is entrapped in endosomes, which hinders the internalization into the nucleus. In comparison to that, the results for sC18 and the dimeric $(sC18)_2$ in MCF-7 cells confirm another uptake way, namely via direct penetration or by endocytosis followed by a vesicle disrupting process, so that the peptides are then free in the cytoplasm and can internalize into the nucleus or other subcellular compartments. [Gronewold, master thesis 2014] [19]. To confirm this theory, a more detailed analysis concerning the different uptake patterns of sC18 and $(sC18)_2$ was performed. The inhibition of all energy- and therefore temperature-dependent pathways like all the steps of endocytosis is realized by minimizing the experimental temperature to 4 °C [91]. So, in this study, MCF-7 and HEK-293 cells were incubated with the same concentration of peptide at 37 °C as well as at 4 °C. Afterwards, they were analyzed by fluorescence microscopy (figure 12).

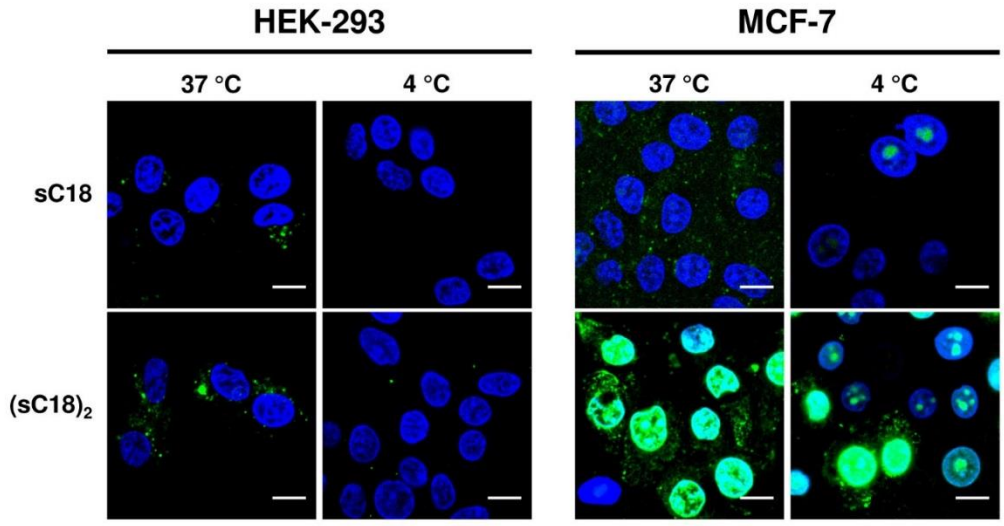

Figure 12: Uptake of CPPs at different temperatures. Fluorescence microscopy images of MCF-7 and HEK-293 cells after 30 min incubation with 10 µM CF-sC18 or CF-$(sC18)_2$ incubated at 4 °C or 37 °C, respectively. Blue: Hoechst nuclear stain, Green: CF-labeled peptides, external fluorescence was quenched with trypan blue for 30 s, Scale bar is 10 µm.

The microscopic analysis of sC18 and $(sC18)_2$ for MCF-7 and HEK-293 cells (figure 12) demonstrated a reduced internalization at 4 °C. This confirmed that the uptake of both CPPs is probably energy-dependent. Nevertheless, the effect for $(sC18)_2$ in MCF-7 cells was not as strong as for HEK-293 cells, which confirmed the hypothesis that the CPPs are entering especially cancer cells, mainly via direct penetration. The internalization in the cancer cells was not affected as much as in the non-cancerous cells, when incubating at 4 °C. The same results could also be obtained using a peptide concentration of 1 µM (data not shown). For the monomeric sC18, also, a decrease in cellular uptake in MCF-7 cells could be detected. Hereby, one can interpret that most of the peptides entered the cells by endocytosis but when inhibiting this pathway, the CPP seemed to be able to overcome the membrane barrier also by direct penetration. In contrast to these results, the difference in the amount of internalized sC18 and $(sC18)_2$ at 37 °C and 4 °C in HEK-293 cells was very high. At 4 °C, almost no peptides could be registered in the embryonic kidney cells. This confirmed the idea, that both peptides internalize HEK-293 cells mainly by endocytosis. At energy-reduction conditions, the peptides are then not capable to internalize in visible amounts into the non-cancer cells.

This result is in correlation with already published data about internalization studies in HEK-293 cells, which revealed that the uptake rates decrease about 80%, if the cells were incubated with CF-sC18 at 4 °C [19].

4.2.2 Uptake studies using flow cytometry

In order to quantify the results of the microscopic analyses, flow cytometric studies were performed using the same cell lines as in the above-mentioned studies (figure 13). For that, the cells were treated with the CPPs at different temperatures in 24-well plates and afterwards removed from the surface using trypsin. Then, they were analyzed in a flow cytometer measuring their green fluorescent signal intensity, whereby the autofluorescence was subtracted from each sample.

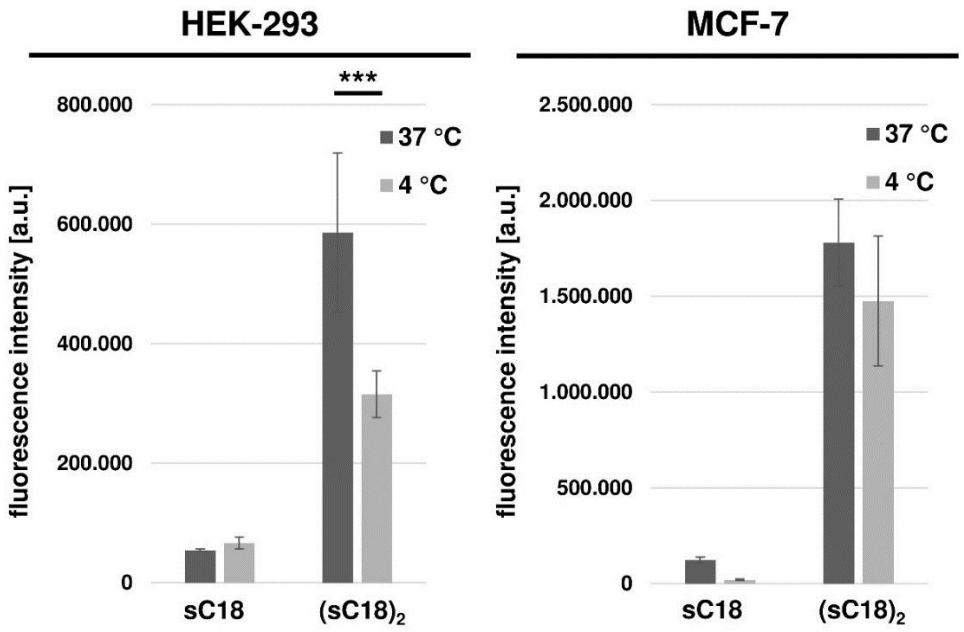

Figure 13: Uptake of CPPs at different temperatures. Flow cytometric analyses of cellular uptake of 10 µM CF-labeled sC18 and $(sC18)_2$ in HEK-293 and MCF-7 cells incubated at 4 °C and 37 °C for 30 min, respectively. Experiments were conducted in triplicate with *n = 3*, error bars represent the standard derivation.

The flow cytometry studies shown in figure 13 confirmed the previous CLSM results, showing that the internalization of the dimeric $(sC18)_2$ was about 10-times higher in relation to the parent monomer sC18 in the two cell lines. This effect was also detected for HEK-293 cells, MCF-7 cells and the human colon adenocarcinoma cell line HT-29 by flow cytometric uptake studies investigating 10 µM peptide solutions that were incubated for 1 h [20]. Furthermore, the internalization rate of the dimeric peptide into MCF-7 cells is clearly higher than for HEK-293 cells, verifying the results of previous studies, and again demonstrating a potential cell selectivity of $(sC18)_2$ [Gronewold, master thesis 2014, figure 12]. Moreover, when incubating MCF-7 cells at 4 °C with $(sC18)_2$, no significant decrease in peptide accumulation could be observed, which confirmed the theory that the CPPs penetrated the cancer cells mainly by direct penetration. In contrast to this, there was a clear difference in the amount of internalized $(sC18)_2$ at 37 °C and 4 °C in HEK-293 cells (*** $p < 0.001$) proving the idea that the peptides enter the non-cancer cells mainly by endocytosis, as it could also be shown in microscope analyses before (figure 12).

4.2.3 Uptake studies with radiolabeled NODAGA-coupled peptides

To proof the former results by other quantification techniques, radiolabeled CPP variants were generated. For this, a chelator had to be introduced first to the peptide sequences at the *N*-terminus, which was achieved by common coupling methods directly on solid phase.

Since the chelator DOTA (1,4,7,10-tetraazacyclododecane-1,4,7,10-tetraacetic acid) did not yield sufficient complexation, and thus satisfying results concerning radiochemical yields, the bifunctional chelator NODAGA (4-(4,7-bis(2-(tert-butoxy)-2-oxoethyl)-1,4,7-triazacyclononan-1-yl)-5-(tert-butoxy)-5-oxopentanoic acid) was used. In table 5, an overview of the NODAGA-coupled peptides is shown.

Table 5: Calculated and experimentally determined molecular weights, purities and yields of the synthesized NODAGA-labeled peptides. For the sequences of sC18 and $(sC18)_2$ see table 3.

Peptide	MW_{calc} [Da]	MW_{exp} [Da]	Net charge	Purity [%]	Yield [%]
NODAGA-sC18	2426.90	2427.63	+ 8	> 99	~ 60
NODAGA-$(sC18)_2$	4479.48	4481.25	+ 16	> 95	~ 39

The chelator was successfully coupled to both sequences and the peptides were obtained in high purity and satisfying yields. The observed high amount of TFA salt adducts in the final products were removed by solving the peptides in 8 mM HCl solution. After repetitive lyophilization steps, the respective chloride salts were obtained.

All following radiolabeling experiments were done in cooperation with the group of Prof. Dr. Schomäcker (by Sergio Muñoz Vásquez and Beate Zimmermanns) from the Institute for Nuclear Medicine, University Hospital, Cologne.

The complexation of these modified peptides with the radionuclide Gallium^{68} worked fine and ended up in a radiochemical yield (RCY) above 95%. Then, the uptake experiments were done to see, whether the Ga^{68}-NODAGA-peptides behave the same as the CF-labeled ones. HEK-293 and MCF-7 cells were incubated with really low concentrations of 0.823 nmol of Ga^{68}-NODAGA-peptides. The radioactivity was measured in a gamma spectrometer and the results are illustrated in figure 14.

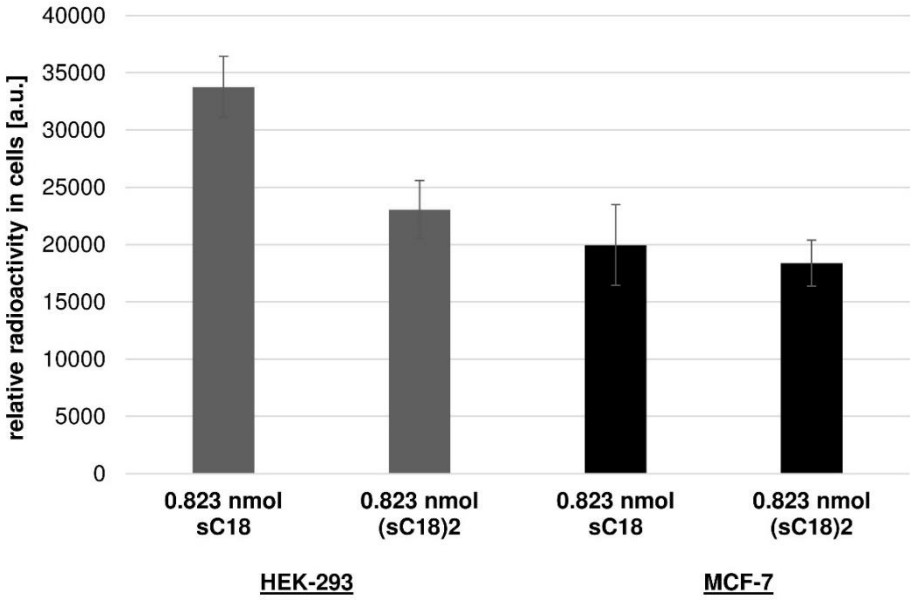

Figure 14: Cellular uptake of ^{68}Ga-NODAGA-modified peptides measured in a gamma spectroscopy system. Relative uptake of 0.0823 nmol ^{68}Ga-NODAGA-modified sC18 or ^{68}Ga-NODAGA-modified $(sC18)_2$ in HEK-293 and MCF-7 cells, respectively. The results are represented in relative amounts of internalized peptide, error bars represent the standard derivation.

Figure 14 shows that the CPPs are still able to internalize into both cell lines, when incubating the cells with very low peptide concentrations of 0.823 nmol. Additionally, when adding Ga^{68}-NODAGA-peptides at these concentrations, the uptake in both cell lines for both peptides is not significantly different. This is in contrast to the results obtained using higher concentrations. It was published by Guterstam *et al.* that the uptake of cell-penetrating peptides is highly depending on various factors. Within this the dependence of CPP concentration is often mentioned. [26] For sC18 and $(sC18)_2$, it could be shown that the different uptake rates in cancer and non-cancer cells occurred with concentration in the micromolar range, but not at lower peptide amounts.

4.2.4 Tracking the intracellular fate of the CPPs after cellular uptake

Next, it should be elucidated where the peptides remain over time after incubation with the cells. It is interesting to verify if the peptides would leave the cells over time or are degraded or if they stay inside and accumulate in certain compartments. Therefore, HEK-293 and MCF-7 cells were incubated with 10 µM of sC18 and $(sC18)_2$ for 30 min. Afterwards, the solutions were removed, the cells were washed and then incubated for 6 h in the appropriate medium containing serum. In figure 15, the results at the time points ‘t = 30 min + 0’ and ‘t = 30 min + 6 h’ are shown.

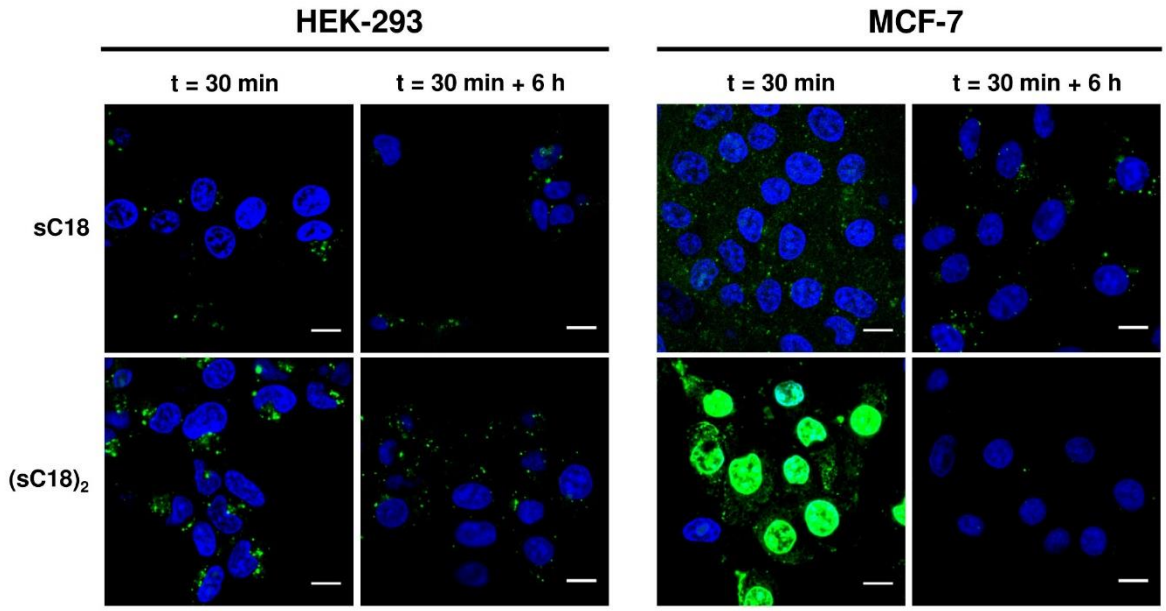

Figure 15: Observation of peptides 6 h after incubation. Fluorescence microscopy images of MCF-7 and HEK-293 cells after 30 min incubation with 10 µM CF-sC18 or CF-$(sC18)_2$ and observation just afterwards or after 6 h in peptide-free medium, respectively. Blue: Hoechst nuclear stain, Green: CF-labeled peptides, external fluorescence was quenched with trypan blue for 30 s, Scale bar is 10 µm.

When comparing the pictures in figure 15, it was visible, that the peptides differed in their internalization pattern depending on the observed cell line. In HEK-293 cells, the amount of peptides, as well as its destination inside the cells (e.g. vesicles) was more or less equal after 6 h. These results are in line with the theory that the uptake in these cells occurs via endocytosis (chapter 4.2.1 and 4.2.2). Thereby, the peptides remained encapsulated in the vesicles and were not released into the cytosol. The endosomes are then undergoing the degradative pathway and will be developed to endolysosomes [92]. The lysosomes contain, among other enzymes, hydrolases to degrade the peptides enzymatically [93]. These lysosomes are visually not distinguishable from endosomes.

On the contrary, in MCF-7 cells, a difference between the time points 0 and 6 was obvious. The amount of sC18 was lower after 6 h and just visible in fluorescent dots, presenting the peptides encapsulated in vesicles. Probably, most of the CPPs that entered the cells by endocytosis was released from the vesicles and could then be degraded in the cytosol. Thus, after 6 h, there were just a few amount of peptide left in the lysosomal pathway. After endosomal release, the free CPPs within the cytoplasm were either degraded by cytosolic enzymes or transported out of the cells. Also for $(sC18)_2$, whereof almost no peptide was left after 6 h, it can be assumed, that it got degraded within the cytoplasm or also released in the surrounding medium. These results are confirming the idea that the internalization in MCF-7 cells happened mainly via direct penetration.

4.2.5 Triggering endosomal release in HEK-293 cells

As previously shown, the cell-penetrating peptides sC18 and $(sC18)_2$ seemed to internalize in the embryonic kidney cells HEK-293 via endocytosis, but staying then encapsulated within the vesicles and not being therefore able to enter the cell nucleus. To examine this hypothesis further, the disruption of the membrane and thus the endosomal release of the peptides in the cytoplasm should be triggered in various ways. For instance, it is possible to use multivalent CPPs, pH-dependent membrane active peptides (PMAPs) and endosomal escape sequence motifs like GALA, KLA or KALA. Also longer peptides as e.g. melittin (26 amino acids) derived from the bee venom can trigger endosomal release by pore-formation [3]. Furthermore, photochemical lysis of the endosomes, or the use of chemicals like $CaCl_2$, chloroquine or sucrose can trigger the disruption of vesicles. [15, 94-96] In this study, the improvement of endosomal release of CPPs was triggered with the chemicals chloroquine, sucrose and $CaCl_2$. Chloroquine (CQ) is a lysosomotropic base, which accumulates in vesicles and can thereby inhibit the acidification of the endosomes, preventing a development to endolysosomes. Furthermore, due to the accumulated ions, the CQ promotes swelling and disruption of the vesicles. [28, 97] This effect could also be shown for sucrose. The sugar accumulates in the endosomes and leads to swelling as well as destabilization, resulting in a release of the vesicle content into the cytosol. [98, 99]. Calcium is attributed to disorder membranes during peptide entry and can therefore trigger the uptake [100, 101].

The cells were incubated for 30 min with 10 µM of the CPPs sC18 and $(sC18)_2$, respectively and the three mentioned agents were added. The pictures after microscopically observation are shown in figures 16 and 17.

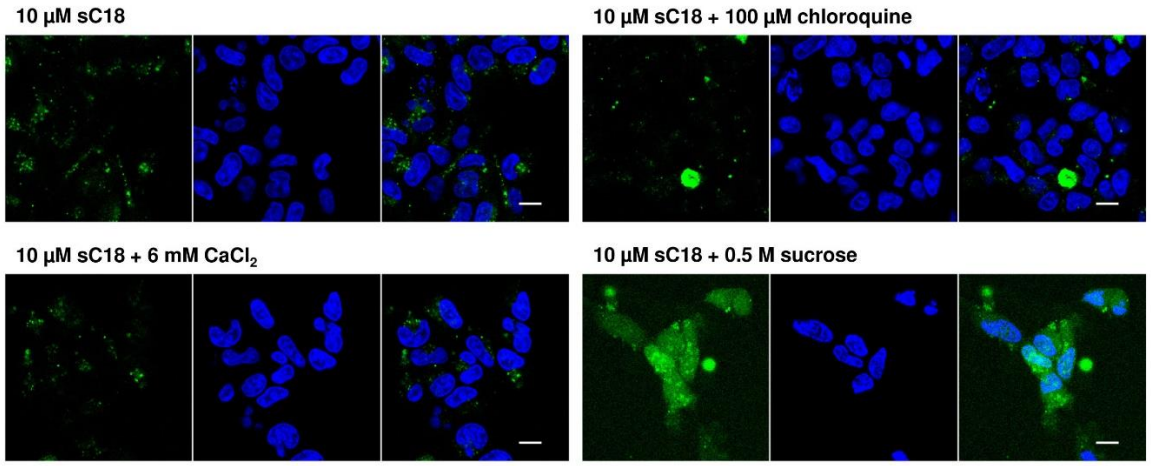

Figure 16: Localization of sC18 after endosomal disruption. Fluorescence microscopy images of HEK-293 cells after 30 min incubation with 10 µM CF-sC18 and additionally 100 µM chloroquine, 6 mM $CaCl_2$ or 0.5 M sucrose, respectively. Blue: Hoechst nuclear stain, Green: CF-labeled peptides, external fluorescence was quenched with trypan blue for 30 s, Scale bar is 10 µm.

Cells treated with 100 µM chloroquine or 6 mM $CaCl_2$ in addition to the peptide sC18, did not show a major difference in peptide distribution within the cells compared to the control. In contrast to that, the cells that were incubated with 0.5 M sucrose in addition to the peptide showed a cytosolic distribution with an especially high accumulation in the nuclei. In those cells, the sucrose seemed to successfully induce the release of the peptides into the cytosol.

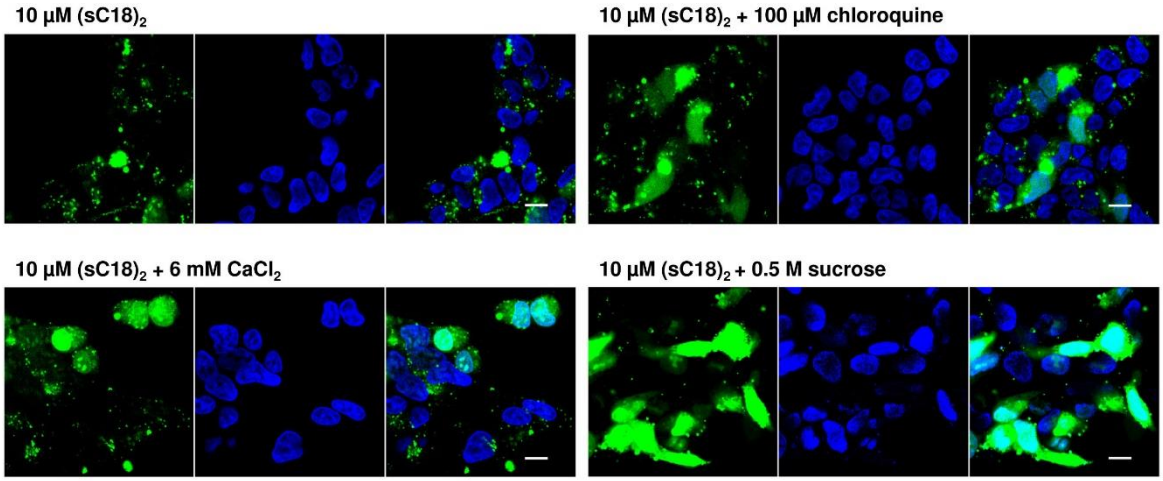

Figure 17: Localization of $(sC18)_2$ after endosomal disruption. Fluorescence microscopy images of HEK-293 cells after 30 min incubation with 10 µM CF-$(sC18)_2$ and additionally 100 µM chloroquine, 6 mM $CaCl_2$ or 0.5 M sucrose, respectively. Blue: Hoechst nuclear stain, Green: CF-labeled peptides, external fluorescence was quenched with trypan blue for 30 s, Scale bar is 10 µm.

For $(sC18)_2$ somehow different results were obtained. Figure 17 shows that the incubation with all tested substances led to a different distribution and localization of $(sC18)_2$ in

HEK-293 cells. The microscopic pictures of the cells treated with CQ and $CaCl_2$ display some cells, where the CPPs were also distributed in the cytoplasm, shown by a diffuse green signal – as well as in the nuclei. This effect was even stronger when incubating the cells with 0.5 M sucrose. Hereby, almost all cells could be observed in the previously described phenotype. The cell nuclei appeared as normal, indicating no toxic effects induced by the agents.

The differences between the two investigated CPPs correlated well with the expectations, since the uptake rate of the dimer at this concentration was about 10-fold higher than that of the monomer, which was already demonstrated in chapter 4.2.2. Thus, the amount of sC18 in the endosomes was less than $(sC18)_2$ and a disruption of the vesicles, filled with the monomeric peptide, did not lead to detectable amounts of CF in the cells.

To underline the hypothesis, that the increase of the green signal did not occur because of the toxic effects induced by the chemicals, cytotoxic tests were performed. The results are shown in figure 18.

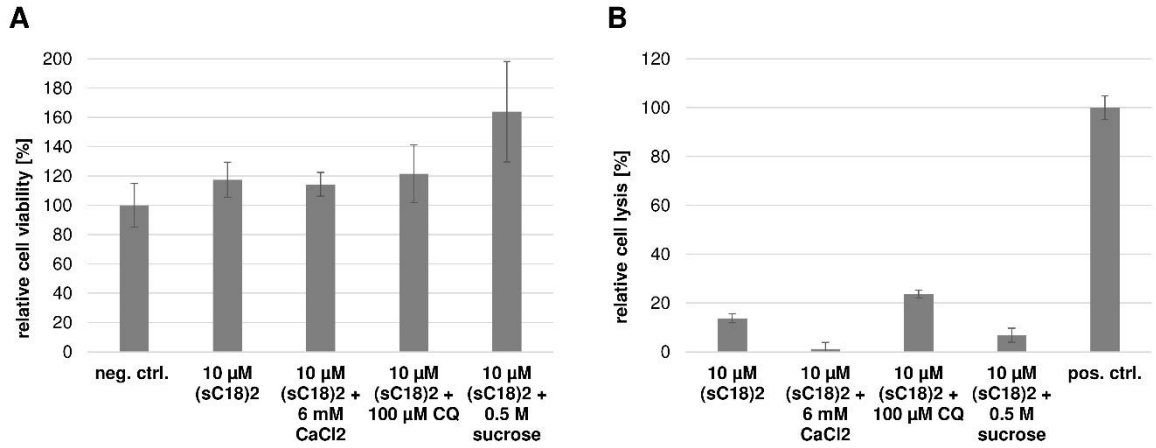

Figure 18: Toxicity profile of endosomal release triggering substances (A) Cell viability assay based on resazurin of 10 µM $(sC18)_2$ alone or co-incubated with 6 mM $CaCl_2$, 100 µM CQ or 0.5 M sucrose, respectively, on HEK-293 cells after incubation for 1 h, untreated cells served as negative control and were set to 100%. 70% EtOH was used as positive control. **(B)** Cell lysis assay based on lactate dehydrogenase release after 1 h incubation of HEK-293 cells with 10 µM $(sC18)_2$ alone or co-incubated with 6 mM $CaCl_2$, 100 µM CQ or 0.5 M sucrose, respectively. Cells treated with lysis solution served as positive control and were set to 100%, untreated cells were used as negative control and were subtracted from each result. Both experiments were conducted in triplicate with *n = 1*. Error bars represent the standard deviations.

The cytotoxicity profile in figure 18 demonstrates that none of the tested substances exhibited any cytotoxic effects in the used concentrations. No decrease in cell viability could be observed (figure 18 A) and just a minimal cell lysis could be detected for the treatment

with CQ (figure 18 B). Despite the fact that these experiments were performed only once, the tendency is supporting the idea that the chemicals did not harm the cells. Therefore, the distribution of the CPPs in figures 16 and 17 were a consequence of the triggered endosomal release.

The endosomal uptake of sC18 and $(sC18)_2$ in HEK-293 cells could be proved by these results. Thereafter, the peptides remained, without any endosomal releasing effect, encapsulated in the vesicles and were not able to penetrate the nuclei as well as other compartments. Furthermore, one can say that an improvement in the application especially of the dimeric peptide could be obtained by adding certain substances as $CaCl_2$, chloroquine and sucrose.

4.2.6 Relevance of membrane composition

From the previous experiments, a certain cell selectivity was observed for the peptides sC18 and $(sC18)_2$ which was in agreement to former results [19, 20, 77]. To confirm the theory, that this selectivity and therefore a better internalization into the negatively charged cancer cells, is correlated with the lipid composition of the membranes, both peptides were also examined on artificial membrane-like systems. The following experiments were established and performed by Mareike Horn. As described above (chapter 4.1.4), the CPPs were tested with giant and large unilamellar vesicles, composed of different lipid formula, that contained an encapsulated dye. The accumulation on the membrane and pore formation in the vesicles could be observed. [77, 81] The results are presented in figure 19.

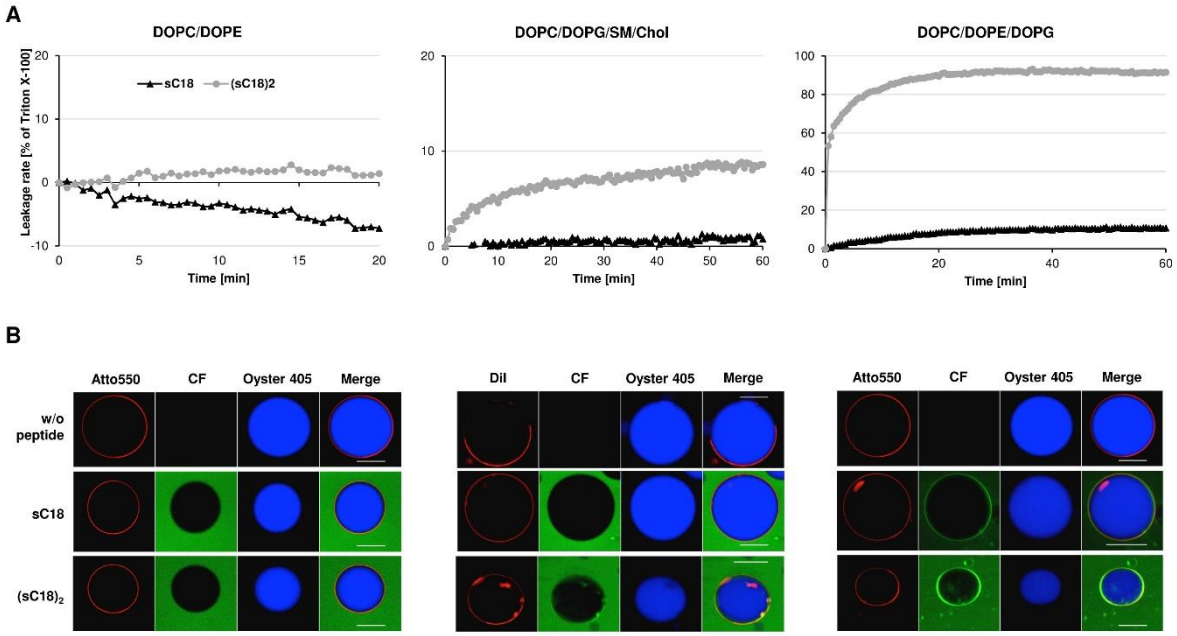

Figure 19: Lipid-peptide interaction studies using artificial membrane systems. (A) Peptide-induced CF leakage experiments from LUVs composed of DOPC/DOPE (50:50), DOPC/DOPG/SM/Chol (25:5:20:20), DOPC/DOPE/DOPG (40:30:30) as a function of time. The results shown are representative of three independent preparations of LUVs. LUVs are treated with 1 µM sC18 and $(sC18)_2$ for 20 or 60 min. **(B)** CLSM analysis of GUVs composed of DOPC/DOPE (50:50), DOPC/DOPG/SM/Chol (25:5:20:20), DOPC/DOPE/DOPG (40:30:30) treated with 10 µM sC18 and $(sC18)_2$ for 90 min. Red: Membrane Stain Atto550 or DiI, Green: CF-labeled peptides and Blue: Oyster 405. Scale bar is 30 µm. Experiments were done by Mareike Horn.

The interaction of both CF-labeled peptides with neutrally charged GUVs was negligible after an incubation time of about 90 min, and no green fluorescent signal was observed on the vesicle membrane as well as no intravesicular blue stain escaped out of the vesicles (figure 19 B left). Also the incubation with the CF-filled LUVs did not show any release of the fluorescent dye from the vesicles (figure 19 A left). This observation indicates a low peptide-lipid interaction and no lytic activities of both peptide variants.

In contrast, the experiments with negatively charged GUVs, that mimic a cancer cell membrane (figure 19 B right), showed an accumulation of the monomeric peptide sC18 on the artificial membrane and a slight release of the blue fluorescent stain Oyster 405. Regarding the experiments with LUVs, one could detect a release of the CF from the vesicles about 10%. For the dimeric peptide $(sC18)_2$, next to the strong accumulation on the GUV membrane, a higher release of the blue stain out of the vesicles could be detected. Moreover, the appearance of the GUV differed from the normal feature of a vesicle, indicating a disrupting event on the lipid membrane. This effect was similar to the well-studied cell-penetrating peptide transportan for which membrane lytic activity has been

already described [102]. This peptide as well as its shorter variant TP10 showed high potential in delivering various cargoes into cells [21, 52]. It is possible that the internalization and the transport capacities of $(sC18)_2$ are comparable to these well studied CPPs. Looking at the results of the experiments with the LUVs containing DOPG in the right graph in figure 19 A, it is visible, that the interactions are the same as observed with the giant unilamellar vesicles. The incubation with sC18 led to a slight release of CF about 10% after 60 min whereas the release of the dye when incubating the vesicles with $(sC18)_2$ occurred very fast at a percentage of 90%. This effect could either take place due to pore-forming events within the vesicle membranes so that the dye could leak from the LUVs, or by a complete disruption of the structures.

Next, the vesicles composed of DOPC, DOPG, sphingomyelin and cholesterol should be elucidated. As described before, cholesterol and sphingomyelin have an influence on the peptide-membrane interaction (chapter 4.1.4) [89]. In figure 19 B in the middle picture, it is illustrated, that sC18 did not accumulate on the GUV membrane. Also in the LUV experiment, no release of carboxyfluorescein from the vesicles could be measured. For the dimeric peptide, an accumulation on the vesicle membrane was visible, but the binding was not that strong as it could be observed for the negatively charged GUVs without cholesterol and sphingomyelin. Also a release of the blue dye was hardly detectable. Furthermore, the leakage rate from the large unilamellar vesicles compared to the maximum leakage using Triton-X, which is completely disrupting the membrane, increased up to a percentage of about 8%, which was considerably less than in the LUVs composed of DOPC/DOPE/DOPG.

Consequently, the results showed that the CPPs were not able to overcome neutrally charged membranes corroborating the importance of negatively charged constituents in the outer leaflet of the membrane. In general, this could explain the fact that the CPPs showed a preference for the cancer cell line MCF-7 in internalization and cell toxicity compared to the non-cancer cell line HEK-293. It is likely that the positively charged CPPs interacted with the anionic DOPG, which led to pore-forming events. These experiments were in coincidence with the previously presented lytic activity of $(sC18)_2$ on MCF-7 cells (figure 10). Anyway, sphingomyelin and cholesterol in the cell membrane seems to hinder the cell membrane disruption.

To prove the idea, that cholesterol hinders the interaction of $(sC18)_2$ with the cell membrane, a cholesterol depletion assay was performed using methyl-β-cyclodextrin (MβCD). Afterwards, the cells were incubated with the peptides as usual and then observed by microscopy or flow cytometry. In figure 20, the results for the cancer cell line MCF-7 are presented.

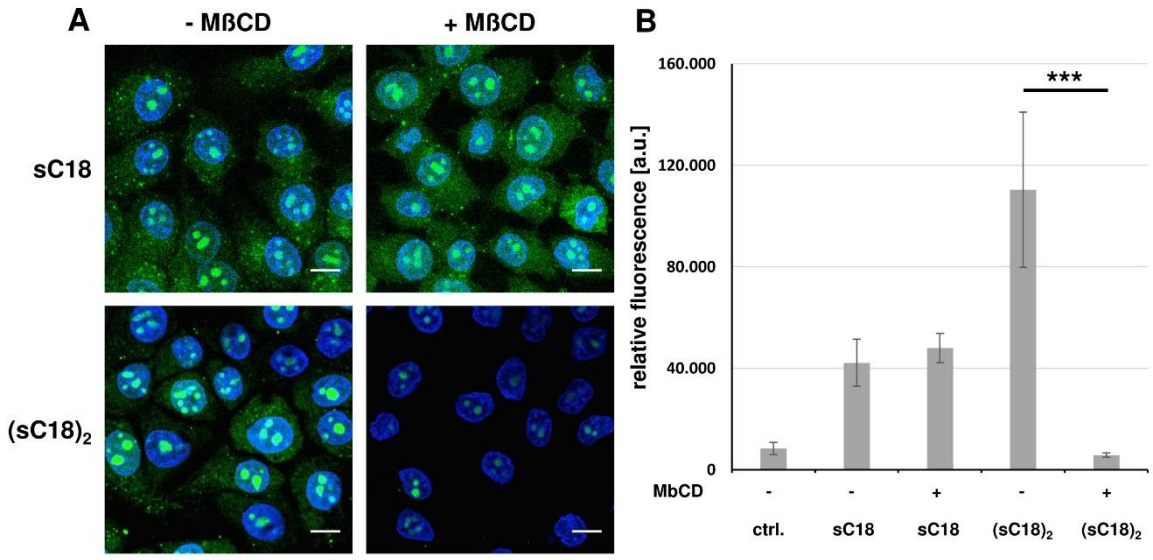

Figure 20: Treatment of MCF-7 cells after cholesterol depletion. (A) Fluorescence microscopy images of MCF-7 incubated with 5 µM CF-sC18 or 1 µM CF-$(sC18)_2$ for 30 min alone or after cholesterol depletion using 10 mM methyl-ß-cyclodextrin for 1 h. Blue: Hoechst nuclear stain, Green: CF-labeled peptides, external fluorescence was quenched with trypan blue for 30 s, Scale bar is 10 µm **(B)** Flow cytometric analyses of cellular uptake of CF-labeled peptides sC18 and $(sC18)_2$ in MCF-7 cells incubated at 37 °C for 30 min with or without earlier cholesterol depletion. Experiments were performed in triplicate with *n = 3*. Experiments were done by Mareike Horn.

It is obvious in both experimental setups that the internalization and intracellular distribution of the monomer was not harmed by cholesterol depletion. This verified the observation, which was shown with the LUVs and GUVs experiments in figure 19, namely that the cholesterol in the membrane was not that important for the sC18 membrane interaction. In the contrary, the internalization rate of the dimeric $(sC18)_2$ was extremely decreased when cholesterol was sequestered from the membranes of MCF-7 cells. In the flow cytometric observations, a significance level of <0.001 could be detected. Furthermore, the peptides just accumulated in the nuclei and almost no green signal could be observed in the cytoplasm of the cells. In addition, the same experiment was performed with HEK-293 cells and similar results could be obtained (data not shown).

It was published previously, that cholesterol depletion inhibits the uptake of a TAT-Cre protein [103]. Furthermore, it is known that the removal of cholesterol disturbs some lipid raft–mediated endocytic pathways like macropinocytosis and caveolae dependent endocytosis. Because the uptake of $(sC18)_2$ was highly reduced after the removal of cholesterol, one could assume that the peptide was penetrating cells via lipid raft–mediated endocytosis. [104, 105]

Anyway, taking these studies in consideration, the highly potent cell selectivity for cancer cells of $(sC18)_2$ is depending on the composition of the target membrane.

4.2.7 Uptake and cytotoxicity screening on various cell lines

To further study a potent cancer selectivity of $(sC18)_2$, several other cell lines, namely HCT-15, HeLa, PC-3, a human prostate cancer cell line [106], and the keratinocyte cell line from adult human skin HaCaT [107] were investigated concerning the cellular uptake and toxicity of sC18 and $(sC18)_2$. Some of them were already used in previous studies [Gronewold, master thesis 2014]. As reference, HEK-293 and MCF-7 cells are again included. In figure 21, the microscopic results for all examined cell lines are shown.

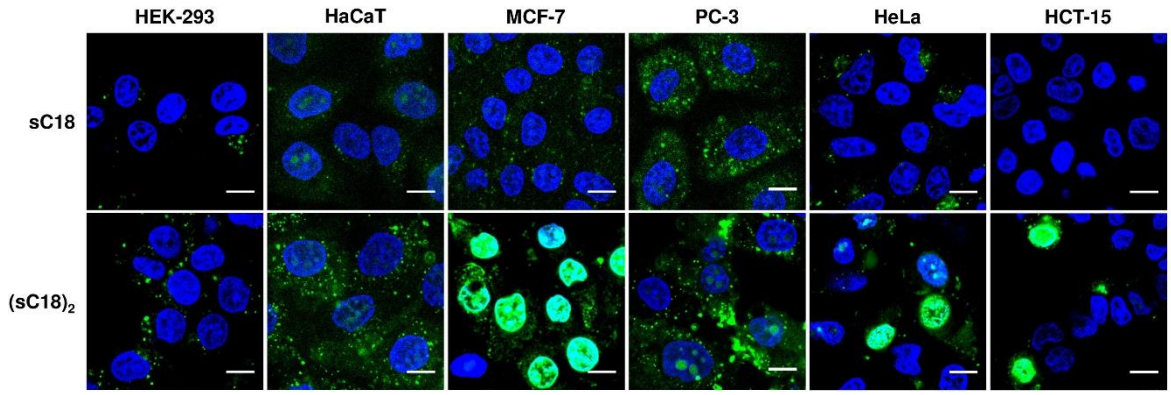

Figure 21: Uptake of sC18 and $(sC18)_2$ in various cell lines. Fluorescence microscopy images of HEK-293, HaCaT, MCF-7, PC-3, HeLa and HCT-15 cells after 30 min incubation with 10 µM CF-sC18 and CF-$(sC18)_2$, respectively. Blue: Hoechst nuclear stain, Green: CF-labeled peptides, external fluorescence was quenched with trypan blue for 30 s, Scale bar is 10 µm.

For all inspected cell lines, it could be detected that after treatment with the dimeric peptide $(sC18)_2$ the intracellular fluorescence intensity was higher than after treating the cells with the linear peptide sC18. The overall punctuate distribution indicated that the peptides entered the cells mainly by endocytosis.

From the microscope pictures of HaCaT cells, showing both peptides with a diffuse and punctuate distribution inside the cytoplasm, as well as accumulation in the cell nucleoli, one can assume that the internalization pattern was different from the one of HEK-293 cells. Hereby, the peptides seemed to enter the cells the same way, they did for MCF-7 cells. The punctual distribution portends an endocytotic way of cell penetration but the diffuse green signal might also be an evidence for direct penetration, or for release of the peptide out of endocytic vesicles [27]. In general, it could be shown, that the previously described cell selectivity for cancer cells is possibly also applicable for keratinocytes.

Having a look at PC-3 cells, one can see that there was a slight increase in uptake of the dimer compared to the monomer. The fluorescent signal for both peptides could be detected as punctuate distribution in the cytoplasm, which is an indicator for endosomal uptake. Furthermore, for $(sC18)_2$ a diffuse signal could also be observed within the cytoplasm, indicating either a direct penetration above the cell membrane or an endosomal uptake with following release from the vesicles. [27] Moreover, the dimeric peptide was also able to cross the cell nuclei membrane and accumulate in the nucleoli, whereas for the monomer only minor uptake into the nuclei was observed.

Regarding the HeLa cells, the fluorescent signal for sC18 could be detected as punctual in the cytoplasm and for $(sC18)_2$ the pictures indicate that the peptide accumulated in the cytoplasm and in the nucleoli as for MCF-7 cells.

For the cell line HCT-15 the gain of the green signal was adjusted to the fluorescence intensity of the dimer. Hence, there was no green signal in the microscope pictures of the monomer. Notably, the fluorescent labeled $(sC18)_2$ peptide was not present in every cell, and in cells, where the peptide was detectable, the signal was present in the cytoplasm as well as in the nuclei. Certainly, the monomer is also entering the HCT-15 cells, but due to the low gain value that was chosen at this time there was no green signal detectable.

These results confirm the differences between the monomeric peptide sC18 and the dimeric peptide $(sC18)_2$, as well as discrepancies in their internalization patterns in different cell lines and a therefore clear detectable selectivity for cancer cells as well as for the epithelial cell line HaCaT. This effect is certainly connected to the different constitutions of the cellular membranes and could be shown for many other cell-penetrating peptides before [83, 108].

It was also very conspicuous that the dimeric peptide $(sC18)_2$ was often localized within the nucleoli when penetrating the cell nuclei. This could be explained by the high amount of ribosomes in the nucleoli. Here, the ribosomes are generated, which are needed for the biosynthesis of proteins in translation afterwards. Ribosomes are composed of ribonucleic acids and proteins. Furthermore, many non-nuclear proteins are present in the nucleoli [109]. This high content of proteins in these cell nuclear regions could be the reason why the cell-penetrating peptides accumulate here, due to an interaction and attraction of the amino acid residues of the CPPs to the proteins present in the nucleoli.

As the variety of the internalization and localization of the CPPs is certainly connected with the membrane constitution of the cells, it is likely that the peptides also have different cytotoxic effects. This should also be investigated on the cell lines used in this thesis. The results of the cell viability assays are presented in figure 22. The results of HEK-293, MCF-7,

HeLa and HCT-15 cells were partly taken from previous studies [Gronewold, master thesis 2014].

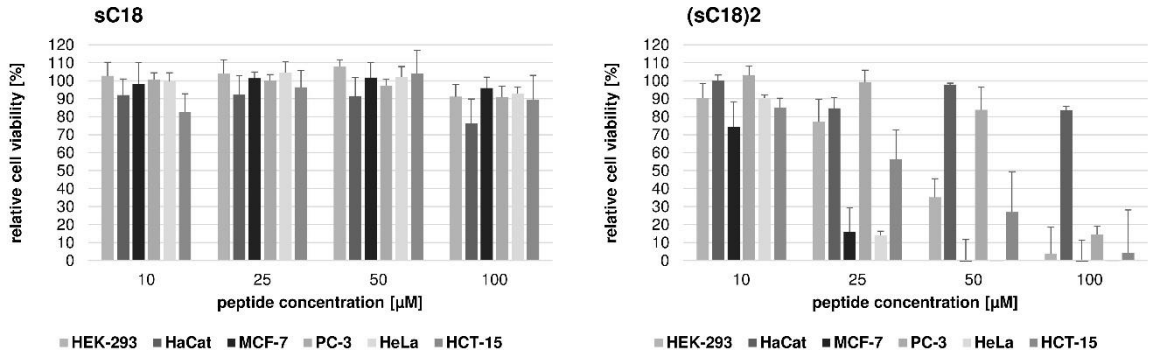

Figure 22: Cytotoxic profile of sC18 and $(sC18)_2$ tested on various cell lines. Cell viability assay on HEK-293, HaCaT, MCF-7, PC-3, HeLa and HCT-15 cells after incubation for 24 h with sC18 or $(sC18)_2$ in various concentrations, untreated cells served as negative control, cells treated for 10 min with 70% EtOH were used as positive control and subtracted from each measurement, experiments were conducted in triplicate with *n = 3* (HEK-293, HaCaT, MCF-7, HeLa and HCT-15) and *n = 1* (PC-3), Error bars represent the standard derivation.

As for all observed cell lines, the monomer sC18 did not show any toxicity in the used concentrations, independently if the CPP was incubated with non-cancer or cancer cells. The relative cell viability of all cell lines stayed around 100% using concentrations up to 100 µM. These examinations are in line with published results [19]. Here, the cell lines HeLa and MCF-7 were tested with the monomeric sC18 in the resazurin based assay, using concentrations of 10 and 100 µM, respectively, and no significant difference to untreated cells could be detected. In the present study, only for the keratinocytes HaCaT, a decrease of cell viability to 75% at a concentration of 100 µM could be seen.

In contrast, after the incubation with the peptide $(sC18)_2$, the relative cell viability decreased with higher concentration of peptide in all cell lines. In HEK-293 cells, the CPP was not toxic up to a concentration of 10 µM, whereas at 50 µM only about 35% of the cells were still viable and all cells were dead at the highest tested concentration of 100 µM. Observing the results of the keratinocytes, one could see that $(sC18)_2$ had no toxic effect on the cells except from a decrease of viable cells to about 85% when incubating with 100 µM peptide solution. As shown for MCF-7 cells before (chapter 4.1.3), the dimer was slightly toxic at 10 µM (75% cell viability) and at concentrations higher than 25 µM, almost no viable cells could be detected. The human prostate cancer cell line PC-3 was not affected by the cell-penetrating peptide up to a concentration of 50 µM. At 100 µM, about 15% of viable cells remained. For HeLa cells, more or less the same outcome than for MCF-7 cells could be noted and the experimental data of HCT-15 cells resembled the ones of HEK-293.

Looking at all examined results for the dimeric CPP $(sC18)_2$, a gradient of cytotoxicity effect on the observed cell lines in the range of 10 – 100 µM can be concluded. The CPP is not toxic to HaCaT cells, slightly toxic to PC-3 cells, followed by HCT-15 and the embryonic kidney cells. The highest toxicity could be observed for the cancer cell lines MCF-7 and HeLa.

To further observe the efficacy of $(sC18)_2$, Ivan Ranđelović of the group of Dr. József Tóvári in Budapest analyzed 16 cancer cell lines (melanoma, liver, pancreas, breast, lung, oral, fibrosarcoma and colon cancer) as well as one human fibroblast cell line using an MTT cell viability assay. The IC_{50} values are shown in table 6.

Table 6: IC_{50} values when incubating $(sC18)_2$ with different cell lines. Toxicity was determined with the MTT assay by Ivan Ranđelović in Budapest as described in Gronewold *et al*. 2017. [77]

Cell line		**IC_{50} [µM]**
Melanoma	A2058	3.9 ± 0,8
	HT168-M1/9	9.2 ± 0,3
	M24	16.2 ± 9,8
Liver	HepG2	5.4 ± 0,1
Prostate	PC-3	8.8 ± 1,4
	DU145	12.3 ± 1,3
Pancreas	Panc-1	23.2 ± 5,0
Breast	MDA-MB-231	30.9 ± 1,2
	MCF-7	6.2 ± 1,0
Lung	A549	27.3 ± 2,0
	H1975	6.5 ± 0,1
	H1650	4.5 ± 0,3
Oral (head and neck)	PE/CA-PJ15	39.6 ± 4,5
	PE/CA-PJ41	36.2 ± 1,1
Fibrosarcoma	HT1080	7.4 ± 0,6
Colon	HT-29	9.5 ± 0,3
Normal fibroblasts	MRC-5	>50

Considering the IC_{50} values depicted in table 6, it is shown that $(sC18)_2$ was again more active against almost all cancer cell lines and the fibroblast cell line was significantly less affected in comparison with an IC_{50} value above 50 µM. The highest cytotoxic effect of the peptide could be examined against the melanoma cell line A2058, the liver cells HepG2, the well-studied breast cancer cell line MCF-7, and the lung cancer cells H1975 and H1650 with averaged IC_{50} values underneath 7 µM. The results for MCF-7 are in line with the ones shown in the previous cell viability assay in figure 22. The estimated IC_{50} value of HCT-15 cells in the previous tests was about 25 µM. The herein tested colon cancer cells HT-29 are with a value of 9.5 in more or less the same range. For the prostate cancer cell line PC-3, another outcome of the cytotoxicity was observed. The experiments with PC-3 cells done in this study (figure 22) were just performed once, so this should be taken with caution.

In conclusion, it could be shown that the dimerization of the linear peptide sC18, which contains a higher number of positive charges, leads to a higher cytotoxicity in a wide range of cells. Overall, the results let assume a high therapeutic potency of $(sC18)_2$ for several cancer models.

4.2.8 Cargo delivery of actinomycin D

Finally, studies on the delivery features were performed to demonstrate that $(sC18)_2$ could serve as a good cellular delivery vector for scientific and therapeutic purposes. Hoyer *et al.* showed in 2012 that $(sC18)_2$ exhibits this property. The covalent binding of two cytostatic agents, precisely a functionalized cymantrene and the anticancer therapeutic chlorambucil, to the peptide led to a significant reduction of cell viability in the cancer cell lines HT-29 and MCF-7 compared to the respective sC18 conjugate and the unconjugated cytostatic compounds. [110]

In this study, it should be elucidated, if sC18 and $(sC18)_2$ are also able to transport non-covalently attached cargo within MCF-7 cells, because the covalent coupling of drugs is of course highly laborious and time-consuming. The antitumor antibiotic actinomycin D, which was used in this experiment, can intercalate with DNA and inhibit the RNA synthesis [111]. As for $(sC18)_2$ a lytic effect on the cell membrane could be shown (figure 10), it is possible that a co-incubation with the antibiotic is sufficient for the transport and successful targeting of the drug into the cells and to the DNA. For this investigation, cells were exposed to the peptides sC18 and $(sC18)_2$ alone, actinomycin D alone and the co-incubated peptide/actinomycin D solution for 24 h. Afterwards a cell viability assay was done to detect the number of viable cells. Therefore, a concentration of actinomycin D was determined before (data not shown), whereby the cells are not affected, so that a toxic effect should be

directly correlated with the transport ability of the CPPs. The results are presented in figure 23.

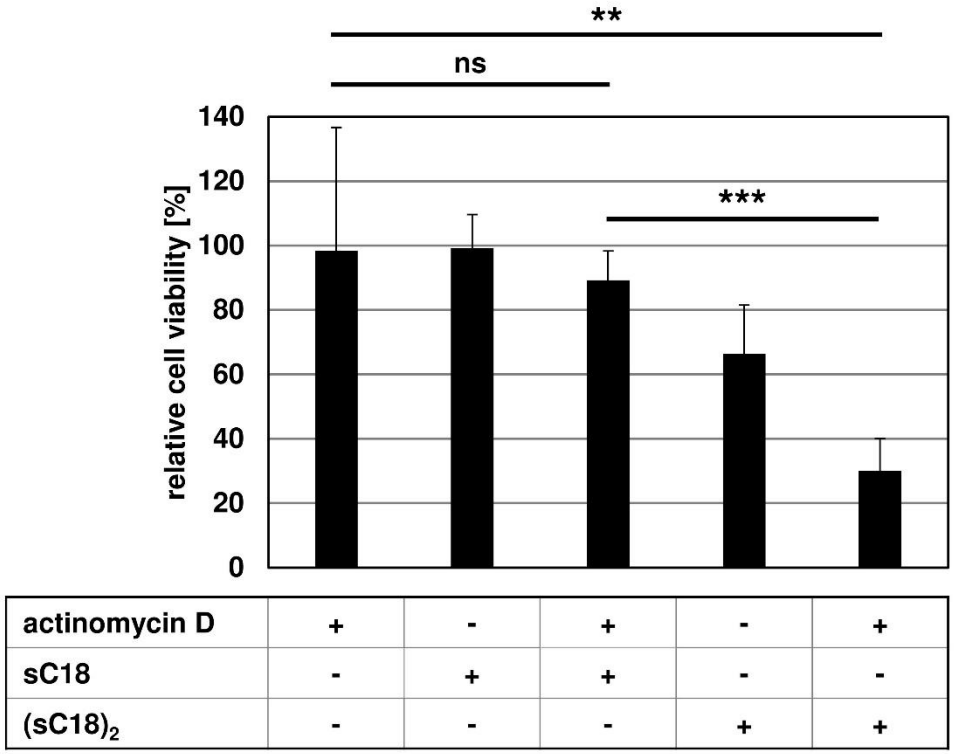

Figure 23: Cargo delivery of actinomycin D in MCF-7 cells. Cytotoxicity assay based on resazurin after incubation with 0.1 µM actinomycin D, 10 µM sC18 or 10 µM $(sC18)_2$ alone or co-incubated with actinomycin D (0.1 µM) for 24 h. Untreated cells served as negative control, cells treated for 10 min with 70% EtOH as positive control and were subtracted from each result. Experiments were conducted in triplicate with *n = 2,* error bars represent the standard derivation.

The results in figure 23 show, that 0.1 µM actinomycin and 10 µM sC18 alone are not toxic to the cancer cells. Also the combination of the drug and the monomeric CPP did not lead to a significant toxic effect. Due to the uptake by endocytosis and no lytic activity, the monomeric peptide sC18 was expected not to be able to efficiently trigger the transport of the drug to the DNA, which could be confirmed in this experiment. Even when the CPP could carry the actinomycin D into the cells via endocytosis, the two compounds might stay enclosed in the vesicles and therefore the agent cannot enter the cell nuclei and fulfil its function.

However, the incubation with $(sC18)_2$ indicated a high decrease of viable cells to around 70% which is in agreement with the results in figure 22. When co-incubating the CPP with the anticancer antibiotic, the cell viability decreases further to about 30%. This indicates that the dimeric CPP was triggering the uptake of actinomycin D into the cells with a significant p-value less than 0.01. The difference between the co-incubation with the

monomer and the dimer was even more defined with a significance level of <0.001. Taking all this in consideration, it seemed that the interaction of $(sC18)_2$ with the negatively charged cancer cell membrane led to pore-forming events and this facilitates the entry of the drug. Actinomycin D was than unbound in the cytosol, could overcome the nuclear membrane and intercalate with the DNA, which led to the inhibition of RNA synthesis and in the end to cell death.

From the detailed observation of $(sC18)_2$, one can conclude that this peptide possesses potential cancer selectivity to many different kind of cancer cells and showed membrane disrupting properties. Furthermore, it was also able to transport a cytotoxic drug efficiently into MCF-7 cells.

4.3 Specific targeting of nuclei and nucleoli using modified CPPs

Within this study, it was tried to create a set of new chimeric CPPs that specifically target the cell nuclei, and act as delivery vectors, potentially even better as the already described branched $(sC18)_2$. For a targeted delivery to the nuclei, the truncated cell-penetrating peptide sC18* was combined with the nuclear localization sequence N50 or the nucleoli-targeting peptide NrTP, respectively. N50 is a nuclear localization sequence of the NFκB1/p50 subunit and NrTP is derived from a toxin sequence [35, 65]. A fusion of NrTP and N50 to CPPs is not published until now.

4.3.1 Peptide synthesis and analysis of the secondary structure

All peptides were synthesized via solid-phase peptide synthesis as previously described. Moreover, unlabeled and carboxyfluorescein-labeled versions were generated. After cleavage from the resin and purification, all peptides were analyzed by HPLC/ESI-MS. The results are shown in table 7.

Table 7: Sequences, calculated and experimentally determined molecular weights, purities and yields of the synthesized peptides, unlabeled and labeled with carboxyfluorescein (CF). The data for sC18* and CF-sC18* can be found in table 3.

Peptide	Sequence	MW_{calc} [Da]	MW_{exp} [Da]	Net charge	Purity [%]	Yield [%]
N50	VQRKRQKLMP-NH_2	1282.61	1282.76	+ 5	> 99	~ 81
CF-N50	CF-VQRKRQKLMP-NH_2	1640.93	1641.11	+ 4	> 93	~ 55
N50-sC18*	VQRKRQKLMPGLRKRLRKFRNK-NH_2	2836.51	2837.20	+ 12	> 99	~ 93
CF-N50-sC18*	CF-VQRKRQKLMPGLRKRLRKFRNK-NH_2	3194.83	3195.65	+ 11	> 97	~ 54
NrTP	YKQCHKKGGKKGSG-NH_2	1504.76	1505.03	+ 6	> 99	~ 59
CF-NrTP	CF-YKQCHKKGGKKGSG-NH_2	1863.08	1863.53	+ 5	> 99	~ 57
NrTP-sC18*	YKQCHKKGGKKGSGGLRKRLRKFRNK-NH_2	3058.67	3059.31	+ 13	> 99	~ 82
CF-NrTP-sC18*	CF-YKQCHKKGGKKGSGGLRKRLRKFRNK-NH_2	3416.99	3417.69	+ 12	> 99	~ 33

As can be depicted in table 7, all peptides could be successfully synthesized and moreover, high purities and yields could be obtained.

For structural characterization of the synthesized peptides, a CD spectrum was recorded with the unlabeled peptides. The peptides were diluted to a concentration of 20 µM in phosphate buffer (pH 7) with or without TFE, respectively, and measured in the CD spectrometer. The spectra are shown in figure 24.

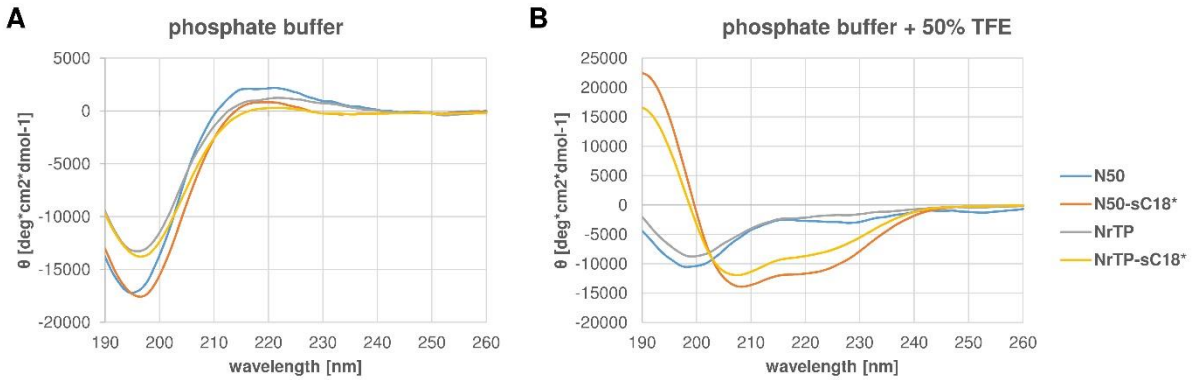

Figure 24: Secondary structure analysis of CPP variants. Circular dichroism spectra of the investigated peptides N50, N50-sC18*, NrTP and NrTP-sC18*. Peptides were measured in a concentration of 20 µM in 10 mM phosphate buffer (pH 7) with **(B)** and without **(A)** 50%-trifluoroethanol (TFE) (*n = 1*).

Judged by the observation of figure 24 A, all peptides exhibited a random coil structure in phosphate buffer without TFE. In the presence of the secondary structure inducing solvent trifluoroethanol [112], the peptides N50 and NrTP also exhibited a random coil structure. On the contrary, in buffer with TFE, for N50-sC18* and NrTP-sC18* the formation of α-helices could be determined (figure 24 B). This was also affirmed by the calculated R-values, which were 0.83 for N50-sC18* and 0.70 for NrTP-sC18*. This proves that the combination of the nuclei-targeting sequences with the CPP sC18* led to the formation of an α-helical structure, whereas the nuclei and nucleoli targeting sequences alone were not able to do so. As depicted in figure 7, sC18* alone is also exhibiting an α-helical character, which was also published recently [73].

4.3.2 Internalization rates of nuclei-targeting sequences

To get a first hint about the internalization features of the new CPP variants, the uptake into two cancer cell lines, namely MCF-7 [113] and HeLa [114], was investigated using flow cytometric analysis. Therefore, cells were treated with CF-labeled peptides, detached and then analyzed in the flow cytometer. The results for both cell lines are shown in figure 25.

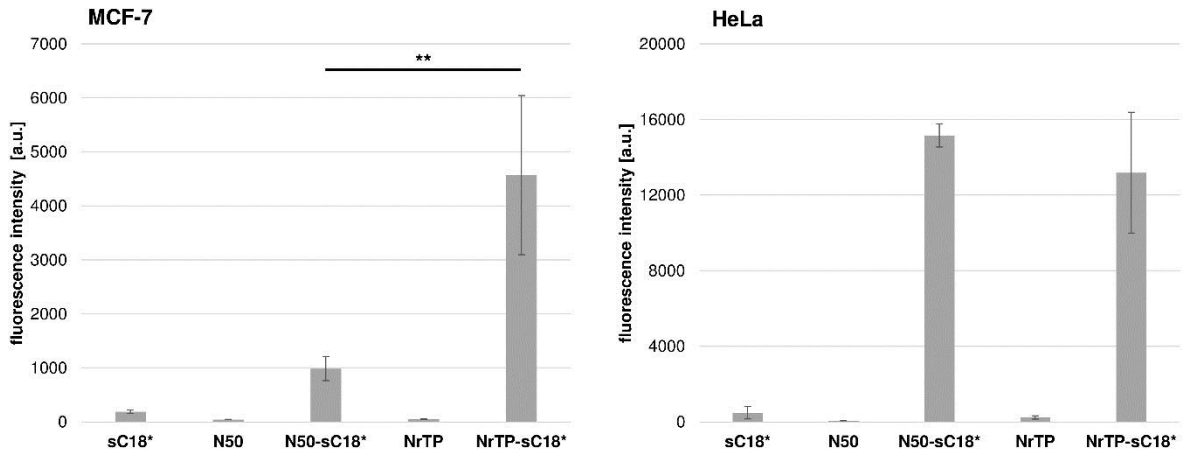

Figure 25: Uptake studies with CPP variants. Flow cytometric analyses of cellular uptake of 10 µM CF-labeled peptides sC18*, N50, N50-sC18*, NrTP and NrTP-sC18* in MCF-7 and HeLa cells incubated at 4 °C and 37 °C for 30 min, respectively. 10'000 events were analyzed, untreated cells served as negative control, experiments were conducted in triplicate with *n = 3* (HeLa) or *n = 2* (MCF-7). Error bars present the standard derivation.

Surprisingly, both new CPP variants, N50-sC18* and NrTP-sC18*, entered the cells extremely efficiently with much higher uptake rates compared to the CPP sC18* alone. In fact, it must be considered that the intensities of N50-sC18* and NrTP-sC18* were such high, that the increased fluorescent signal was diminished with the aim to still measure all signals. Therefore, the internalization of sC18* seemed to be very low. Anyway, the measured signals for the NLS-sequence N50 and the nucleoli-targeting sequence NrTP alone were that minor that one cannot assume any internalization ability for these peptides from these experiments. Rádis-Baptista *et al*. showed that rhodamine B-labeled NrTP can enter into three different tumor cell lines (human ductal mammary gland carcinoma (BT-474), human pancreatic adenocarcinoma (Bx-PC3) and murine neuroblastome (N2A) cells) at a concentration of 50 µM after incubation for 45 min [35]. In this present study, a concentration of 10 µM was used for 30 min; therefore the cell-penetrating capability of the NrTP sequence can probably be increased by augmenting the concentration. Another study also claimed very low cell-penetrating properties for N50 at a concentration of 10 µM in 4 different cell lines (African green monkey kidney (Cos-7), human embryonal kidney (HEK-293), human cervix carcinoma (HeLa) and Madin-Darby canine kidney (MDCK)) [115]. However, the fusion of the NLS and NrTP sequences with sC18* resulted in uptake rates that were much higher compared to the sC18* alone. In detail, for the MCF-7 cells, the internalization of N50-sC18* was about 5-times higher, whereas for NrTP-sC18* the uptake was even about 20-times higher than the ones of the cell-penetrating sequence alone. NrTP-sC18* seemed to internalize better into the breast cancer cells than N50-sC18*. In HeLa cells, the measured values were actually above the ones in MCF-7 cells, indicating a better penetration within the cervix cancer cells. Furthermore, the

values for the chimeric peptides were about 30-times higher than for sC18*. Hereby, it is obvious that the internalization rates for N50-sC18* and NrTP-sC18* were different from the ones in MCF-7 cells.

Anyway, the evident increase of internalized peptides confirmed the hypothesis, that due to the potent formation of α-helices, the chimeric sequences N50-sC18* and NrTP-sC18* were able to interact with the cell membranes in an even better way than sC18* alone, and the peptides could then translocate into the cells in highly efficient rates.

4.3.3 Defining the intracellular localization cells after internalization

Despite the fact that the newly described CPPs N50-sC18* and NrTP-sC18* translocated into the two observed cancer cells in high rates, it is not known how they behave afterwards and especially where they are located within the cells. As they carry a sequence that should trigger the transport to the nuclei or nucleoli, they presumable localize within the cell nuclei. To verify this idea, microscopic analyses were performed after incubating the cells with 10 µM of the CPPs. The results for HeLa cells are presented in figure 26.

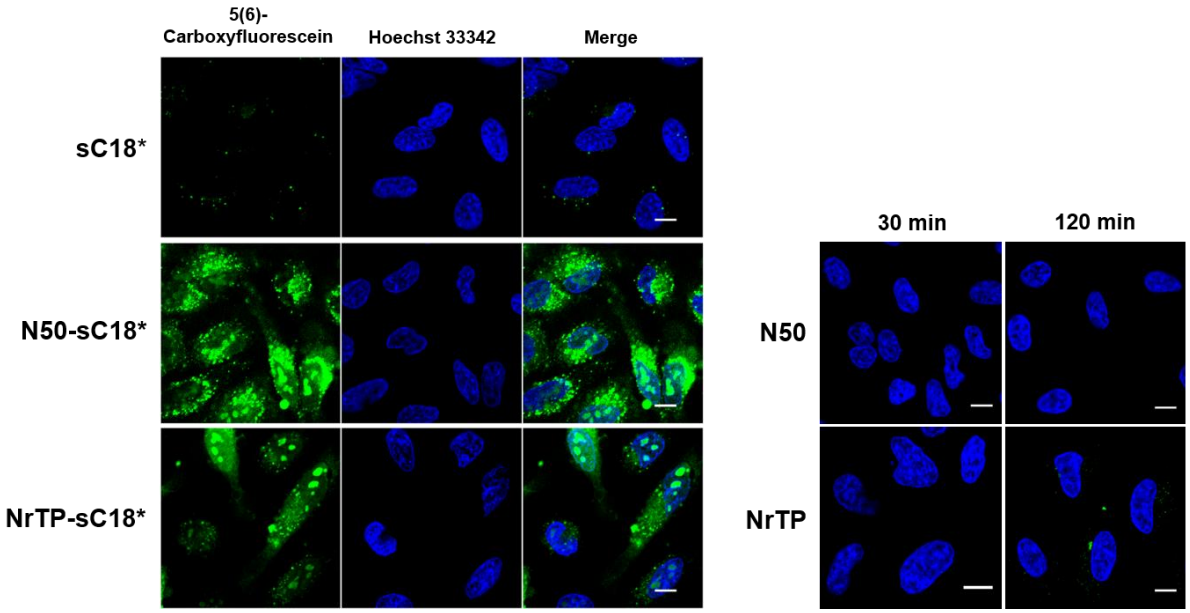

Figure 26: Uptake and distribution of CPP variants in HeLa cells. Fluorescence microscopy images after 30 min incubation with 10 µM CF-labeled peptides sC18*, N50, N50-sC18*, NrTP and NrTP-sC18* at 37 °C, respectively. For the right merge pictures, cells were incubated with 10 µM of the peptides N50 and NrTP for 30 or 120 min, Blue: Hoechst nuclear stain, Green: CF-labeled peptides, external fluorescence was quenched with trypan blue for 30 s, Scale bar is 10 µm.

It could be shown that sC18*, as expected from the flow cytometry results, was only marginally taken up compared to N50-sC18* and NrTP-sC18*. Only small dots were detectable, which

were probably representing vesicles, since an endocytotic uptake way for this CPP and its longer version sC18 were already demonstrated (chapter 4.1) [19, 73, 77]. Observing the microscopic pictures on the right side of the figure, the nuclear localization sequence N50 alone was not noticeable present within the cells at this concentration, not even after a longer incubation period of two hours. In contrast, the uptake rate of the fusion peptide N50-sC18* was much higher compared to the two peptides sC18* and N50 alone, which was also confirmed by the flow cytometry results (figure 25). Examining the localization of the CPP, it is obvious that the CF-labeled peptide was distributed in the whole cell. It seemed to accumulate within the cytoplasm, especially around the nucleus, but also a diffuse green signal could be registered, indicating free peptide, which was not enclosed in vesicles. In addition to that, the peptide was capable to overcome the cell nuclei membrane and also accumulated in the nuclei. The same localization pattern and amount of internalized peptides could be observed after 2 hours of incubation (data not shown).

More or less the same results could be examined for the peptides NrTP and NrTP-sC18*. The NrTP sequence alone was not detectable after incubation of HeLa cells for 30 min, but after a longer incubation period of two hours, some green signals within the cytoplasm could be observed. Notably, for the fusion peptide NrTP-sC18* a much higher internalization rate could be detected and especially for this CPP a strong accumulation within the nucleoli was visible. This confirmed the theory that the NrTP sequence is targeting these regions in the nuclei [35]. Also for this fusion peptide, studies after 120 minutes were done and the uptake was even slightly higher after this period of incubation (data not shown). As the internalization with 10 µM of the peptides was already really high and the accumulation, especially for N50-sC18* was not precisely detectable caused by an intense green signal in the whole cell, another set of microscopic observations was performed using a lower peptide concentration of 1 µM. The results for the fusion peptides are presented in figure 27.

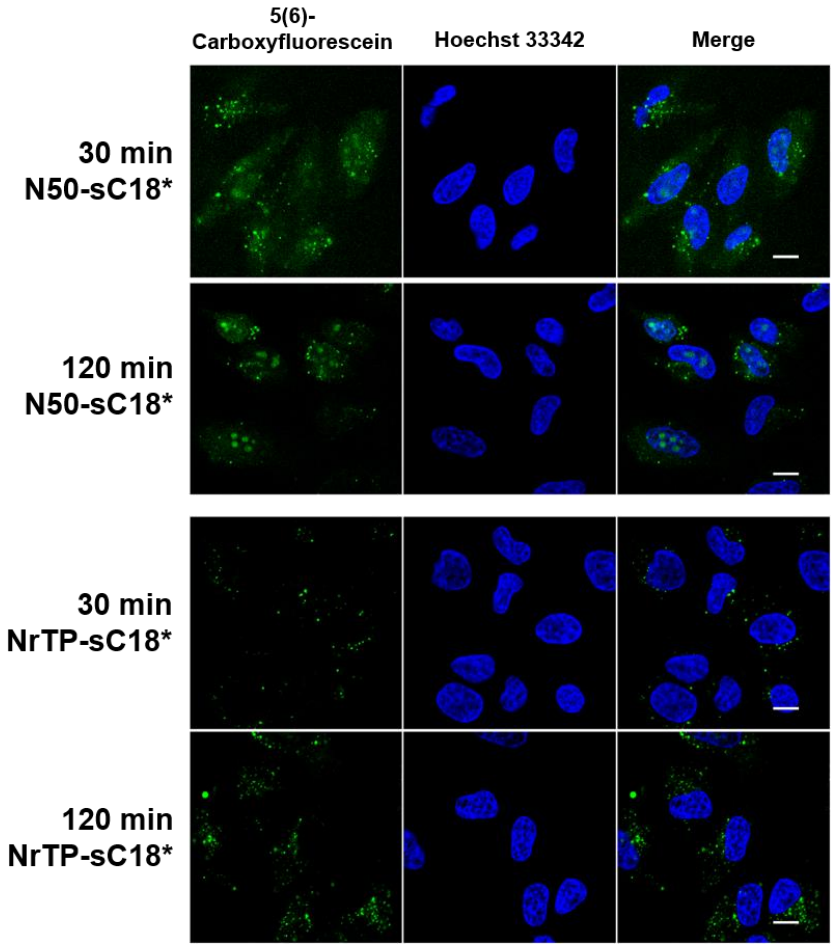

Figure 27: Uptake and distribution of CPP variants in HeLa cells at low concentrations. Fluorescence microscopy images after 30 or 120 min incubation with 1 µM CF-labeled peptides N50-sC18* or NrTP-sC18* at 37 °C, respectively. Blue: Hoechst nuclear stain, Green: CF-labeled peptides, external fluorescence was quenched with trypan blue for 30 s, Scale bar is 10 µm.

Next to this, also the shorter fractions, namely sC18*, N50 and NrTP alone were tested at these concentrations for 30 and 120 min, but hereby no green signal could be registered (data not shown). On the contrary, the pictures in figure 27 show that both fusion peptides were able to internalize the cells in efficient ways. Obviously, the uptake was less compared to the rates at a concentration of 10 µM.

For the upper pictures representing the peptide N50-sC18*, also an adequate signal within the nuclei could be identified. Next to this, a diffuse signal within the cytoplasm was visible, supporting the idea, that the peptides entered the cells by direct penetration or by endocytosis with a subsequent release from the vesicles. Then, they are able to overcome the nuclear membrane [27]. After exposing the peptides for 2 h to the HeLa cells, the diffuse signal in the cytoplasm seemed to decrease and a more precise accumulation within the nuclei was detectable.

In contrast to this, the uptake of 1 µM of NrTP fused to sC18* indicated that the CPP at this concentration was able to enter the cells, but then seemed to accumulate in endosomes or somewhere else within the cytoplasm. The peptide was neither detectable in the nuclei nor in the nucleoli. The distribution was punctual so it is possible that the peptides entered into the cells at this concentration via endocytosis, but the concentration of the CPP was probably not high enough to escape from the vesicles. Hence, it was not possible for the peptides to interact with the nuclei membranes. This observation was different from the one that was made in figure 26, but it is known that the internalization ways of CPPs are depending among many factors besides their concentration [10]. So, one can conclude, that for NrTP-sC18*, the concentration should be higher than 1 µM for an efficient intracellular targeting to the organelle. Also a longer incubation time, as shown for 120 min, is not triggering the endosomal release, even when the intensity of green signal within the cells was slightly higher than after 30 min of incubation.

Consequently, it can be said that the fusion of N50 and NrTP to sC18* led to higher internalization rates and localization in the nuclei and nucleoli at a certain concentration, respectively. Taking all observations in consideration, the cell-penetrating peptide sC18* was probably bringing the CPPs within the cells and the combination of the amino acids of N50 and NrTP was triggering the transport to the cell nuclei and nucleoli. Anyway, showing much higher uptake rates of the fusion peptides, one can suggest that the combination of the two peptides also increased the ability to interact with the plasma membrane, probably due to the higher amount of positive charges, which could end in longer and stabilized α-helices.

Next, MCF-7 cells were investigated regarding the uptake of the new CPP variants. The microscopic analyses are depicted in the figures 28 and 29.

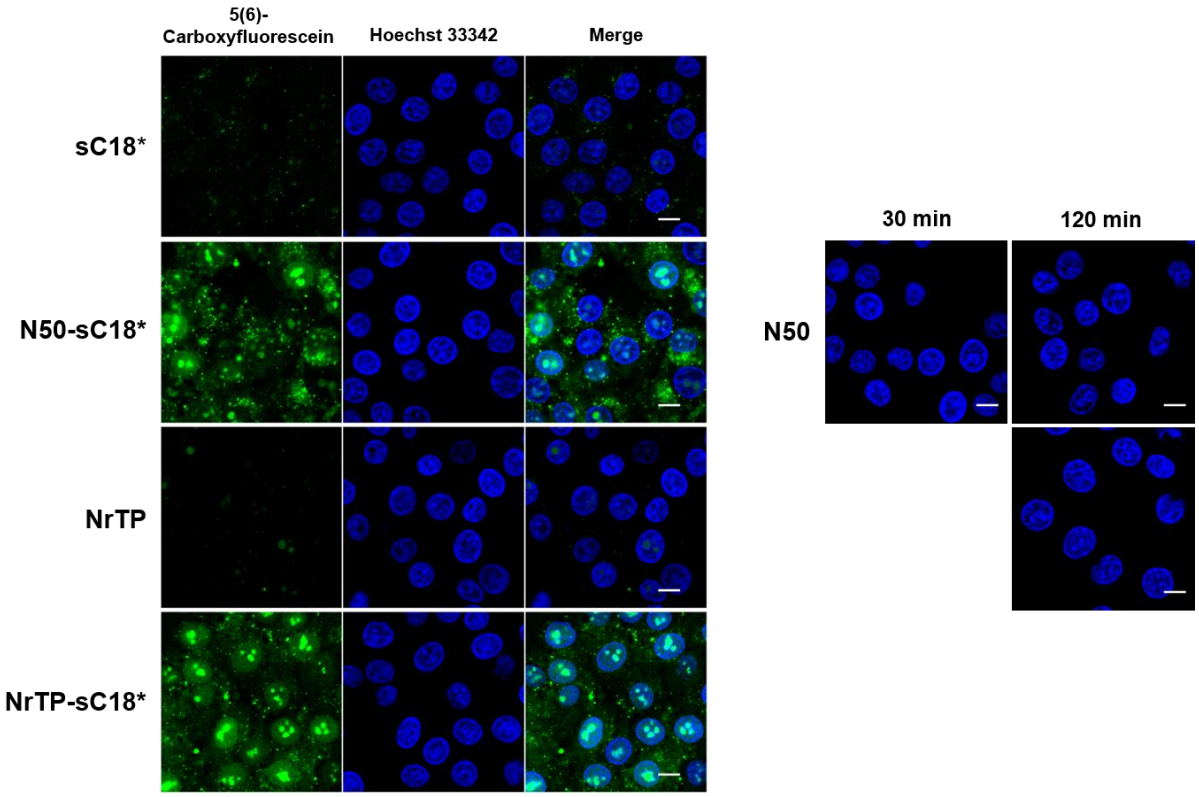

Figure 28: Uptake and distribution of CPP variants in MCF-7 cells. Fluorescence microscopy images cells after 30 min incubation with 10 µM CF-labeled peptides sC18*, N50, N50-sC18*, NrTP and NrTP-sC18* at 37 °C, respectively. For the right merge pictures, cells were incubated with 10 µM of the peptides N50 and NrTP for 30 or 120 min, Blue: Hoechst nuclear stain, Green: CF-labeled peptides, external fluorescence was quenched with trypan blue for 30 s, Scale bar is 10 µm.

Evaluating figure 28 on the left side, the peptide sC18* internalized into MCF-7 cells probably via endocytosis. Moreover, the uptake seemed to be higher compared to HeLa cells. Again, no green fluorescence could be detected within the cell nuclei. Next to this, no visible uptake of the N50 sequence alone could be noticed, not even after an incubation time of 120 min. In contrast to this, the fusion peptide N50-sC18* was taken up by the cancer cells in high amounts, and furthermore, the peptides were able to localize within in the cell nuclei. Within the cytoplasm, a diffuse distribution as well as various agglomerations of green signal could be observed. So, the fusion of N50 to sC18* leads to higher internalization rates and a successful localization in the nuclei. The intensity of the green signal of labeled N50-sC18* is slightly reduced after an incubation time of 120 min (data not shown). This could be explained by a certain more precise dispersion towards the target and a degradation of unbound peptide in the cytoplasm. For a deeper understanding of the remaining CPPs after a longer exposition, more experiments should be performed.

Regarding the internalization of NrTP and NrTP-sC18*, a slightly different outcome compared to HeLa cells could be seen. Evaluating the microscopic pictures depicted in figure 28, the peptide NrTP was also capable to internalize in the cells by itself in small amounts and

localized mainly in the nucleoli as it is thought for. This effect could not be observed after 120 min (figure 28 right side). Anyway, as described above, the fusion of the two peptide sequences led to higher uptake rates and a strong co-localization with the cell nuclei and, especially visible in MCF-7 cells, with the nucleoli. Hereby, again the uptake after 120 min seemed to be less diffuse than after 30 min (data not shown). For a superior explanation of this phenomenon, more investigations need to be done. Also here, MCF-7 were treated with a concentration of 1 µM of the fusion peptides for 30 and 120 min, the results are presented in figure 29.

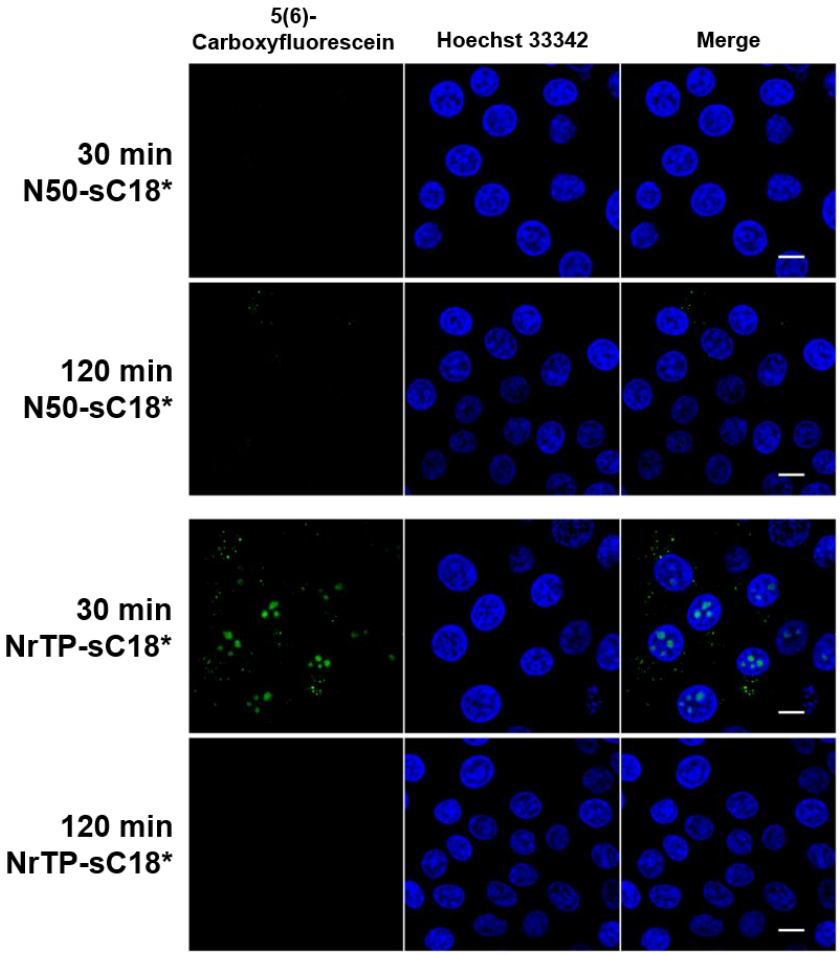

Figure 29: Uptake and distribution of CPP variants in MCF-7 cells at low concentrations. Fluorescence microscopy images after 30 or 120 min incubation with 1 µM CF-labeled peptides N50-sC18* or NrTP-sC18* at 37 °C, respectively. Blue: Hoechst nuclear stain, Green: CF-labeled peptides, external fluorescence was quenched with trypan blue for 30 s, Scale bar is 10 µm.

Hereby, the results were different from the ones with HeLa cells shown in figure 27. The only visible signal, which could be detected at this concentration, was after the treatment with NrTP-sC18* for 30 min. No uptake for sC18*, N50 and NrTP alone (data not shown), N50-sC18* (30 and 120 min) and NrTP-sC18* after 120 min could be seen. Comparing these results with the ones of the flow cytometer shown in figure 25, it could be proven that the uptake of

NrTP-sC18* is higher than the uptake of N50-sC18* also at low concentrations. The fact, that the CPP NrTP-sC18* was not visible after 120 min is also in correlation to the previously presented microscopic results (figure 28). Anyway, a prominent localization within the cell nucleoli in the MCF-7 cells could be noted.

4.3.4 Microscopic analysis of uptake at 4 °C

From previous studies, it was presumed that the CPPs enter the cells by direct penetration or by endocytosis followed by an endosomal release, which could already be shown for the CPP $(sC18)_2$ (chapter 4.2). Otherwise, they would not be untrapped in the cytosol and could not penetrate the cell nuclei membranes [27]. Another uptake study performed at 4 °C was done to get detailed insights into the mechanism of internalization. Hereby, the energy dependent pathways were shut down and the CPPs could just enter the cells by direct penetration [91]. MCF-7 and HeLa cells were treated with the fusion sequences for 30 min at 4 °C and were observed using a confocal laser scanning microscope. The pictures are presented in figure 30 for HeLa cells, and the results for MCF-7 cells are shown in figure 31.

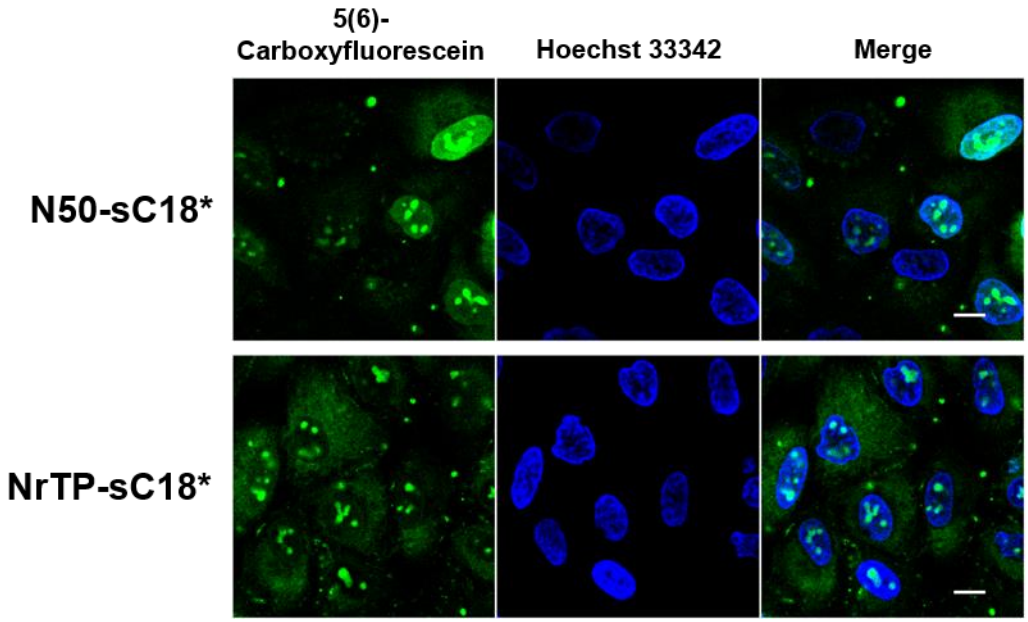

Figure 30: Uptake of CPP variants in HeLa cells at 4 °C. Fluorescence microscopy images after 30 min incubation with 10 µM CF-labeled peptides N50-sC18* or NrTP-sC18* at 4 °C, respectively. Blue: Hoechst nuclear stain, Green: CF-labeled peptides, external fluorescence was quenched with trypan blue for 30 s, Scale bar is 10 µm.

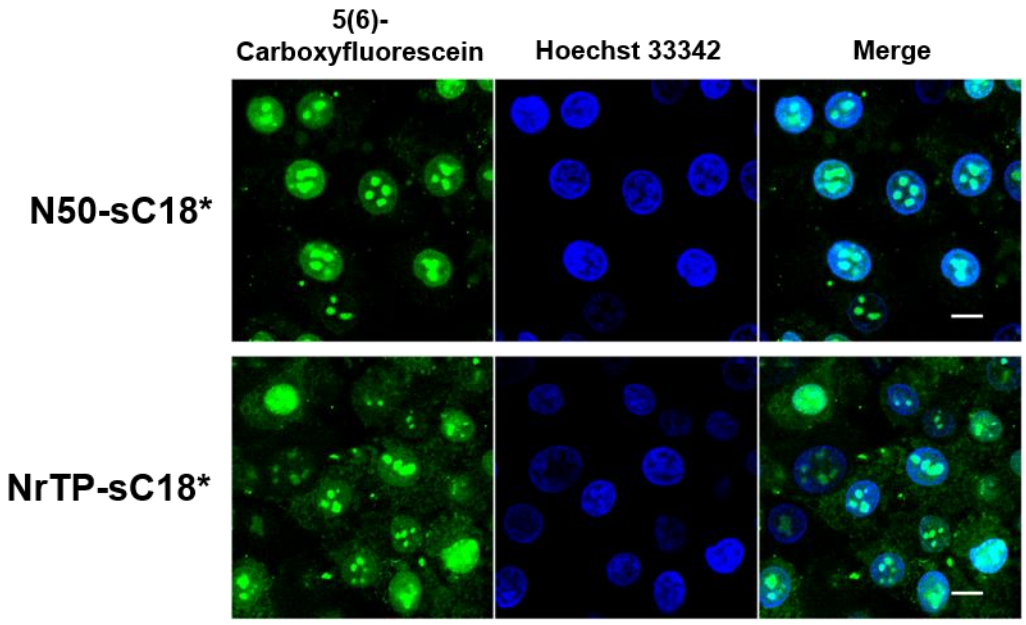

Figure 31: Uptake of CPP variants in MCF-7 cells at 4 °C. Fluorescence microscopy images after 30 min incubation with 10 µM CF-labeled peptides N50-sC18* or NrTP-sC18* at 4 °C, respectively. Blue: Hoechst nuclear stain, Green: CF-labeled peptides, external fluorescence was quenched with trypan blue for 30 s, Scale bar is 10 µm.

As shown in the previous figures, a prominent green signal for both cell-penetrating peptides N50-sC18* and NrTP-sC18* in HeLa and MCF-7 cells could be registered, which was visible in a diffuse signal distributed in the cytoplasm and strong accumulations in the cell nuclei and nucleoli. This leads to the interpretation that the sequences internalized into the cells in high amounts by direct penetration, because an internalization by endocytosis is suppressed at 4 °C [91]. These results are in coincidence with the uptake at 37 °C, whereby the peptides are capable to overcome the nuclei membranes. Therefore, the CPPs need to be free in the cytoplasm and an encapsulation within vesicles would hinder them in this step.

This uptake by direct penetration could already be published for many well studied cell-penetrating peptides, for example for the arginine-rich peptide TAT(48-60), which was used in numerous applications as delivery vectors [16, 116].

4.3.5 Defining the intracellular localization of CPPs

Until now, it is not clear, if the green signals that were distributed in the cytoplasm were just randomly spread peptides or if the CPPs accumulate in specific organelles. To get a better understanding about this, additional ER- and lysosomal tracker were used to stain the organelles in red. If the CF-labeled peptides accumulated in these compartments, the overlay of the green and red signals would appear yellow.

The studies with the endoplasmic reticulum marker in MCF-7 and HeLa cells did not show any co-localization of N50-sC18* or NrTP-sC18* with the ER. Therefore, an accumulation within the ER could not be determined. (data not shown)

Using the lysotracker in MCF-7 cells, no satisfying staining could be obtained (data not shown). The obtained results in HeLa cells appeared better and are shown in figure 32.

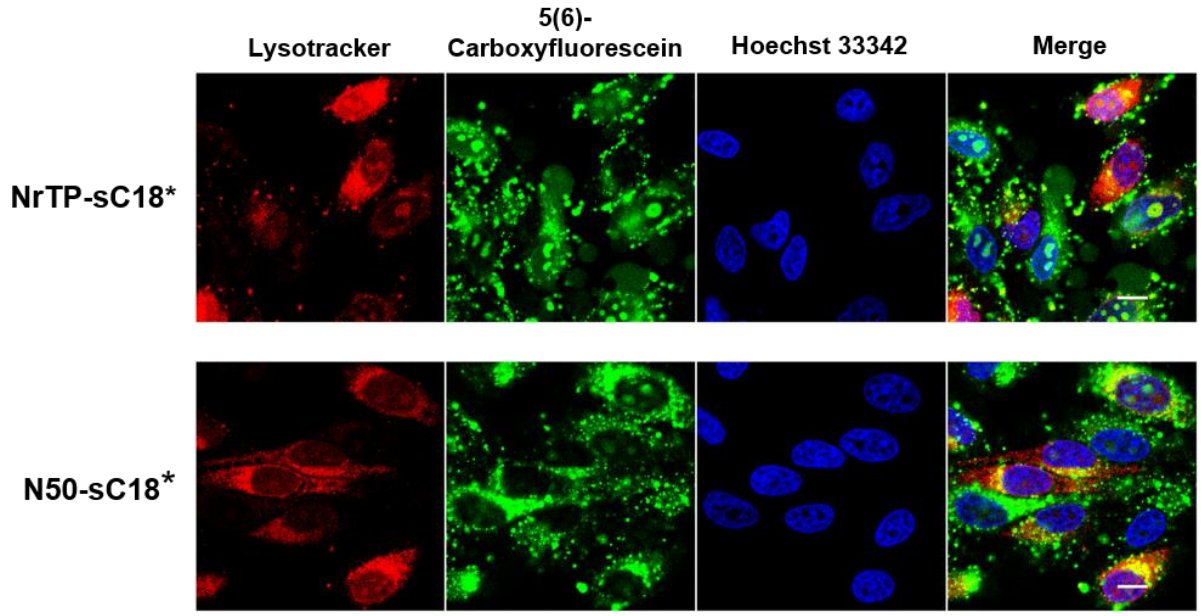

Figure 32: Intracellular localization of NrTP-sC18* and N50-sC18* in HeLa cells. Fluorescence microscopy images after 30 min incubation with 10 µM CF-labeled peptides N50-sC18* or NrTP-sC18* and 75 nM of lysosomal marker, respectively. Blue: Hoechst nuclear stain, Green: CF-labeled peptides, Red: Lysotracker, external fluorescence was quenched with trypan blue for 30 s, Scale bar is 10 µm.

As depicted in figure 32, the lysosomal staining in HeLa cells was successful. In merge pictures, one could notice some yellow regions indicating a localization of the CPPs in the lysosomes. Anyway, there were also many regions, where the peptides accumulated in other regions within the cytoplasm. It is possible that this accumulation did not occur in specific organelles in the cells, but just in agglomerations of the peptides in higher amounts. Some parts of the nuclei showed red fluorescence, indicating that the staining was not lysosome specific and should be improved further.

4.3.6 Cytotoxic profile of nuclei-targeting CPPs

After detailed investigation of the internalization and localization of the peptides, a closer look at their cytotoxicity profiles was taken. Therefore, MCF-7 and HeLa cells were exposed for 24 h to the CPPs sC18*, N50, N50-sC18*, NrTP and NrTP-sC18* in various concentrations

and then, the number of viable cells was determined. The results of the experiments are shown in figure 33.

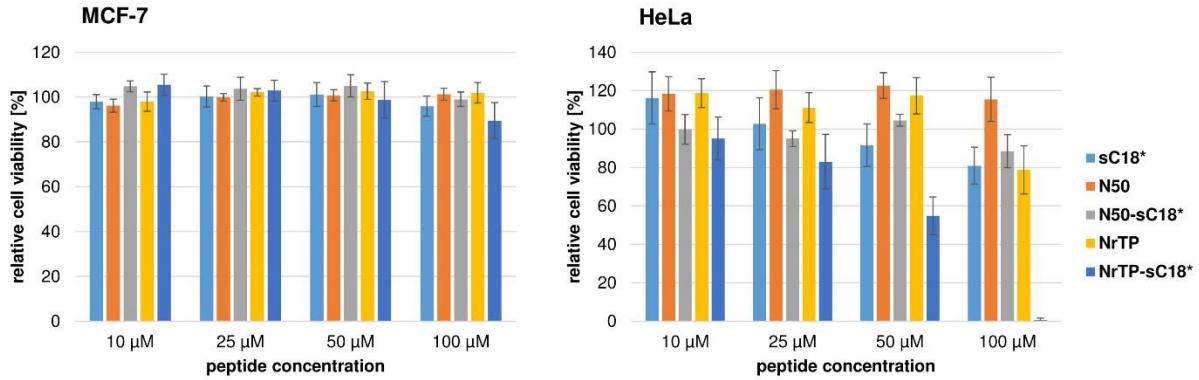

Figure 33: Cytotoxic profile of CPP variants for MCF-7 and HeLa cells. Cell viability assay based on resazurin after incubation with the CPPs sC18*, N50, N50-sC18*, NrTP and NrTP-sC18* for 24 h in various concentrations, untreated cells served as negative control and were set to 100%. 70% EtOH was used as positive control, which was subtracted from all results. Experiments were conducted in triplicate with *n = 2*. Error bars represent the standard deviations.

It is observable that none of the peptides was toxic to MCF-7 cells up to a concentration of 100 µM. Also after treating HeLa cells with the peptides, no significant toxicity for the CPPs sC18*, N50, N50-sC18* and NrTP up to a concentration of 50 µM could be observed. At 100 µM, the incubation with sC18*, N50-sC18* and NrTP resulted in a decrease of viable cells to about 80%. Horn *et al*. showed that sC18* is not toxic to MCF-7 and HEK-293 cells up to a concentration of 200 µM. To HeLa and HCT-15 cells, the CPP demonstrated slight cytotoxic effects at a concentration of 200 µM. [73] This is in correlation with the results obtained in this work. In contrast, for the chimeric peptide sequence NrTP-sC18* in HeLa cells at a concentration of 50 µM, about 50% of the cells were still viable whereas at a concentration of 100 µM all cells were dead. This observation is in agreement with the previously presented results of flow cytometric analyses, whereby it could be shown that the internalization rates of the chimeric variants are much higher in HeLa cells than in MCF-7 cells. Therefore, it is likely, that the interaction with the cervix cancer cell membranes was stronger and led to a disruption of the membrane, which caused cell death in the end. This idea could be confirmed by the execution of a cell lysis assay described above. However, all uptake experiments that were done with the peptides were conducted at concentrations between 1 and 10 µM, whereby they did not show toxic effects on the cells.

4.3.7 Complexation capability with pEGFP-N1 and pGL4.13

As described in the introduction, in many approaches, it is necessary to deliver DNA into cells and certainly into the nucleus. An electromobility shift assay (EMSA) with N50-sC18* and NrTP-sC18* was performed to register if the peptides are able to form complexes with plasmid DNA, which is necessary for its transport into the cells. Both sequences carry a high number of positive charges (12 for N50-sC18* and 13 for NrTP-sC18*), which theoretically enable them to interact with negatively charged plasmid DNA [117]. These differently charged components should form electrostatic complexes for efficient transport of the DNA to the cells. The ratios were calculated according to the negative charge of the DNA and the positive charges of the CPPs. For the EMSAs, a plasmid concentration of 100 ng was taken for good visibility on the agarose gel. If a complexation takes place, the electrophoretic migration rate of the DNA is reduced in comparison to naked DNA and therefore, the plasmid remains in the loading pocket of the gel. In figure 34, the assay is shown for the vector pEGFP-N1, the concentrations of N50-sC18* were 0.62 µM (1:1), 3.09 µM (5:1), 6.18 µM (10:1) and 18.56 µM (30:1), respectively. NrTP-sC18* was used in the following concentrations: 0.57 µM (1:1), 2.86 µM (5:1), 5.71 µM (10:1) and 17.14 µM (30:1).

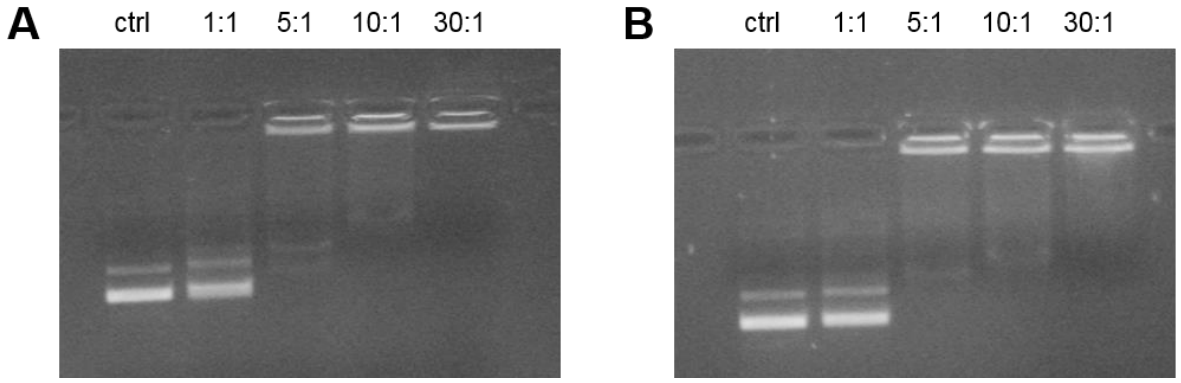

Figure 34: Complexation studies of CPPs with pEGFP-N1. Electromobility shift assay (EMSA) using the CPPs N50-sC18* **(A)** or NrTP-sC18* **(B)** and the plasmid pEGFP-N1 after complexation for 30 min in different charge ratios (1:1, 5:1, 10:1, 30:1), pEGFP-N1 plasmid alone served as negative control.

Evaluating the EMSAs in figure 34, one can notice that both peptides, namely N50-sC18* and NrTP-sC18*, were able to form complexes with the plasmid pEGFP-N1 in the ratios 5:1, 10:1 and 30:1. At a ratio of 1:1, the DNA could still move to the positively charged anode like the control plasmid, whereas the bigger complexes were not able to move through the agarose matrix. For the complexation at 5:1 ratio, still some traces of free DNA were visible. Hence, for the transfection using the EGFP-plasmid, a charge ratio of 10:1 was used.

Additionally, another plasmid was used in this study and therefore another EMSA was performed using the luciferase encoding vector pGL4.13 [luc2/SV40] (figure 35). The ratios were also calculated from the charges of CPPs and plasmid and a vector concentration of 100 ng was chosen. The concentrations of N50-sC18* were 0.63 µM (1:1), 3.16 µM (5:1), 6.31 µM (10:1) and 18.94 µM (30:1) and of NrTP-sC18* 0.58 µM (1:1), 2.91 µM (5:1), 5.83 µM (10:1) and 17.48 µM (30:1).

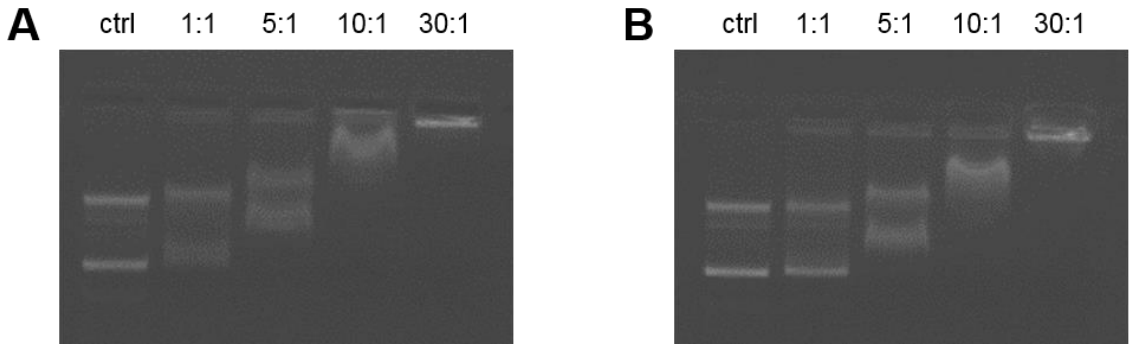

Figure 35: Complexation studies of CPPs with pGL4.13. Electromobility shift assay (EMSA) using the CPPs N50-sC18* **(A)** or NrTP-sC18* **(B)** and the plasmid pGL4.13 [luc2/SV40] after complexation for 30 min in different charge ratios (1:1, 5:1, 10:1, 30:1), pGL4.13 plasmid alone served as negative control.

In figure 35, it is visible that the complexation of the CPPs with the plasmid pGL4.13 occurred at a concentration of 30:1. At lower ratios, only partly complexation was visible. Consequently, the ratio of 30:1 was used in further experiments.

4.3.8 Transfection of MCF-7 and HeLa cells

Next, it was investigated, if the fusion peptides are able to deliver pDNA into cells. For transfection with the GFP encoding plasmid pEGFP-N1, cells were seeded in 8-well ibidis and treated with the peptide/vector complexes for 6 hours. After 48 hours, meanwhile the cells could express the green fluorescent protein, they were observed under the microscope. The pictures are presented in figure 36.

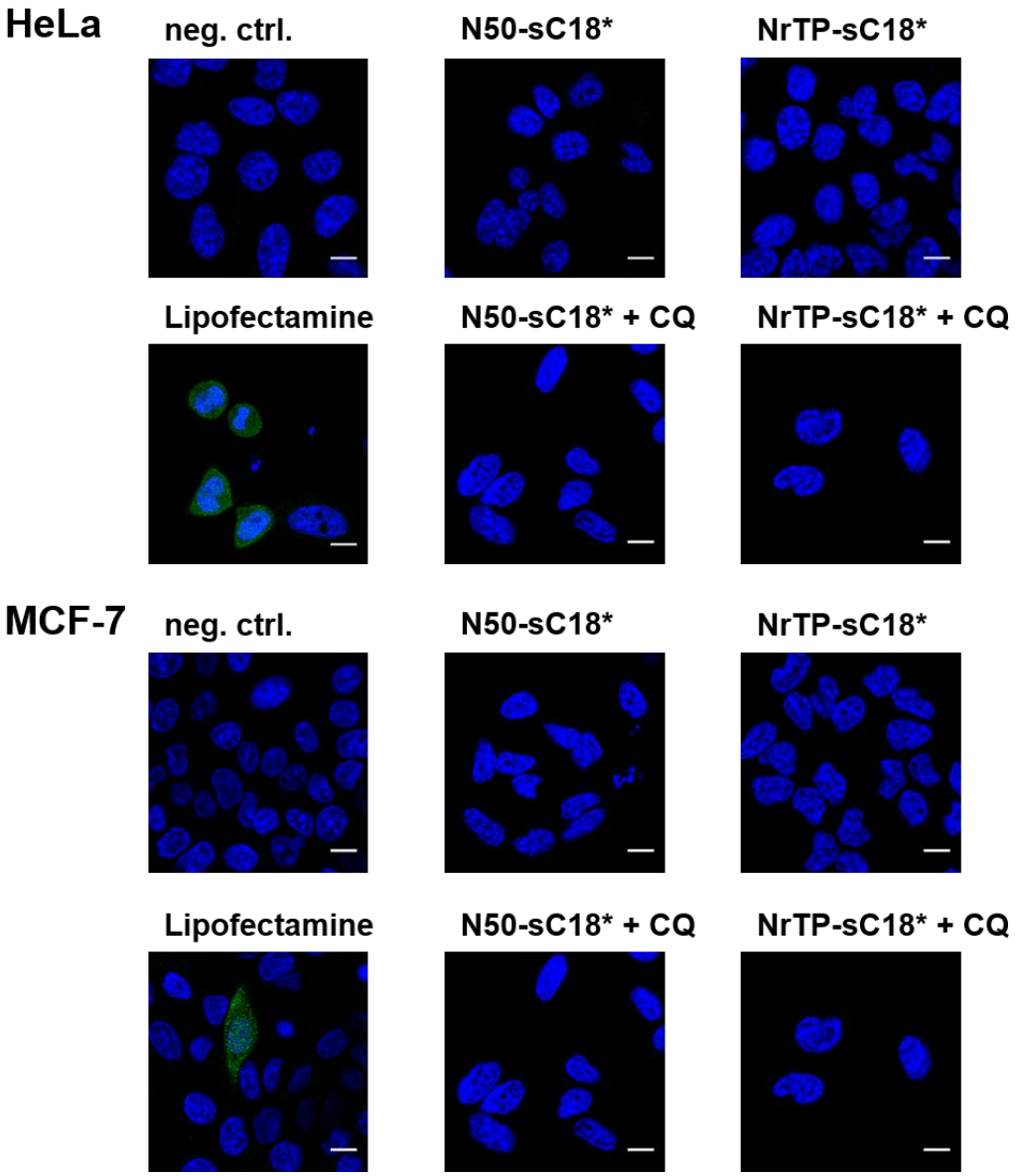

Figure 36: Transfection studies of CPPs with pEGFP-N1. Transfection of MCF-7 and HeLa cells with the plasmid pEGFP-N1 after complexation for 30 min with the peptides N50-sC18* or NrTP-sC18* with or without 100 µM chloroquine at a ratio of 10:1. 300 ng of plasmid were used, plasmid alone served as negative control, for positive control Lipofectamine®2000 was complexed with the vector for 5 min, Merge pictures are shown, Scale bar is 10 µm.

It is visible that in the negative control, whereby just plasmid alone was given to the cells, no green signal could be detected. On the contrary, after treating the MCF-7 and HeLa cells with the transfection reagent Lipofectamine®2000 and the vector, some green cells, which expressed the green fluorescent protein, could be detected. This confirms a successful positive control of the experimental setup. However, for both cell lines, not any transfected cell after treatment with the CPP/plasmid complexes was observed. Furthermore, also the addition of the endosomal release triggering agent chloroquine did not lead to successful transfection. Notably, if the peptides internalize into the cells by direct penetration, as it is assumed from

the former studies, the chloroquine would be redundant and should not have any effect on the cells. Hence, other ways for the improvement of transfection efficiency should be tried in the future.

The transfection experiments were furthermore performed using the other plasmid DNA, namely the pGL4.13 vector that encodes for the firefly luciferase enzyme. Cells were seeded in 96-well plates and treated with the complexes for 6 hours. As for the previously described assay, the cells were afterwards incubated for 48 hours and thereafter, a luciferase assay reagent containing beetle luciferin, which can be oxidized by luciferase to oxiluciferin, was added to each well. During this reaction, a flash of light is generated that can be detected with a plate reader measuring the luminescence [118]. To improve the transfection rate, chloroquine was added as well. The results of these experiments can be seen in figure 37.

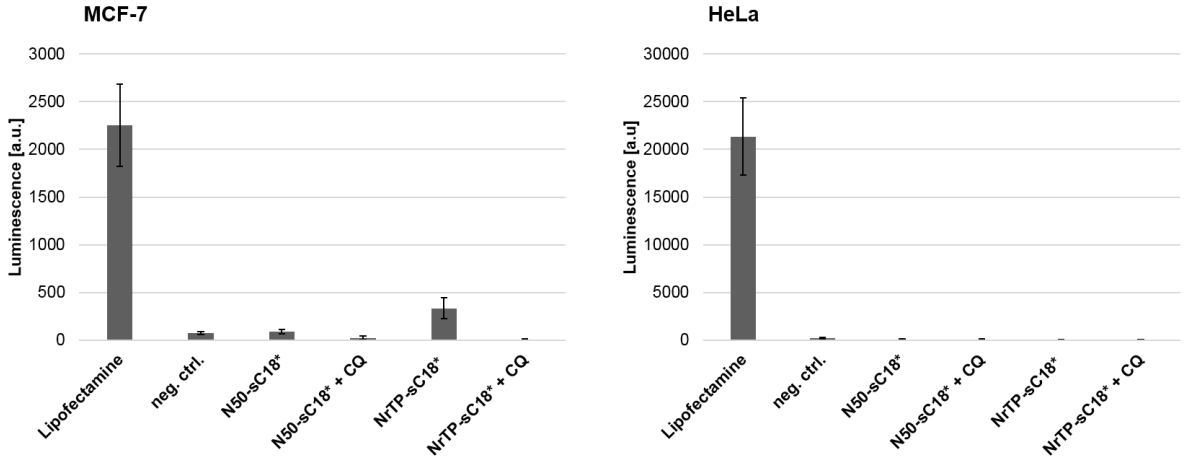

Figure 37: Transfection studies of CPPs with pGL4.13. Transfection of MCF-7 and HeLa cells with the plasmid pGL4.13 [luc2/SV40] after complexation for 30 min with the peptides N50-sC18* or NrTP-sC18* with or without 100 µM chloroquine at a ratio of 30:1. 300 ng of plasmid were used, plasmid alone served as negative control, for positive control Lipofectamine was complexed with the vector for 5 min. Experiments were conducted in triplicate with *n = 2* (except for the CQ experiments with *n = 1*), error bars represent the standard derivation.

First, it can be concluded that in both cell lines, the positive control using the transfection reagent Lipofectamine was able to successfully transfect the cells. The results are evidently better in HeLa than in MCF-7 cells, which was similar to the results for the transfections with the pEGFP-N1 vector (figure 36). Apart from that, one can say that the transfection with the tested CPPs was not successful. Looking at the HeLa cells, no transfection at all could be noticed. In MCF-7 cells, a slight signal of the cells transfected with the peptide NrTP-sC18* could be executed, but this result was not statistically significant. Taking the uptake studies of the two combined CPPs in MCF-7 cells in consideration, whereby the NrTP-sC18* show apparent higher internalization than N50-sC18* (figure 25), one can conclude that this was

correlated to the transfection efficiency. NrTP-sC18* is taken up in higher amounts and can therefore probably bring more plasmid DNA into the cancer cells, which results in low expression of the luciferase-encoding vector.

The results of the experiments using the endosomal release triggering agent chloroquine, that were incidentally just done once, need to be considered cautiously. Hereby, the chloroquine was added directly to the solution when mixing the reagents for the complexation. Maybe, a higher output can be observed, adding the CQ later, when giving the complexes to the cells, as Rennert *et al.* did in their studies in 2008 [119]. Furthermore, there are other possibilities to enhance the transfection potential of cell-penetrating peptides. Cationic polymers like polyethyleneimines (PEI) could be added in low concentrations, so that the acidification process which is essential for the transition from endosomes to lysosomes is slowed down [120]. Another possibility to improve the transfection rate is the addition of inactivated viral particles or recombinant proteins. They have the capability to disrupt endosomes or free radicals and could therefore cause membrane damage [121, 122]. A further alternative is the introduction of a fatty acid. Futaki *et al.* showed in 2001 that in this way the transfection efficiency of octaarginine could be enhanced. [123] Also the delivery of siRNA could be improved by fatty acid-CPPs conjugates [110].

Another aspect that needs to be considered is the fact that the peptides seem to enter the cells by direct penetration. Their ability to form complexes with the negatively charged plasmid DNA does not say anything about the entering pathway of the peptide/DNA complexes. As it is known that CPPs can internalize cells in various pathways and direct penetration and endocytosis can also occur simultaneously, it is possible that some peptide/plasmid complexes can enter the cells via endocytosis [26]. Maybe, the DNA is transported by the CPPs within the cells, but then the interaction capability is disturbed by intracellular proteins or peptides and the DNA is degraded by cellular DNases before entering the cell nuclei [124]. Anyway, due to the fact that the effective gene delivery is subordinated to the endosomal uptake pathway and the transfection efficiency was low in both experiments, the results confirmed an uptake by direct penetration for the CPPs N50-sC18* and NrTP-sC18*. [125, 126]

4.3.9 Cargo delivery of Doxorubicin

Since the pDNA delivery studies were not successful in the first try, the transport capability of N50-sC18* and NrTP-sC18* were investigated in further experiments with smaller cargoes. Therefore, HeLa and MCF-7 cells were exposed to the chemotherapeutic drug doxorubicin (DOX) that is already used to treat cancer [http://www.cytrx.com/aldoxorubicin, 24.09.2017]. Doxorubicin interacts with DNA by intercalation and thereby inhibits the macromolecular biosynthesis [127, 128]. Some publications reported that the covalent binding of doxorubicin

to different CPPs induced cell death in various cell lines [129, 130]. Furthermore, doxorubicin is known to be fluorescent [131] and this property was used in a first approach to test, if the peptides were able to trigger the transport of the drug into the cells. Therefore, DOX and the sequences N50-sC18* and NrTP-sC18* were co-incubated with HeLa and MCF-7 cells, respectively and observed for red fluorescence afterwards. The results are shown in figures 38 and 39.

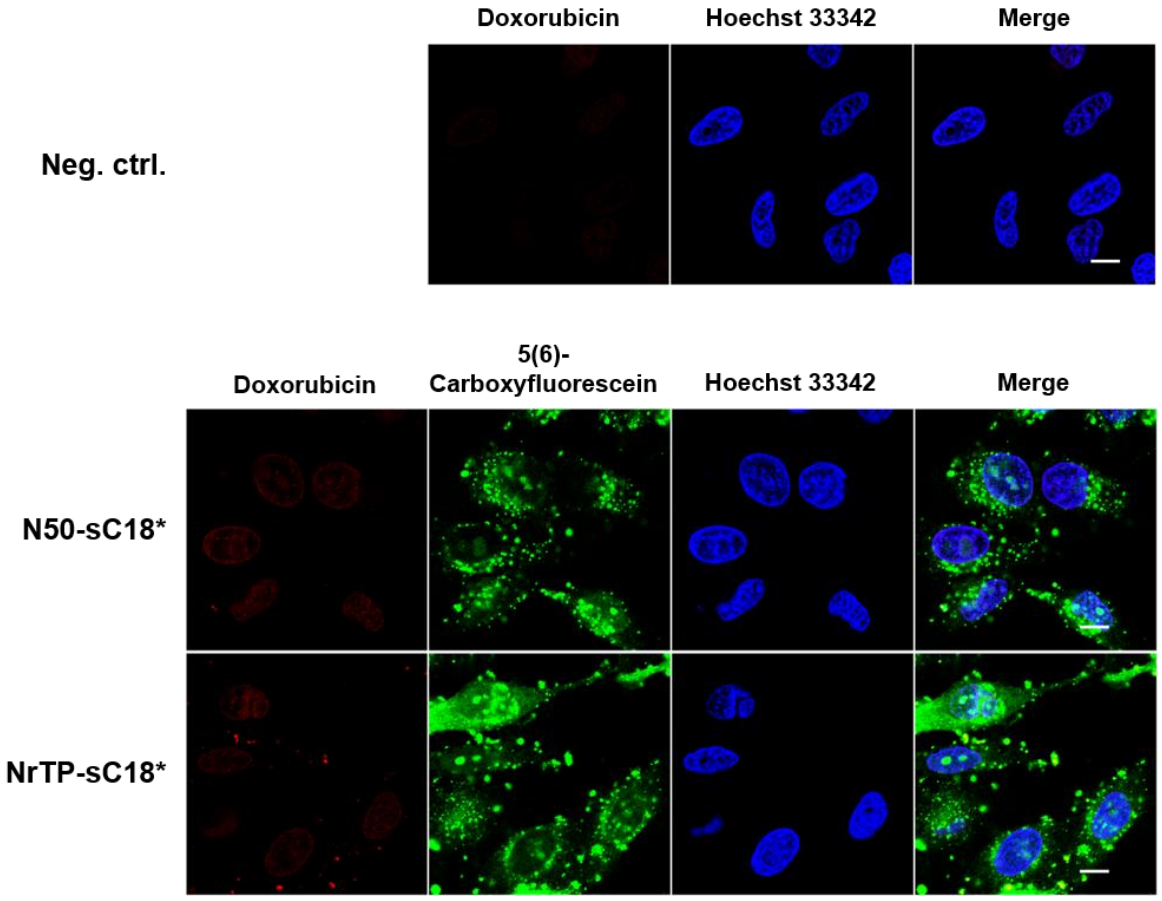

Figure 38: Uptake and delivery of DOX into HeLa cells. Fluorescence microscopy images after 30 min incubation with 10 µM CF-labeled peptides N50-sC18* or NrTP-sC18* co-incubated with 10 µg/ml doxorubicin at 37 °C, respectively. Cells treated with DOX alone served as negative control, Blue: Hoechst nuclear stain, Green: CF-labeled peptides, Red: doxorubicin, external fluorescence was quenched with trypan blue for 30 s, Scale bar is 10 µm.

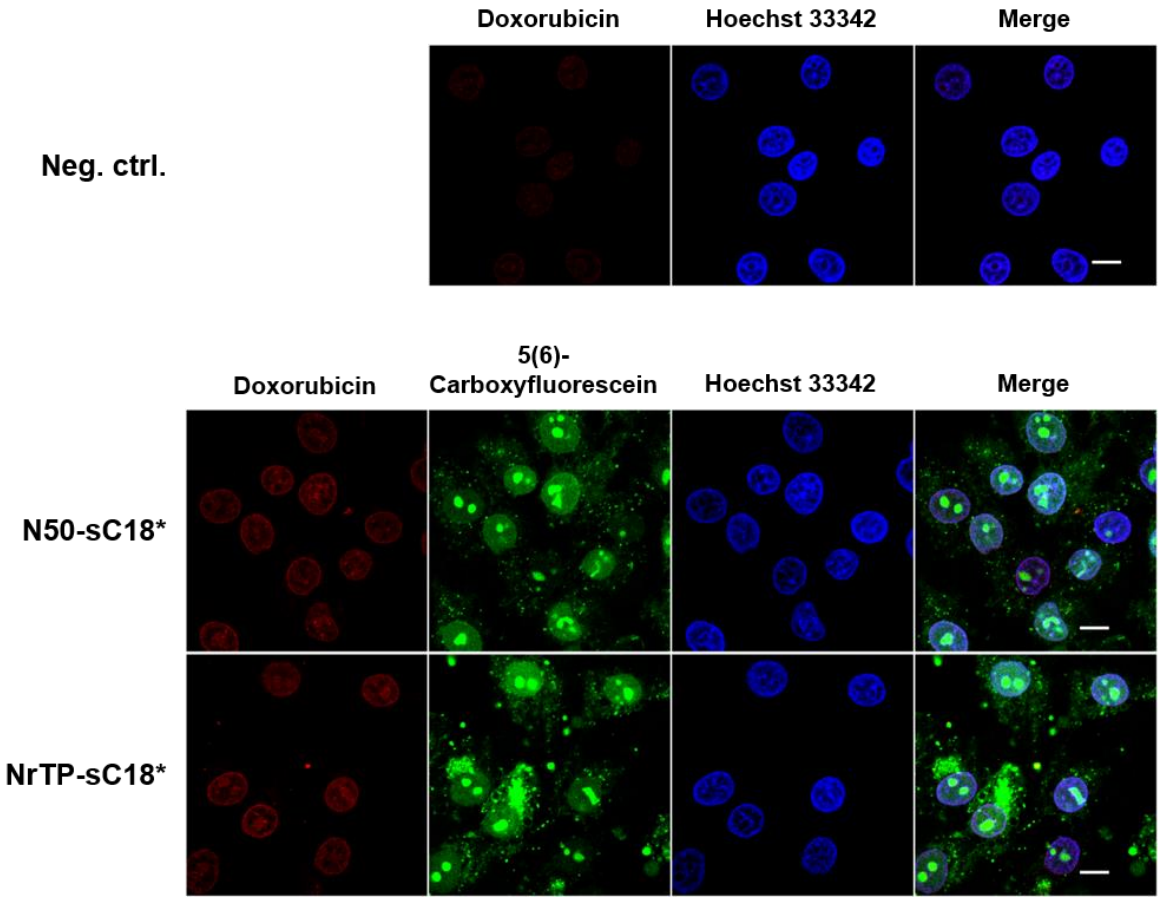

Figure 39: Uptake and delivery of DOX into MCF-7 cells. Fluorescence microscopy images after 30 min incubation with 10 µM CF-labeled peptides N50-sC18* or NrTP-sC18* co-incubated with 10 µg/ml doxorubicin at 37 °C, respectively. Cells treated with DOX alone served as negative control, Blue: Hoechst nuclear stain, Green: CF-labeled peptides, Red: doxorubicin, external fluorescence was quenched with trypan blue for 30 s, Scale bar is 10 µm.

As depicted in the figures 38 and 39 the cell nuclei appeared in normal shape confirming the applied concentrations not to be toxic when given for 30 min to the cells. Furthermore, a slight red fluorescence could be detected in the negative control, indicating that the chemotherapeutic drug was also able to translocate in the cells by itself at this concentration. Apart from that, looking at the bottom pictures showing the co-incubation of DOX with the CPPs, one can say that the intensities of the red fluorescent signals visible in the cell nuclei were more intense compared to the negative control. This effect was more intense in MCF-7 cells. As a result, these pictures could give a first hint about the drug transport capability of the peptides N50-sC18* and NrTP-sC18* in the two observed cancer cells lines. As this is just a first estimation, in the following, a killing assay was established to verify the transport and toxic effects of the drug.

Therefore, doxorubicin was incubated for 48 hours at different concentrations. It turned out that 5, 10 and 15 µg/ml doxorubicin was to high for these experiments, because no viable cells

could be detected after the treatment (data not shown). At 0.1 and 0.5 µg/ml all cells remain viable after the experiment (data not shown), so these concentrations were too low. At a concentration of 1 µg/ml in MCF-7 cells, the cell viability decreased to about 60%. At this concentration doxorubicin seemed to be high enough to theoretically kill the cells, thus the following assay was done under these conditions. Hence, 48 h after the treatment with the drug alone or co-incubated with 10 µM of the peptides sC18*, N50-sC18* and NrTP-sC18*, a cell viability assay was performed, whose results are shown in figure 40.

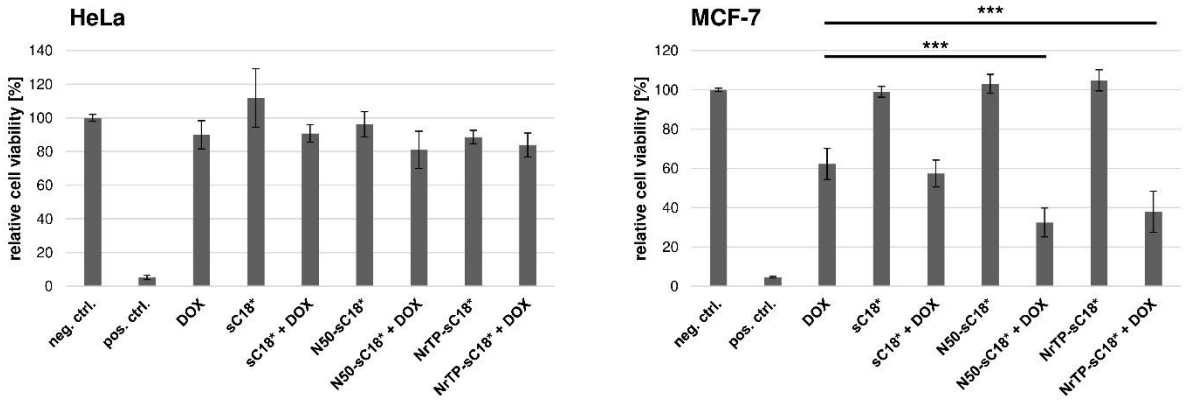

Figure 40: Cargo delivery of doxorubicin in HeLa and MCF-7 cells. Cytotoxicity assay based on resazurin after incubation with 1 µg/ml doxorubicin, 10 µM sC18*, N50-sC18* or NrTP-sC18* alone or co-incubated with 1 µg/ml doxorubicin for 48 h, respectively. Untreated cells served as negative control, cells treated for 10 min with 70% EtOH as positive control. Experiments were conducted in triplicate with *n = 2,* error bars represent the standard derivation.

As it is depicted in figure 40, the cargo delivery ability of the CPPs was different according to both cancer cell lines. In HeLa cells, the doxorubicin alone and also the CPPs alone did not show any toxicity. Furthermore, the co-incubation of the agent with the chimeric peptides N50-sC18* and NrTP-sC18* also did not lead to a decreased cell viability. The results for the positive control were successful with a remaining number of viable cells of about 5%, so the assay was per se working properly. For the doxorubicin control, it seemed that the applied concentration of 1 µg/ml is not high enough to harm the cells. The tests on HeLa cells should be repeated using another, higher doxorubicin concentration.

In contrast to that, the experiments on MCF-7 cells were more successful. As shown in figure 40 on the left hand side, the treatment with doxorubicin alone ended up in a number of viable cells about 60%. The peptides alone were not toxic at a concentration of 10 µM, which was already mentioned in chapter 4.3.6. In contrast, when co-incubating the CPPs and the chemotherapy drug, the toxic effect of doxorubicin could be improved. After treatment with N50-sC18*, the number of viable cells was around 30%, for NrTP-sC18* around 40%. The effect of doxorubicin could be enhanced about 20 – 30% when triggering its transport to the

cell nuclei in MCF-7 cells. To show that this effect was not caused by the sC18* sequence, this CPP was tested in co-incubation in the same conditions. Hereby, no difference to the treatment with doxorubicin alone could be observed. This proved that the combination of the nuclear targeting sequences N50 and NrTP and the cell-penetrating peptide sC18* led to an increased transport of the drug to the cells and their nuclei. Then, the chemotherapeutic drug could fulfil its function, intercalated with the DNA and finally led to cell death in a high number of cells.

These results show that the CPPs N50-sC18* and NrTP-sC18* support the transport of the chemotherapeutic drug doxorubicin into breast cancer cells. Interestingly, the herein presented non-covalent approach is very efficient, compared to a recent described CPP-mediated DOX transport, where the drug was covalently coupled to the CPP [130].

Summarizing the fusion of the nuclear localization sequences N50 and NrTP to the CPP sC18* resulted in two peptides, that showed extremely high uptake rates and specific localization in the cell nucleus.

5 CONCLUSION AND OUTLOOK

5.1 Summary and conclusion of studies with linear and branched dimeric sC18 versions

This chapter examined the investigation of the two cell-penetrating peptides sC18 and sC18*, as well as their dimeric, precisely branched and linear, versions.

All peptide variants were successfully synthesized via solid-phase peptide synthesis in an unlabeled and CF-labeled version. The results of circular dichroism spectroscopy revealed that all peptide variants were able to exhibit an α-helical structure in the presence of TFE. Moreover, all variants internalized in higher extent into cancer cells than in non-cancer cells, pointing to a potential cell selectivity. Furthermore, the internalization rate of the dimeric peptides $(sC18)_2$, $(sC18^*)_2$, $lin(sC18)_2$ and $lin(sC18^*)_2$ was increased compared to their monomeric forms, however no significant difference between the dimerized versions could be obtained. The cytotoxic profiles revealed that the short peptide versions did not exhibit cytotoxic effects to both cell lines in the tested concentrations and furthermore, no cell lysis could be detected. In contrast to this, all dimeric CPPs exhibited a more toxic effect on MCF-7 cells than on HEK-293 cells and showed also high membrane lysis events in the cancer cell line. The two branched variants in HEK-293 cells did not show a difference in toxicity, whereas in MCF-7 cells the truncated version $(sC18^*)_2$ was less toxic and fewer membrane lysis compared to the longer version $(sC18)_2$ could be demonstrated. Also the linear variants showed the same toxicity as the branched ones in HEK-293 cells, but in MCF-7 the linear sequences were slightly more toxic. One can conclude that the branching of the peptide sequence led to a reduction of the cytotoxicity.

The selectivity of the peptides for the different cell types could be explained by investigating different artificial membrane systems, whereby it could be demonstrated that the CPPs were not able to overcome neutrally charged membranes, which represent the plasma membranes of non-cancer cells. In contrast to this, the accumulation of the peptides on negatively charged vesicles, symbolizing cancer cell membranes, was very high. This might be an explanation for the increased internalization and cytotoxicity of the CPPs into the cancer cell line MCF-7.

The microscopic analysis illustrated that the different toxicity profiles were not correlated to the amount of CPP within the cell, since all longer peptide versions exhibited an equal uptake rate. This leads to the conclusion, that a membrane disrupting process during internalization of the peptides was responsible for the different cytotoxicities. The LDH release assay revealed an efficient membrane disrupting event at a concentration of 10 µM for 1 h of the longer peptides

versions. Since the microscopic analyses were performed using 10 µM for 30 min, it is likely that the high uptake rates are correlated with the membrane destabilization induced by the CPPs. As the cell nuclei appeared normally and healthy, an evocation of toxicity did not happen after this short period of time. The toxicity assays were performed after 24 hours of incubation with the peptides. So, it is likely that the membrane disruption of the CPPs led to higher penetration rates with a followed cell death induced some hours later.

Stephanie Natividad-Tietz investigated in previous experiments the transfection capacity of all variants in HEK-293 cells. Thereby, it was shown that the branched and linear peptides revealed slightly higher transfection rates than the monomeric peptides sC18 and sC18*. Anyway, there were no significant differences among each other and the transfection rate for all tested sC18 derivatives were extremely poor compared to the commonly used transfection reagent Lipofectamine®2000. [Natividad-Tietz, Dissertation 2016]

Taking all results of this study in consideration, it can be concluded, that the longer dimeric branched variant $(sC18)_2$ showed the highest potential for a lytic anticancer peptide. Without the branching, the sequence forms a longer helix, compared to the branched versions, which exhibited two α-helical structures linked by a peptide bond. Maybe this was triggering the more intense membrane disruption by lin$(sC18)_2$. Thus, the branching decreased the unselective toxic property, resulting in a higher selectivity against cancer cells.

5.2 Summary and conclusion of $(sC18)_2$ studies

In chapter 4.2, a more detailed investigation of the dimeric cell-penetrating peptide $(sC18)_2$ in comparison to its monomeric parent peptide sC18 was performed. In flow cytometric analysis, the different uptake rates of the CPPs could be affirmed. The translocation rates of $(sC18)_2$ were much higher than the ones of the monomer sC18 in both cell lines. Moreover, the internalization into the cancer cell line MCF-7 was much higher than into the non-cancer cells HEK-293. Nevertheless, at very low concentrations of 0.823 nmol, which could be elucidated with the radiolabeled NODAGA-coupled peptides, no difference in the internalization rates of both peptides in both cell lines occurred. This demonstrated, that the peptide selectivity was only given at concentrations in the micromolar range.

Besides, it could be demonstrated that the internalization rates were decreased at 4 °C, whereby all energy-dependent mechanisms were highly reduced in the cells. This effect was very distinct in HEK-293 cells, leading to the hypothesis that sC18 and $(sC18)_2$ penetrate the cells mainly by endocytosis. This theory was confirmed by observing the cells six hours after incubation with the peptides, where still all green signals were present in vesicles. The CPPs seemed to be entrapped in endosomes and be then degraded in the lysosomal pathway, which

is also explaining why they never occurred in the nuclei of the non-cancer cells. Anyway, various reagents like chloroquine, calcium and sucrose could trigger the endosomal release in this cell line. The experiment with endosomal release triggering substances was more efficient for the dimer than for the monomer, but was not caused by toxic or lytic effects.

In the cancer cells, the CPPs also occurred within the nuclei, indicating an endosomal release, so that they were able to overcome the nuclei membrane. The internalization was not fully inhibited at 4 °C, indicating a combination of endocytosis and direct penetration, which could still occur at low temperatures. Furthermore, six hours after incubation with the CPPs, almost no green signal could be detected in the cells. It is likely, that the peptides were able to leave the endosomes, could translocate in the nuclei and were degraded within the cytoplasm after distinct amount of time.

An internalization and cytotoxicity screening of sC18 and $(sC18)_2$ on several different cell lines confirmed that the uptake in cancer cell lines was increased compared to the non-cancer cells HEK-293. Furthermore, also the toxicity studies approved a specific preference for the neoplastic plasma membranes. The IC_{50} values were in the lower micromolar range in all different types of cancer cells that were investigated.

The cancer cell selectivity of $(sC18)_2$ was a consequence of the peptide-lipid interactions depending on the lipid charge, which was verified on various artificial membrane systems. It was demonstrated that the interaction of both peptides with neutrally charged membranes were minimal and no disruption could be observed. In contrast, looking at the experiments with the negatively charged membranes, that were more resembling cancer cell membranes, the accumulation of the CPPs was very outstanding. Furthermore, $(sC18)_2$ was even able to disrupt the vesicles, which led to a release of the enclosed dyes. It could also be shown that cholesterol played an important role for the interaction with the membranes, even when the disrupting effect was diminished compared to the negatively charged vesicles.

Additionally, an efficient transport capability of the active drug actinomycin D could be presented, which resulted in the effective reduction of viable cells in comparison to the cells incubated with the drug or peptide alone, respectively. In future, the delivery of other drugs or covalently bound agents should be observed.

In conclusion, $(sC18)_2$ could be presented in various studies as a lytic peptide with cancer selective properties, that was able to overcome the membrane likely by pore formation and also accumulated in the cell nuclei. Moreover, it could also be used as cargo delivery system.

5.3 Summary and conclusion of N50 and NrTP studies

In the third part of the thesis, two fusion peptides were investigated regarding their internalization and transport capability. The nuclear targeting sequence N50 and the nucleolar targeting sequence NrTP were conjugated to the CPP sC18* to gain higher uptake rates and a specific targeting to the cell nucleus. All peptide sequences were successfully synthesized via SPPS and high purities could be obtained. The CD spectra showed that N50 and NrTP alone were not exhibiting a defined secondary structure, but when coupled to sC18*, the peptides formed an α-helical structure in the presence of TFE. As it was already shown that sC18* alone was also able to form a helix, thus the coupling of the NLS-sequences to this amphipathic peptide was the determining factor of the structure formation.

Due to this, the peptides were also different in their cellular uptake amounts. In both tested cell lines (HeLa and MCF-7), the internalization rates of the fusion peptides were extremely increased in contrast to the ones of sC18*, N50 and NrTP alone, which was demonstrated by flow cytometric and microscopic analysis. It could also be demonstrated that the uptake of the fusion peptides in HeLa cells seemed to be higher than in MCF-7 cells, whereby the translocation of the peptides were equal in both cell lines. In MCF-7, the internalization of NrTP-sC18* was about four times higher than of N50-sC18*. In more detailed microscopic studies, it could be observed that both NLS-CPPs localized in the cytoplasm as well as in high extent in the nuclei and especially NrTP-sC18* accumulated in the nucleoli. This result was also confirmed for HeLa cells but only at low concentrations, whereas in MCF-7 cells, just NrTP-sC18* was present in the nucleoli after 30 min of incubation. Interestingly, the amount of peptides in the breast cancer cells decreased with longer incubation times, indicating a fast degradation of the peptides in the cytoplasm. The incubation of the cells with the CPPs at low temperatures did not harm their translocation and localization pattern. This indicated an energy-independent direct penetration for their uptake mechanism, which was followed by a translocation over the cell nuclei membrane and later on peptide degradation.

In addition, the peptides cytotoxic profiles differed from each other comparing the cell lines. In MCF-7, no toxicity for all peptides could be detected up to a concentration of 100 µM. On the contrary, in HeLa cells sC18*, NrTP and N50-sC18* were slightly toxic at 100 µM, whereas the fusion of NrTP and sC18* resulted in a toxic peptide version. At 100 µM, no viable cell could be examined any more. This was probably correlated to the higher uptake rates in HeLa cells, in general. Higher amounts of peptides in the cells could evoke higher cytotoxicity.

N50-sC18* and NrTP-sC18* were also capable to form complexes with the two DNA vectors pEGFP-N1 and pGL4.13, respectively. This was verified by an electromobility shift assay and thus a complexation rate could be determined for transfection experiments. Anyway, both

transfection studies did not lead to an efficient expression of the reporter genes that were encoded on the plasmid DNA. The only slightly promising result was obtained for NrTP-sC18* in MCF-7 cells, even when the transfection rate was far below the one with Lipofectamine. In general, the transfection rate with Lipofectamine was about 10-times higher in HeLa cells than in MCF-7 cells. It is known, that the transfection of cells is a very challenging tool that is depending on many various factors such as temperature, concentration, membrane composition etc. Other cell lines as well as different protocols should be taken into consideration regarding a successful transfection. Within this, also higher peptide/vector rates should be investigated, leading to better results.

Nevertheless, another important property of these fusion peptides could be observed. N50-sC18* and NrTP-sC18* were able to efficiently transport the anticancer drug doxorubicin in MCF-7 cells, which resulted in a decrease of cell viability. This effect could not be seen in HeLa cells and also the microscopic observation led to the hypothesis that the transport of the drug was not that high as in the MCF-7 cells. It occurred that the uptake of the CPPs alone was higher in HeLa cells, but when complexed with DNA or co-incubated with doxorubicin, the treatment of MCF-7 cells was more efficient. This was presumably correlated with the interaction of the peptides with the two different cancer plasma membranes.

In conclusion, one can say that the fusion of a nuclear or nucleolar targeting sequence with a cell-penetrating peptide could highly increase the cellular uptake and a selective targeting of the nucleus of cancer cells. The two presented new fusion CPPs N50-sC18* and NrTP-sC18* already showed interesting features and this work formed the basis for further more detailed studies of these promising potential nuclei-targeting peptides.

To get a better understanding in the translocation of the CPPs N50-sC18* and NrTP-sC18* over the cell nuclei membranes of the cancer cells, experiments with fractionated cells and isolated nuclei should be performed. Next to this, it should also be investigated, if these fusion peptides do also exhibit a certain cell selectivity. Uptake and cytotoxicity studies should also be performed with these new CPP variants on non-cancer cells.

The ability of N50-sC18* and NrTP-sC18* as transport vehicles was only studied with doxorubicin. This could be further investigated using other therapeutic agents, covalently bound drugs or chemicals that are known to improve the uptake. Moreover, transfection studies were just done in a few attempts. Hereby, one could improve the protocol, decrease the peptide/plasmid rate or test other cell lines that are known to be better transfectable.

Furthermore, the exact uptake mechanism of all presented CPPs is still not fully understood. By inhibiting specific uptake pathways, the uptake behavior could be further investigated.

6 REFERENCES

[1] Whitehead, K. A., Langer, R., and Anderson, D. G. (**2009**) Knocking down barriers: advances in siRNA delivery, *Nat Rev Drug Discov 8*, 129-138.

[2] Mitragotri, S. (**2013**) Devices for overcoming biological barriers: the use of physical forces to disrupt the barriers, *Adv Drug Deliv Rev 65*, 100-103.

[3] Dowdy, S. F. (**2017**) Overcoming cellular barriers for RNA therapeutics, *Nat Biotechnol 35*, 222-229.

[4] Hille, B. (**1986**) Ionic channels: molecular pores of excitable membranes, *Harvey Lect 82*, 47-69.

[5] Perland, E., and Fredriksson, R. (**2017**) Classification Systems of Secondary Active Transporters, *Trends Pharmacol Sci 38*, 305-315.

[6] Huber, P. E., Jenne, J., Debus, J., Wannenmacher, M. F., and Pfisterer, P. (**1999**) A comparison of shock wave and sinusoidal-focused ultrasound-induced localized transfection of HeLa cells, *Ultrasound Med Biol 25*, 1451-1457.

[7] Tata, D. B., Dunn, F., and Tindall, D. J. (**1997**) Selective clinical ultrasound signals mediate differential gene transfer and expression in two human prostate cancer cell lines: LnCap and PC-3, *Biochem Biophys Res Commun 234*, 64-67.

[8] Allen, T. M., and Cullis, P. R. (**2013**) Liposomal drug delivery systems: from concept to clinical applications, *Adv Drug Deliv Rev 65*, 36-48.

[9] Li, Y., Pei, Y., Zhang, X., Gu, Z., Zhou, Z., Yuan, W., Zhou, J., Zhu, J., and Gao, X. (**2001**) PEGylated PLGA nanoparticles as protein carriers: synthesis, preparation and biodistribution in rats, *J Control Release 71*, 203-211.

[10] Madani, F., Lindberg, S., Langel, U., Futaki, S., and Graslund, A. (**2011**) Mechanisms of cellular uptake of cell-penetrating peptides, *J Biophys 2011*, 414729.

[11] Bechara, C., and Sagan, S. (**2013**) Cell-penetrating peptides: 20 years later, where do we stand?, *FEBS Lett 587*, 1693-1702.

[12] Dissanayake, S., Denny, W. A., Gamage, S., and Sarojini, V. (**2017**) Recent developments in anticancer drug delivery using cell penetrating and tumor targeting peptides, *J Control Release 250*, 62-76.

[13] Jarver, P., and Langel, U. (**2006**) Cell-penetrating peptides--a brief introduction, *Biochim Biophys Acta 1758*, 260-263.

[14] Snyder, E. L., and Dowdy, S. F. (**2005**) Recent advances in the use of protein transduction domains for the delivery of peptides, proteins and nucleic acids in vivo, *Expert Opin Drug Deliv 2*, 43-51.

[15] Reissmann, S. (**2014**) Cell penetration: scope and limitations by the application of cell-penetrating peptides, *J Pept Sci 20*, 760-784.

[16] Vives, E., Brodin, P., and Lebleu, B. (**1997**) A truncated HIV-1 Tat protein basic domain rapidly translocates through the plasma membrane and accumulates in the cell nucleus, *J Biol Chem 272*, 16010-16017.

[17] Derossi, D., Joliot, A. H., Chassaing, G., and Prochiantz, A. (**1994**) The third helix of the Antennapedia homeodomain translocates through biological membranes, *J Biol Chem 269*, 10444-10450.

[18] Krauss, U., Kratz, F., and Beck-Sickinger, A. G. (**2003**) Novel daunorubicin-carrier peptide conjugates derived from human calcitonin segments, *J Mol Recognit 16*, 280-287.

[19] Neundorf, I., Rennert, R., Hoyer, J., Schramm, F., Löbner, K., Kitanovic, I., and Wölfl, S. (**2009**) Fusion of a Short HA2-Derived Peptide Sequence to Cell-Penetrating Peptides Improves Cytosolic Uptake, but Enhances Cytotoxic Activity, *Pharmaceuticals 2*, 49-65.

[20] Hoyer, J., Schatzschneider, U., Schulz-Siegmund, M., and Neundorf, I. (**2012**) Dimerization of a cell-penetrating peptide leads to enhanced cellular uptake and drug delivery, *Beilstein J Org Chem 8*, 1788-1797.

[21] Pooga, M., Hallbrink, M., Zorko, M., and Langel, U. (**1998**) Cell penetration by transportan, *FASEB J 12*, 67-77.

[22] Futaki, S., Suzuki, T., Ohashi, W., Yagami, T., Tanaka, S., Ueda, K., and Sugiura, Y. (**2001**) Arginine-rich peptides. An abundant source of membrane-permeable peptides having potential as carriers for intracellular protein delivery, *J Biol Chem 276*, 5836-5840.

[23] Deshayes, S., Heitz, A., Morris, M. C., Charnet, P., Divita, G., and Heitz, F. (**2004**) Insight into the mechanism of internalization of the cell-penetrating carrier peptide Pep-1 through conformational analysis, *Biochemistry 43*, 1449-1457.

[24] Rennert, R., Neundorf, I., and Beck-Sickinger, A. G. (**2008**) Calcitonin-derived peptide carriers: mechanisms and application, *Adv Drug Deliv Rev 60*, 485-498.

[25] Larrick, J. W., Hirata, M., Balint, R. F., Lee, J., Zhong, J., and Wright, S. C. (**1995**) Human CAP18: a novel antimicrobial lipopolysaccharide-binding protein, *Infect Immun 63*, 1291-1297.

[26] Guterstam, P., Madani, F., Hirose, H., Takeuchi, T., Futaki, S., El Andaloussi, S., Graslund, A., and Langel, U. (**2009**) Elucidating cell-penetrating peptide mechanisms of action for membrane interaction, cellular uptake, and translocation utilizing the hydrophobic counter-anion pyrenebutyrate, *Biochim Biophys Acta 1788*, 2509-2517.

[27] Jones, A. T., and Sayers, E. J. (**2012**) Cell entry of cell penetrating peptides: tales of tails wagging dogs, *Journal of Controlled Release 161*, 582-591.

[28] Radis-Baptista, G., Campelo, I. S., Morlighem, J. R. L., Melo, L. M., and Freitas, V. J. F. (**2017**) Cell-penetrating peptides (CPPs): From delivery of nucleic acids and antigens to transduction of engineered nucleases for application in transgenesis, *J Biotechnol 252*, 15-26.

[29] Alves, I. D., Goasdoue, N., Correia, I., Aubry, S., Galanth, C., Sagan, S., Lavielle, S., and Chassaing, G. (**2008**) Membrane interaction and perturbation mechanisms induced by two cationic cell penetrating peptides with distinct charge distribution, *Biochim Biophys Acta 1780*, 948-959.

[30] van den Berg, A., and Dowdy, S. F. (**2011**) Protein transduction domain delivery of therapeutic macromolecules, *Curr Opin Biotechnol 22*, 888-893.

[31] Maiolo, J. R., Ferrer, M., and Ottinger, E. A. (**2005**) Effects of cargo molecules on the cellular uptake of arginine-rich cell-penetrating peptides, *Biochim Biophys Acta 1712*, 161-172.

[32] Jones, A. T. (**2007**) Macropinocytosis: searching for an endocytic identity and role in the uptake of cell penetrating peptides, *J Cell Mol Med 11*, 670-684.

[33] Ben-Dov, N., and Korenstein, R. (**2015**) The uptake of HIV Tat peptide proceeds via two pathways which differ from macropinocytosis, *Biochim Biophys Acta 1848*, 869-877.

[34] Kaplan, I. M., Wadia, J. S., and Dowdy, S. F. (**2005**) Cationic TAT peptide transduction domain enters cells by macropinocytosis, *J Control Release 102*, 247-253.

[35] Radis-Baptista, G., de la Torre, B. G., and Andreu, D. (**2012**) Insights into the uptake mechanism of NrTP, a cell-penetrating peptide preferentially targeting the nucleolus of tumour cells, *Chem Biol Drug Des 79*, 907-915.

[36] Mitra, A. K., Agrahari, V., Mandal, A., Cholkar, K., Natarajan, C., Shah, S., Joseph, M., Trinh, H. M., Vaishya, R., Yang, X., Hao, Y., Khurana, V., and Pal, D. (**2015**) Novel delivery approaches for cancer therapeutics, *J Control Release 219*, 248-268.

[37] DeSantis, C. E., Lin, C. C., Mariotto, A. B., Siegel, R. L., Stein, K. D., Kramer, J. L., Alteri, R., Robbins, A. S., and Jemal, A. (**2014**) Cancer treatment and survivorship statistics, 2014, *CA Cancer J Clin 64*, 252-271.

[38] Ran, S., Downes, A., and Thorpe, P. E. (**2002**) Increased exposure of anionic phospholipids on the surface of tumor blood vessels, *Cancer Res 62*, 6132-6140.

[39] Schweizer, F. (**2009**) Cationic amphiphilic peptides with cancer-selective toxicity, *Eur J Pharmacol 625*, 190-194.

[40] Schroder-Borm, H., Bakalova, R., and Andra, J. (**2005**) The NK-lysin derived peptide NK-2 preferentially kills cancer cells with increased surface levels of negatively charged phosphatidylserine, *FEBS Lett 579*, 6128-6134.

[41] Lim, K. J., Sung, B. H., Shin, J. R., Lee, Y. W., Kim, D. J., Yang, K. S., and Kim, S. C. (**2013**) A cancer specific cell-penetrating peptide, BR2, for the efficient delivery of an scFv into cancer cells, *PLoS One 8*, e66084.

[42] Nguyen, L. T., Yang, X. Z., Du, X., Wang, J. W., Zhang, R., Zhao, J., Wang, F. J., Dong, Y., and Li, P. F. (**2015**) Enhancing tumor-specific intracellular delivering efficiency of cell-penetrating peptide by fusion with a peptide targeting to EGFR, *Amino Acids 47*, 997-1006.

[43] Liu, Y., Mei, L., Xu, C., Yu, Q., Shi, K., Zhang, L., Wang, Y., Zhang, Q., Gao, H., Zhang, Z., and He, Q. (**2016**) Dual Receptor Recognizing Cell Penetrating Peptide for Selective Targeting, Efficient Intratumoral Diffusion and Synthesized Anti-Glioma Therapy, *Theranostics 6*, 177-191.

[44] Desgrosellier, J. S., and Cheresh, D. A. (**2010**) Integrins in cancer: biological implications and therapeutic opportunities, *Nat Rev Cancer 10*, 9-22.

[45] Ronson, A., Tvito, A., and Rowe, J. M. (**2016**) Treatment of Relapsed/Refractory Acute Lymphoblastic Leukemia in Adults, *Curr Oncol Rep 18*, 39.

[46] Dietz, G. P., and Bahr, M. (**2004**) Delivery of bioactive molecules into the cell: the Trojan horse approach, *Mol Cell Neurosci 27*, 85-131.

[47] Bolhassani, A., Safaiyan, S., and Rafati, S. (**2011**) Improvement of different vaccine delivery systems for cancer therapy, *Mol Cancer 10*, 3.

[48] Li, Y., Zheng, X., Cao, Z., Xu, W., Zhang, J., and Gong, M. (**2012**) Self-assembled peptide (CADY-1) improved the clinical application of doxorubicin, *Int J Pharm 434*, 209-214.

[49] Zhang, P., Cheetham, A. G., Lock, L. L., and Cui, H. (**2013**) Cellular uptake and cytotoxicity of drug-peptide conjugates regulated by conjugation site, *Bioconjug Chem 24*, 604-613.

[50] Dubikovskaya, E. A., Thorne, S. H., Pillow, T. H., Contag, C. H., and Wender, P. A. (**2008**) Overcoming multidrug resistance of small-molecule therapeutics through conjugation with releasable octaarginine transporters, *Proc Natl Acad Sci U S A 105*, 12128-12133.

[51] Soler, M., Gonzalez-Bartulos, M., Soriano-Castell, D., Ribas, X., Costas, M., Tebar, F., Massaguer, A., Feliu, L., and Planas, M. (**2014**) Identification of BP16 as a non-toxic cell-penetrating peptide with highly efficient drug delivery properties, *Org Biomol Chem 12*, 1652-1663.

[52] Izabela, R., Jaroslaw, R., Magdalena, A., Piotr, R., and Ivan, K. (**2016**) Transportan 10 improves the anticancer activity of cisplatin, *Naunyn Schmiedebergs Arch Pharmacol 389*, 485-497.

[53] Mussbach, F., Pietrucha, R., Schaefer, B., and Reissmann, S. (**2011**) Internalization of nucleoside phosphates into live cells by complex formation with different CPPs and JBS-nucleoducin, *Methods Mol Biol 683*, 375-389.

[54] Morris, M. C., Vidal, P., Chaloin, L., Heitz, F., and Divita, G. (**1997**) A new peptide vector for efficient delivery of oligonucleotides into mammalian cells, *Nucleic Acids Res 25*, 2730-2736.

[55] Rittner, K., Benavente, A., Bompard-Sorlet, A., Heitz, F., Divita, G., Brasseur, R., and Jacobs, E. (**2002**) New basic membrane-destabilizing peptides for plasmid-based gene delivery in vitro and in vivo, *Mol Ther 5*, 104-114.

[56] Liu, B. R., Huang, Y. W., Aronstam, R. S., and Lee, H. J. (**2016**) Identification of a Short Cell-Penetrating Peptide from Bovine Lactoferricin for Intracellular Delivery of DNA in Human A549 Cells, *PLoS One 11*, e0150439.

[57] McBride, H. M., Neuspiel, M., and Wasiak, S. (**2006**) Mitochondria: more than just a powerhouse, *Curr Biol 16*, R551-560.

[58] Chan, D. C. (**2006**) Mitochondria: dynamic organelles in disease, aging, and development, *Cell 125*, 1241-1252.

[59] Horton, K. L., Stewart, K. M., Fonseca, S. B., Guo, Q., and Kelley, S. O. (**2008**) Mitochondria-penetrating peptides, *Chem Biol 15*, 375-382.

[60] Strouboulis, J., and Wolffe, A. P. (**1996**) Functional compartmentalization of the nucleus, *J Cell Sci 109 (Pt 8)*, 1991-2000.

[61] Paine, P. L., Moore, L. C., and Horowitz, S. B. (**1975**) Nuclear envelope permeability, *Nature 254*, 109-114.

[62] Hariton-Gazal, E., Feder, R., Mor, A., Graessmann, A., Brack-Werner, R., Jans, D., Gilon, C., and Loyter, A. (**2002**) Targeting of nonkaryophilic cell-permeable peptides into the nuclei of intact cells by covalently attached nuclear localization signals, *Biochemistry 41*, 9208-9214.

[63] Lewis, H. D., Husain, A., Donnelly, R. J., Barlos, D., Riaz, S., Ginjupalli, K., Shodeinde, A., and Barton, B. E. (**2010**) Creation of a novel peptide with enhanced nuclear localization in prostate and pancreatic cancer cell lines, *BMC Biotechnol 10*, 79.

[64] Hoesel, B., and Schmid, J. A. (**2013**) The complexity of NF-kappaB signaling in inflammation and cancer, *Mol Cancer 12*, 86.

[65] Zienkiewicz, J., Armitage, A., and Hawiger, J. (**2013**) Targeting nuclear import shuttles, importins/karyopherins alpha by a peptide mimicking the NFkappaB1/p50 nuclear localization sequence, *J Am Heart Assoc 2*, e000386.

[66] O'Sullivan, J. M., Pai, D. A., Cridge, A. G., Engelke, D. R., and Ganley, A. R. (**2013**) The nucleolus: a raft adrift in the nuclear sea or the keystone in nuclear structure?, *Biomol Concepts 4*, 277-286.

[67] Woods, S. J., Hannan, K. M., Pearson, R. B., and Hannan, R. D. (**2015**) The nucleolus as a fundamental regulator of the p53 response and a new target for cancer therapy, *Biochim Biophys Acta 1849*, 821-829.

[68] Fretz, M. M., Penning, N. A., Al-Taei, S., Futaki, S., Takeuchi, T., Nakase, I., Storm, G., and Jones, A. T. (**2007**) Temperature-, concentration- and cholesterol-dependent translocation of L- and D-octa-arginine across the plasma and nuclear membrane of CD34+ leukaemia cells, *Biochem J 403*, 335-342.

[69] Rodrigues, M., de la Torre, B. G., Radis-Baptista, G., Santos, N. C., and Andreu, D. (**2011**) Efficient cellular delivery of beta-galactosidase mediated by NrTPs, a new family of cell-penetrating peptides, *Bioconjug Chem 22*, 2339-2344.

[70] Kaiser, E., Colescott, R. L., Bossinger, C. D., and Cook, P. I. (**1970**) Color test for detection of free terminal amino groups in the solid-phase synthesis of peptides, *Anal Biochem 34*, 595-598.

[71] Manning, M. C., and Woody, R. W. (**1991**) Theoretical CD studies of polypeptide helices: examination of important electronic and geometric factors, *Biopolymers 31*, 569-586.

[72] Dagert, M., and Ehrlich, S. D. (**1979**) Prolonged incubation in calcium chloride improves the competence of Escherichia coli cells, *Gene 6*, 23-28.

[73] Horn, M., Reichart, F., Natividad-Tietz, S., Diaz, D., and Neundorf, I. (**2016**) Tuning the properties of a novel short cell-penetrating peptide by intramolecular cyclization with a triazole bridge, *Chem Commun (Camb) 52*, 2261-2264.

[74] Neundorf, I., Hoyer, J., Splith, K., Rennert, R., Peindy N'dongo H, W., and Schatzschneider, U. (**2008**) Cymantrene conjugation modulates the intracellular distribution and induces high cytotoxicity of a cell-penetrating peptide, *Chem Commun (Camb)*, 5604-5606.

[75] Deshayes, S., Konate, K., Aldrian, G., Heitz, F., and Divita, G. (**2011**) Interactions of amphipathic CPPs with model membranes, *Methods Mol Biol 683*, 41-56.

[76] Dev, S., Khan, R. H., and Surolia, A. (**2006**) 2,2,2-Trifluoroethanol-Induced structural change of peanut agglutinin at different pH: A comparative account, *IUBMB Life 58*, 473-479.

[77] Gronewold, A., Horn, M., Randelovic, I., Tovari, J., Munoz Vazquez, S., Schomacker, K., and Neundorf, I. (**2017**) Characterization of a Cell-Penetrating Peptide with Potential Anticancer Activity, *ChemMedChem 12*, 42-49.

[78] Anoopkumar-Dukie, S., Carey, J. B., Conere, T., O'Sullivan, E., van Pelt, F. N., and Allshire, A. (**2005**) Resazurin assay of radiation response in cultured cells, *Br J Radiol 78*, 945-947.

[79] Korzeniewski, C., and Callewaert, D. M. (**1983**) An enzyme-release assay for natural cytotoxicity, *J Immunol Methods 64*, 313-320.

[80] Kreutzberger, M. A., Tejada, E., Wang, Y., and Almeida, P. F. (**2015**) GUVs melt like LUVs: the large heat capacity of MLVs is not due to large size or small curvature, *Biophys J 108*, 2619-2622.

[81] Ziegler, A. (**2008**) Thermodynamic studies and binding mechanisms of cell-penetrating peptides with lipids and glycosaminoglycans, *Advanced Drug Delivery Reviews 60*, 580-597.

[82] Tsumoto, K., Matsuo, H., Tomita, M., and Yoshimura, T. (**2009**) Efficient formation of giant liposomes through the gentle hydration of phosphatidylcholine films doped with sugar, *Colloids Surf B Biointerfaces 68*, 98-105.

[83] Zachowski, A. (**1993**) Phospholipids in animal eukaryotic membranes: transverse asymmetry and movement, *Biochem J 294 (Pt 1)*, 1-14.

[84] Jobin, M. L., and Alves, I. D. (**2014**) On the importance of electrostatic interactions between cell penetrating peptides and membranes: a pathway toward tumor cell selectivity?, *Biochimie 107 Pt A*, 154-159.

[85] Dobrzynska, I., Szachowicz-Petelska, B., Sulkowski, S., and Figaszewski, Z. (**2005**) Changes in electric charge and phospholipids composition in human colorectal cancer cells, *Mol Cell Biochem 276*, 113-119.

[86] Jobin, M. L., Bonnafous, P., Temsamani, H., Dole, F., Grelard, A., Dufourc, E. J., and Alves, I. D. (**2013**) The enhanced membrane interaction and perturbation of a cell penetrating peptide in the presence of anionic lipids: toward an understanding of its selectivity for cancer cells, *Biochim Biophys Acta 1828*, 1457-1470.

[87] Martin, S. J., Reutelingsperger, C. P., McGahon, A. J., Rader, J. A., van Schie, R. C., LaFace, D. M., and Green, D. R. (**1995**) Early redistribution of plasma membrane phosphatidylserine is a general feature of apoptosis regardless of the initiating stimulus: inhibition by overexpression of Bcl-2 and Abl, *J Exp Med 182*, 1545-1556.

[88] Edidin, M. (**2003**) The state of lipid rafts: from model membranes to cells, *Annu Rev Biophys Biomol Struct 32*, 257-283.

[89] Saalik, P., Niinep, A., Pae, J., Hansen, M., Lubenets, D., Langel, U., and Pooga, M. (**2011**) Penetration without cells: membrane translocation of cell-penetrating peptides in the model giant plasma membrane vesicles, *J Control Release 153*, 117-125.

[90] Brown, D. A., and London, E. (**2000**) Structure and function of sphingolipid- and cholesterol-rich membrane rafts, *J Biol Chem 275*, 17221-17224.

[91] Langel, Ü. (2006) *Cell-penetrating Peptides: Processes and Applications*, 2 ed., CRC Press, Boca Raton, Fla, USA.

[92] Huotari, J., and Helenius, A. (**2011**) Endosome maturation, *EMBO J 30*, 3481-3500.

[93] Mukherjee, S., Ghosh, R. N., and Maxfield, F. R. (**1997**) Endocytosis, *Physiol Rev 77*, 759-803.

[94] Erazo-Oliveras, A., Muthukrishnan, N., Baker, R., Wang, T. Y., and Pellois, J. P. (**2012**) Improving the endosomal escape of cell-penetrating peptides and their cargos: strategies and challenges, *Pharmaceuticals (Basel) 5*, 1177-1209.

[95] Ciftci, K., and Levy, R. J. (**2001**) Enhanced plasmid DNA transfection with lysosomotropic agents in cultured fibroblasts, *Int J Pharm 218*, 81-92.

[96] Shiraishi, T., and Nielsen, P. E. (**2006**) Enhanced delivery of cell-penetrating peptide-peptide nucleic acid conjugates by endosomal disruption, *Nat Protoc 1*, 633-636.

[97] Mellman, I., Fuchs, R., and Helenius, A. (**1986**) Acidification of the endocytic and exocytic pathways, *Annu Rev Biochem 55*, 663-700.

[98] Kato, T., Okada, S., Yutaka, T., and Yabuuchi, H. (**1984**) The effects of sucrose loading on lysosomal hydrolases, *Mol Cell Biochem 60*, 83-98.

[99] Abes, S., Williams, D., Prevot, P., Thierry, A., Gait, M. J., and Lebleu, B. (**2006**) Endosome trapping limits the efficiency of splicing correction by PNA-oligolysine conjugates, *J Control Release 110*, 595-604.

[100] Lorents, A., Kodavali, P. K., Oskolkov, N., Langel, U., Hallbrink, M., and Pooga, M. (**2012**) Cell-penetrating peptides split into two groups based on modulation of intracellular calcium concentration, *J Biol Chem 287*, 16880-16889.

[101] Melikov, K., Hara, A., Yamoah, K., Zaitseva, E., Zaitsev, E., and Chernomordik, L. V. (**2015**) Efficient entry of cell-penetrating peptide nona-arginine into adherent cells involves a transient increase in intracellular calcium, *Biochem J 471*, 221-230.

[102] Islam, M. Z., Ariyama, H., Alam, J. M., and Yamazaki, M. (**2014**) Entry of Cell-Penetrating Peptide Transportan 10 into a Single Vesicle by Translocating Across Lipid Membrane and Its Induced Pores, *Biochemistry 53*, 386-396.

[103] Wadia, J. S., Stan, R. V., and Dowdy, S. F. (**2004**) Transducible TAT-HA fusogenic peptide enhances escape of TAT-fusion proteins after lipid raft macropinocytosis, *Nat Med 10*, 310-315.

[104] Anderson, R. G. (**1998**) The caveolae membrane system, *Annu Rev Biochem 67*, 199-225.

[105] Nichols, B. J., and Lippincott-Schwartz, J. (**2001**) Endocytosis without clathrin coats, *Trends Cell Biol 11*, 406-412.

[106] Kaighn, M. E., Narayan, K. S., Ohnuki, Y., Lechner, J. F., and Jones, L. W. (**1979**) Establishment and characterization of a human prostatic carcinoma cell line (PC-3), *Invest Urol 17*, 16-23.

[107] Boukamp, P., Petrussevska, R. T., Breitkreutz, D., Hornung, J., Markham, A., and Fusenig, N. E. (**1988**) Normal keratinization in a spontaneously immortalized aneuploid human keratinocyte cell line, *J Cell Biol 106*, 761-771.

[108] Raucher, D., and Ryu, J. S. (**2015**) Cell-penetrating peptides: strategies for anticancer treatment, *Trends Mol Med*.

[109] Raska, I., Shaw, P. J., and Cmarko, D. (**2006**) Structure and function of the nucleolus in the spotlight, *Curr Opin Cell Biol 18*, 325-334.

[110] Hoyer, J., and Neundorf, I. (**2012**) Knockdown of a G protein-coupled receptor through efficient peptide-mediated siRNA delivery, *J Control Release 161*, 826-834.

[111] Perry, R. P., and Kelley, D. E. (**1970**) Inhibition of RNA synthesis by actinomycin D: characteristic dose-response of different RNA species, *J Cell Physiol 76*, 127-139.

[112] Roccatano, D., Colombo, G., Fioroni, M., and Mark, A. E. (**2002**) Mechanism by which 2,2,2-trifluoroethanol/water mixtures stabilize secondary-structure formation in peptides: a molecular dynamics study, *Proc Natl Acad Sci U S A 99*, 12179-12184.

[113] Soule, H. D., Vazguez, J., Long, A., Albert, S., and Brennan, M. (**1973**) A human cell line from a pleural effusion derived from a breast carcinoma, *J Natl Cancer Inst 51*, 1409-1416.

[114] Scherer, W. F., Syverton, J. T., and Gey, G. O. (**1953**) Studies on the propagation in vitro of poliomyelitis viruses. IV. Viral multiplication in a stable strain of human malignant epithelial cells (strain HeLa) derived from an epidermoid carcinoma of the cervix, *J Exp Med 97*, 695-710.

[115] Mueller, J., Kretzschmar, I., Volkmer, R., and Boisguerin, P. (**2008**) Comparison of cellular uptake using 22 CPPs in 4 different cell lines, *Bioconjug Chem 19*, 2363-2374.

[116] Bolhassani, A., Jafarzade, B. S., and Mardani, G. (**2017**) In vitro and in vivo delivery of therapeutic proteins using cell penetrating peptides, *Peptides 87*, 50-63.

[117] Hoyer, J., and Neundorf, I. (**2012**) Peptide vectors for the nonviral delivery of nucleic acids, *Acc Chem Res 45*, 1048-1056.

[118] Fan, F., and Wood, K. V. (**2007**) Bioluminescent assays for high-throughput screening, *Assay Drug Dev Technol 5*, 127-136.

[119] Rennert, R., Neundorf, I., Jahnke, H. G., Suchowerskyj, P., Dournaud, P., Robitzki, A., and Beck-Sickinger, A. G. (**2008**) Generation of carrier peptides for the delivery of nucleic acid drugs in primary cells, *ChemMedChem 3*, 241-253.

[120] Sonawane, N. D., Szoka, F. C., Jr., and Verkman, A. S. (**2003**) Chloride accumulation and swelling in endosomes enhances DNA transfer by polyamine-DNA polyplexes, *J Biol Chem 278*, 44826-44831.

[121] Curiel, D. T., Agarwal, S., Wagner, E., and Cotten, M. (**1991**) Adenovirus enhancement of transferrin-polylysine-mediated gene delivery, *Proc Natl Acad Sci U S A 88*, 8850-8854.

[122] Kloeckner, J., Prasmickaite, L., Hogset, A., Berg, K., and Wagner, E. (**2004**) Photochemically enhanced gene delivery of EGF receptor-targeted DNA polyplexes, *J Drug Target 12*, 205-213.

[123] Futaki, S., Ohashi, W., Suzuki, T., Niwa, M., Tanaka, S., Ueda, K., Harashima, H., and Sugiura, Y. (**2001**) Stearylated arginine-rich peptides: a new class of transfection systems, *Bioconjug Chem 12*, 1005-1011.

[124] Ramamoorth, M., and Narvekar, A. (**2015**) Non viral vectors in gene therapy- an overview, *J Clin Diagn Res 9*, GE01-06.

[125] Medina-Kauwe, L. K., Xie, J., and Hamm-Alvarez, S. (**2005**) Intracellular trafficking of nonviral vectors, *Gene Ther 12*, 1734-1751.

[126] Al-Dosari, M. S., and Gao, X. (**2009**) Nonviral gene delivery: principle, limitations, and recent progress, *AAPS J 11*, 671-681.

[127] Gewirtz, D. A. (**1999**) A critical evaluation of the mechanisms of action proposed for the antitumor effects of the anthracycline antibiotics adriamycin and daunorubicin, *Biochem Pharmacol 57*, 727-741.

[128] Yang, F., Teves, S. S., Kemp, C. J., and Henikoff, S. (**2014**) Doxorubicin, DNA torsion, and chromatin dynamics, *Biochim Biophys Acta 1845*, 84-89.

[129] Aroui, S., Brahim, S., Hamelin, J., De Waard, M., Breard, J., and Kenani, A. (**2009**) Conjugation of doxorubicin to cell penetrating peptides sensitizes human breast MDA-MB 231 cancer cells to endogenous TRAIL-induced apoptosis, *Apoptosis 14*, 1352-1365.

[130] Liang, J. F., and Yang, V. C. (**2005**) Synthesis of doxorubicin-peptide conjugate with multidrug resistant tumor cell killing activity, *Bioorg Med Chem Lett 15*, 5071-5075.

[131] Bhattacharya, A., Seshadri, M., Oven, S. D., Toth, K., Vaughan, M. M., and Rustum, Y. M. (**2008**) Tumor vascular maturation and improved drug delivery induced by methylselenocysteine leads to therapeutic synergy with anticancer drugs, *Clin Cancer Res 14*, 3926-3932.

7 ATTACHEMENT

7.1 List of abbreviations

aa	amino acid
ACN	acetonitrile
Boc	*tert*-butyloxycarbonyl
CD	circular dichroism
CF	5(6)-carboxyfluorescein
Chol	cholesterol
CH_2Cl_2	dichloromethane
CLMS	confocal laser scanning microscopy
CPP	cell-penetrating peptide
DCM	dichloromethane
Dde	1-(4,4-dimethyl-2,6-dioxocyclohex-1-ylidene)ethyl
DIC	*N,N*-diisopropylcarbodiimide
DiI	1,1'-dioctadecyl-3,3,3',3'-tetramethylindocarbocyanine perchlorate
DIPEA	*N,N*-diisopropylethylamine
DMEM	Dulbecco's Modified Eagle Medium
DMF	*N,N*-dimethylformamide
DMSO	dimethyl sulfoxide
DNA	deoxyribonucleic acid
DOPC	1,2-dioleoyl-*sn*-glycero-3-phosphocholine
DOPE	1,2-dioleoyl-*sn*-glycero-3-phophoethanolamine
DOPG	1,2-dioleoyl-sn-glycero-3-[phospho-rac-(1-glycerol)]
DOTA	1,4,7,10-tetraazacyclododecane-1,4,7,10-tetraacetic acid
DOX	doxorubicin hydrochloride
EGFP	enhanced green fluorescent protein
EGFR	epidermal growth factor receptor

EMSA	electrophoretic mobility shift assay
eq.	equivalent
ER	endoplasmic reticulum
ESI	electrospray ionization
Et_2O	diethyl ether
EtOH	ethanol
FBS	fetal bovine serum
Fmoc	9-fluorenylmethyloxycarbonyl
GPMV	giant plasma membrane vesicles
GUV	giant unilamellar vesicle
HaCaT	human aneuploid immortal keratinocyte cell line
HATU	*O*-(7-azabenzotriazol-1-yl)-1,1,3,3-tetramethyluronium hexafluorophosphate
HCl	hydrogen chloride
hCT	human calcitonin
HCT-15	human colon adenocarcinoma cell line
HEK-293	human embryonic kidney 293 cell line
HeLa	human cervix carcinoma cell line
HIV	human immunodeficiency virus
Hoechst	bisbenzimide H33342
HPLC	high performance liquid chromatography
KCN	potassium cyanide
LB	Luria/Miller
LDH	lactate dehydrogenase
LUV	large unilamellar vesicle
m/z	mass-to-charge ratio
MßCD	methyl-ß-cyclodextrin
MCF-7	human breast adenocarcinoma cell line
MEM	Minimum Essential Medium Eagle

MeOH	methanol
MS	mass spectrometry
MW	molecular weight
m/z	mass to charge ratio
NFκB	Nuclear factor-κB
NMP	*N*-methyl-2-pyrrolidone
NODAGA	4-(4,7-bis(2-tert-butoxy-2-oxoethyl)-1,4,7-triazonan-1-yl)-5-tert-butoxy-5-oxopentaoic acid
NLS	nuclear localization signal
NrTP	nucleolar targeting peptides
ns	not significant
o/N	over night
PB	pyrenebutyrate
PBS	phosphate buffered saline
PC-3	human prostate cancer cell line
PCR	polymerase chain reaction
PEI	polyethyleneimine
pGL4.13	Luciferase Reporter Vector
PMAPs	pH-dependent Membrane Active Peptides
RCY	radiochemical yield
Resazurin	7-hydroxy-3*H*-phenoxazin-3-one-10-oxide
RNA	ribonucleic acid
RPMI-1640	Roswell Park Memorial Institute, Cell culture medium
RT	room temperature
SM	sphingomyelin (porcine brain)
SPPS	solid-phase peptide synthesis
TAE	tris-acetate-EDTA
t-Bu	*tert.* butyl
^{t}BuOH	*tert*. butyl alcohol

TFA	trifluoroacetic acid
TFE	trifluoroethanol
TIS/TIPS	triisopropylsilane
v/v	volume per volume
w/o	without

Amino acids:

A	Ala	alanine
C	Cys	cysteine
D	Asp	aspartic acid
E	Glu	glutamic acid
F	Phe	phenylalanine
G	Gly	glycine
H	His	histidine
I	Ile	isoleucine
K	Lys	lysine
L	Leu	leucine
M	Met	methionine
N	Asn	asparagine
P	Pro	proline
Q	Gln	glutamine
R	Arg	arginine
S	Ser	serine
T	Thr	threonine
V	Val	valine
W	Trp	tryptophane
Y	Tyr	tyrosine

7.2 List of figures

7.3 List of tables

7.4 Erklärung

Ich versichere, dass ich die von mir vorgelegte Dissertation selbstständig angefertigt, die benutzten Quellen und Hilfsmittel vollständig angegeben und die Stellen der Arbeit – einschließlich Tabellen, Karten und Abbildungen –, die anderen Werken im Wortlaut oder dem Sinn nach entnommen sind, in jedem Einzelfall als Entlehnung kenntlich gemacht habe; dass diese Dissertation noch keiner anderen Fakultät oder Universität zur Prüfung vorgelegen hat; dass sie – abgesehen von unten angegebenen Teilpublikationen – noch nicht veröffentlicht worden ist, sowie, dass ich eine solche Veröffentlichung vor Abschluss des Promotionsverfahrens nicht vornehmen werde. Die Bestimmungen der Promotionsordnung sind mir bekannt.

Die von mir vorgelegte Dissertation ist von Frau Prof. Dr. Ines Neundorf betreut worden.

Teilpublikationen:

Gronewold A., Horn M., Ranđelović I., Tóvári J., Muñoz Vázquez S., Schomäcker K., Neundorf I. (2017). Characterization of a Cell-Penetrating Peptide with Potential Anticancer Activity. *ChemMedChem.,* 12(1): 42-49.

Gronewold A., Horn M., Ranđelović I., Tóvári J., Muñoz Vázquez S., Schomäcker K., Neundorf I. (2017). Corrigendum Characterization of a Cell-Penetrating Peptide with Potential Anticancer Activity. *ChemMedChem.,* 12(9): 712.

Posterpräsentationen:

Gronewold A., Horn M., Neundorf I. (2015). Cell selectivity and uptake mechanisms of the positively charged cell-penetrating peptide $(sC18)_2$. 12^{th} German Peptide Symposium, Darmstadt

Gronewold A., Horn M., Neundorf I. (2015). Specific targeting of cancer cells using a positively charged lytic peptide. International Symposium CPP, Paris

_____ _____

Ort, Datum (Anja Gronewold)